Suppression of Nonlinear Distortion in Radio-over-Fibre Systems

Taimur Nazir Mirza

PhD

2020

Royal Holloway University of London

Suppression of Nonlinear Distortion in Radio-over-Fibre Systems

By

Taimur Nazir Mirza

Department of Electronics Engineering

Royal Holloway University of London

A Thesis submitted to the Royal Holloway University of London
for the Degree of Doctor of Philosophy

05 February 2020

Declaration

I, Taimur Nazir Mirza declare that the work presented in this thesis is my own and it has been generated by me as a result of my own original research. Some of my research work has been submitted for Patent grant under application number GB1900552.9, which is filed by Leonardo UK Ltd on 15th January 2019. This work is strictly **confidential** and should not be shared with anyone without prior consent of the PhD Supervisor (Dr. Shyqyri Haxha). The author rights for the Patent have been equally distributed among myself, Dr. Shyqyri Haxha (PhD supervisor), and Dr. Ian Flint (Leonardo Employee).

I confirm that this thesis has not been submitted before for any examination or degree in any University.

Name of Candidate: Taimur Nazir Mirza

Signature: 

Date: 05/02/2020

Abstract

Radio over fibre (RoF) is a promising technology in the communication world. Since the establishment of wireless technology, a research society in this area has been actively growing because of its intrinsic benefits such as great reliability, immunity to electromagnetic interference (EMI), high bandwidth, low loss and less cost. The RoF system being such an advantageous system, also possesses some limitations such as distortion products caused by nonlinear properties of the RoF system and poor Spurious-free Dynamic Range (SFDR) as compared to the electronic devices. These limitations need to be addressed to improve the RoF system performance so that its intrinsic benefits can be fully exploited.

In this thesis, a literature review of the RoF system with a focus on the linearisation techniques for Analogue Photonic Links (APL), has been presented and are critically analysed. Initially, a background study of APL was conducted which includes an optical fibre and its dispersions, techniques to compensate the fibre dispersion, optical modulation process, Balanced detection, and nonlinearities in the APL system. Later, the study was performed on reviewing various linearisation techniques for the elimination of Harmonics and Intermodulation distortions, which are generally produced due to a nonlinear transfer function of the Electro-Optic modulator. The core objective of the thesis is to develop linearisation techniques for the elimination of Intermodulation distortions in the APL and in the Frequency Mixers.

Three different linearisation methods have been proposed and presented in Chapter 3 to Chapter 5 of this thesis. Proposed models reduce the effect of distortions on the required frequencies, by eliminating them. The first proposed method eliminates the second-order distortion products by using two Dual-Parallel Mach Zehnder

Modulators (DPMZM) and a Balanced Photodetector (BPD) circuitry. Both DPMZMs process a double sideband suppressed carrier signal (DSBSC), and an independent polarisation-maintained fibre link is used to transmit an unmodulated optical carrier. Both optical links are coupled and then detected by the BPD. The method of using two DPMZMs improves the suppression of optical carrier, and an additional optical link for the transmission of optical Carrier helps improve the dynamic range. The BPD circuitry eliminates the Second-order distortion products and thus, significantly improves the SFDR with respect to Second-order Intermodulation Distortion (IMD2) and Third-order Intermodulation Distortion (IMD3). This proposed method is then used for the implementation of a dual RF channel APL, where the performance of both RF channels is optimised over a single optical carrier wavelength. Spurious-free Dynamic Range (SFDR) and Signal-to-Interference ratio (S/I) are the defined performance indicators for the the proposed linearisation techniques. The second and third method are the novel designs for eliminating the beat frequencies of Intermodulation Distortions in a Two-Tone Microwave Photonic Mixer, which is discussed in Chapter 4 and 5. The second method eliminates the IMD2 and Second-order harmonic Distortions (SHD) produced due to a beating between the Two-Tone input signals. Whereas the third method performs exactly the same task as a configuration proposed in the second method, but with an additional capability of eliminating the second order harmonic of the LO signal (2LO), which lies close to the upconverted frequencies or image frequencies. Both configurations are capable of linearly downconverting and upconverting the Two-Tone signals, simultaneously. Dynamic range of the eliminated distortions are presented in the form of a SFDR graph. These models have been submitted for the Patent application with a support from Leonardo UK Ltd .

Acknowledgement

Firstly, I would like to thank the God Almighty for giving me strength, confidence, and patience throughout the research duration. Without these benedictions, I would not have been able to successfully complete my research. Secondly, I would like to express my sincere gratitude to my PhD supervisor Dr. Shyqyri Haxha for his continuous support, and without his efforts, this work would not have been possible. Finally, I would like to thank my parents and my two sisters for their prayers, and continuous encouragement, which has motivated me to work hard.

Table of Contents

List of Figures

List of Tables

Abbreviations and Acronyms

- AMPL Analogue Microwave Photonic Link
- APL Analogue Photonic Link
- ASE Amplified Spontaneous Emission
- BER Bit Error Rate
- BNL Background Noise level
- BPD Balanced Photodetector
- CIR Carrier to Interference Ratio
- CW Continuous Wave
- DC Direct Current
- DCF Dispersion Compensation Fibre
- DCM Dispersion Compensation Method
- DDMZM Dual-Drive Mach Zehnder Modulator
- D-DPMZM Double-Dual Parallel Mach Zehnder Modulator
- DEMZM Dual-Electrode Mach Zehnder Modulator
- DEMUX De-Multiplexer
- DFB Distributed Feedback
- DPMZM Dual-Parallel Mach Zehnder Modulator
- DSB Double Sideband
- DSBSC Double Sideband Suppressed Carrier
- DSBFC Double Sideband Full Carrier
- DSF Dispersion Shifted Fibre
- EDFA Erbium Doped Fibre Amplifiers
- EO Electro-Optic
- ER Extinction Ratio
- FBG Fibre Bragg Grating
- FWM Four Wave Mixing
- GVD Group Velocity Division
- IF Intermediate Frequency
- IIP3 Third-order Input Intercept Point
- IMD Intermodulation Distortion
- IMD2 Second-order Intermodulation Distortion
- IMD3 Third-order Intermodulation Distortion
- IP3 Third-order Intercept Point

- ISI Intersymbol Interference
- ISNL Input System Noise Level
- LD Laser Diode
- LO Local Oscillator
- LSB Lower Sideband
- MDS Minimum Detectable Signal
- MMF Multimode Fibre
- MOS Minimum Operational Sensitivity
- MPM Microwave Photonic Mixer
- MWP Microwave Photonic
- MUX Multiplexer
- MZI Mach-Zehnder Interferometer
- MZM Mach-Zehnder Modulator
- NF Noise Figure/Factor
- NLCFBG Nonlinearity group-delay Chirped Fibre Bragg Grating
- NRZ Non-Return to Zero
- NZDSF Non-zero Dispersion Shifter Fibre
- OC Optical Coupler
- OCS Optical Carrier Suppression
- OEO Opto-Electric Oscillator
- OIP3 Third-order Output Intercept Point
- OPC Optical Phase Conjugator
- OSNL Output System Noise Level
- PON Passive Optical Network
- PMD Polarisation Mode Dispersion
- PMF Polarisation Maintaining Fibre
- QF Quality Factor
- RE Responsivity Error
- RF Radio Frequency
- RIN Relative Intensity Noise
- RoF Radio Over Fibre
- RZ Return to Zero
- S/I Signal to Interference Ratio
- SDMZM Single-Drive Mach Zehnder Modulator
- SFDR Spurious-Free Dynamic Range

- SHD Second-order Harmonic Distortion
- SMF Single-Mode Fibre
- SNR Signal to Noise Ratio
- SPM Self-Phase Modulation
- SSB Single Sideband
- SSBSC Single Sideband Suppressed Carrier
- USB Upper Sideband
- VOA Variable Optical Attenuator
- WDM Wavelength-Division Multiplexing
- XMD Cross-Modulation Distortion
- XPM Cross-phase Modulation

Chapter 1

1. Introduction

1.1 Introduction to Optics Communication

With the continuous growth in the demand for telecommunication devices, the mode of communications is rapidly evolving, and innovations in the field are emerging. The advancement of the communication system from the wire to wireless surfaced in the early 1900s when radio technology was being used as radiotelegraphy [1]. Today the need for telecommunication in the various areas of life such as residential areas, industrial societies and defence/military, is more than ever. Many companies and governments are investing billions of dollars on the new technologies to comply with the demand and to transmit a large amount of information in seconds. Around the 1960s, the transmission of high data rates through optical waves was introduced and implemented in around the 1980s using optical fibres, which has an enormous potential to carry data-rates of 100Gbps and beyond due to wide bandwidth of light waves [2]. In the Photonic systems, data is carried from one end to another by a carrier wave frequency, which ranges from a few megahertz to several thousand terahertz [3]. Before the evolution of optical fibre, coaxial cable was being used, and the initial transmission capability of coaxial cable was to transmit 300 voice channels or one television channel [3, 4]. Compared to coaxial cable, optical fibre is much faster and reliable, which makes it a strong contender for future telecommunication systems.

Since 1990 [5], radio over fibre system has become a great interest for researchers, because of its capability to relay digital baseband and radio frequency signals through a wide bandwidth of optical fibre. However, the system possesses some inevitable limitations due to its intrinsic impairments e.g. the nonlinear conversion

of signals from electrical to optical by an electro-optic modulator. Also, some other optical components in the link like optical fibres, optical amplifiers and optical filters all introduce some limitation in the form of optical signal dispersion, amplified noise and coupling loss.

With a continuous increase in the demand for ultra-wide bandwidth and lossless system, the need for a highly equipped system is required. Much progress has been made on the realisation of high bandwidth and low loss system by using microwave photonics (MWP). In MWP, the transmission can be achieved using a Digital Photonic Link (DPL) or Analogue Photonic Link (APL). However, digital links have a much less complicated performance requirement than analogue photonic links. Moreover, the availability of different components like laser diode, optical modulators and photodetectors, have allowed APLs to perform multiple functionalities [6]. APLs are best used for the transmission of radio signals from antennas to the Base unit, where signals are digitally processed. The commonly used applications of APLs are in radars, satellite, aircraft, Anonymous signal detection sensors, and defence & military.

1.2 Radio over Fibre Systems

Radio over fibre is a technique, which transmits the radio frequency signals over optical fibre. One should always keep in mind that RoF is fundamentally an analogue communication link, but it is also capable of transmitting digital signals [7]. Taking an example of RoF in wireless networks, where an analogue optical link can be defined as a link that has a sufficiently small modulation depth or *always On* laser to analyse small signals in many links. However, in case of a digital optical link, the optical modulation depth increases to 100%, or the laser switches ON and OFF subjective to the data sequence. [8].

The architecture of the RoF system consists of various components that fulfil the requirement of this system, such as Laser diode, Optical modulator, optical fibre, optical amplifiers, filters and Photodiode. Figure 1.1 illustrates the block diagram of the RoF structure, where the downlink and uplink transmission can be seen between the control station and base station [9]. At a transmitter in the control station, the radio signal along with an optical signal from a laser diode (LD) is modulated and then transmitted over the fibre. The receiver on the other end converts the signals back into an electrical signal by using a Photodetector.

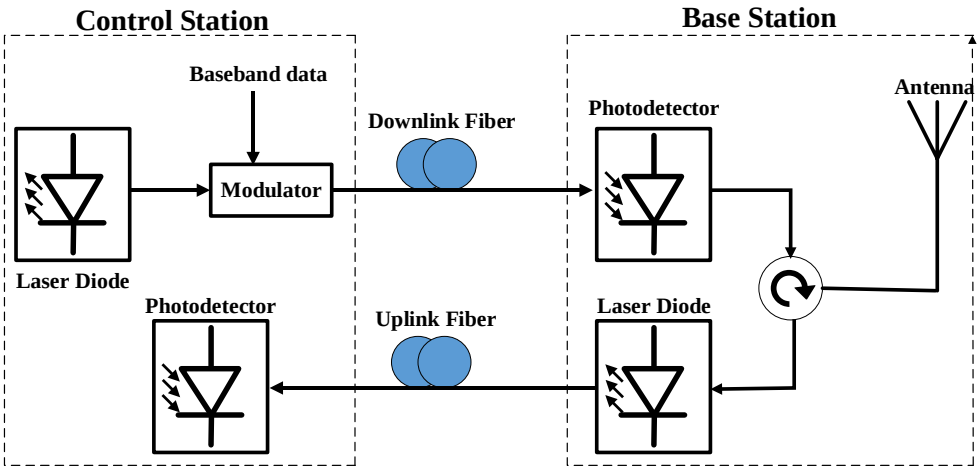

Figure 1.1: RoF architecture shows downlink and uplink between control and base station [9]

1.2.1 Applications of RoF system

RoF system has many applications in the existing communication infrastructure, and it also has a great scope in future communication networks considering its benefits over an existing coaxial network. The applications of RoF system are enormous such as, mobile communication system, broadcasting system, Airport system, and Train communication systems [10]. In the mobile communication system, RoF provides the flexibility of transmitting any modulation format such as Wideband Code Division Multiple Access (W-CDMA), and Long-Term Evolution (LTE). The broadcasting system includes the digital terrestrial transmission like Studio to

Transmitter Links (STLs), Transmitter to Studio Links (TSLs), Transmitter to Transmitter Links (TTLs), and Field Pick-up Units (FPU); and it is also used for television broadcasting [11, 12]. The applications in airport systems include Multilateration system that is an aircraft surveillance system, secondly, a foreign object and debris detection radar system that detects any object on the surface which may cause damage to the aircraft [13]. RoF system can also be extensively used in the railway communication networks as a millimetre-wave fronthaul and backhaul systems.

Furthermore, these can be categorised in three applicable links; transmit optical links, distribution optical links and receive optical links [14].

- Transmit Optical Links (TOL) carries RF signals from a source to an antenna. The known applications for this type of link are the radar transmitting function and the Personal Communication Service/Cellular antenna remoting function. Radar systems typically transmit a single signal at a time, which means the distortions in the system are not the main limiting factors. On the other side, PCS/Cellular links transmit multiple frequencies at the same time, which consequently produce many distortion products and makes the system limited [15].
- Distributed optical links (DOL) spread the same radio signal to multiple optical links. For instance, in the Cable Television (CATV) system, the microwave carrier is distributed over the whole system, which was credited as the first CATV distributed system based on RoF system [16, 17]. The typical applications of DOL are phased array Radars, and CATV distributed networks. Like TOL, the radar also transmits only one signal at a time and distortion is not a significant issue. Conversely, the broadcasting system transmits multiple signals simultaneously and faces many sources of distortion. Moreover, due to the distribution of signal into multiple links, the

splitting loss becomes a major concern in the performance of the RoF system. Usually, this loss is compensated by deploying optical amplifiers after the splitters. It should be noted that in a system of 100 distributions, the splitting loss can be of 20dB, and the optical loss of 20dB is translated to 40dB of RF loss, which is between the input RF and one of the output RF [14].

- Receive optical link (ROL) is a link between an antenna and a remotely located RF receiver [18]. The signal is detected by an antenna and then transmitted through a RoF link to a distantly located receiver. The noise picked up at the antennas generally limit ROL, which can be optimised by using linearisation techniques in the system.

1.3 Advantages and Disadvantages of RoF System

Radio over Fibre system has various advantages over a conventional coaxial link due to the intrinsic properties of the RoF system such as low losses, less complexity, and lower cost [19-21]. The prime purpose of using RoF is to transmit and process a radio frequency over an optical link without being digitised. It is capable of modulating and demodulating RF signals ranging from a few kilohertz to gigahertz, with a very low propagation loss as compared to the old coaxial links [10, 22]. The wide frequency range of RoF provides an excellent opportunity for the transmission of multiple channels with a large bandwidth, which has a high demand in the existing telecommunication infrastructure.

Even though RoF systems have many advantages, they also possess some limitations which are mainly due to the fabrication materials. One must know that processing an optical signal through a medium, with even minor defects, is going to have severe implications for the system performance. These implications count towards the disadvantages of the RoF system such as poor dynamic range, high-order harmonics and Intermodulation distortions, and chromatic dispersion [23]. When a radio

frequency is modulated over an optical carrier in the RoF system, it produces multiple high-order distortions, and in case of multiple RF modulation, the Intermodulation Distortions (IMD) are generated due to the nonlinear behaviour of the modulator. These distortions limit the system bandwidth and make it challenging to filter the fundamental frequencies at the receiver. The nonlinearities produced from the electro-optic modulator are compensated by optimising the modulation index, and optical power of the link.

Furthermore, the dynamic range of the system is limited by Relative Intensity Noise (RIN) and shot noise produced due to an increasing optical power. However, these noises can be reduced by using low optical power or by using coherent balanced photodetectors. RoF system includes an optical fibre as a connecting link between the transmitter and a receiver. The signal propagating through an optical fibre faces chromatic dispersion, which is due to a nonlinearity of the material used in the core of fibre. Chromatic dispersion can be reduced by deploying a single sideband (SSB) modulation technique or by using a Dispersion Compensation Fibre (DCF) in the RoF System.

1.4 Motivation

The demand for high speed and high data communication system is increasing, and the existing infrastructure is becoming inundated with the data flow. Therefore, RoF systems are considered the way forward in the communication links to improve their capacity. Nevertheless, the RoF system also comes with some intrinsic severe disabilities, which can potentially be a bottleneck to the communication link performance. Considering the enormous benefits of the RoF system, it is viable to overcome the inherent nonlinearities of the system by integrating the distortion compensation techniques in the links. In the RoF system, electro-optic modulator is considered a key component, which converts the radio signals into an optical signal. The prime focus of this research is to optimise the Radio over Fibre system for the

suppression of harmonics and intermodulation distortions, which are produced due to the nonlinear properties of the electro-optic modulator. This research will have a great importance in radar systems, aircraft or debris detection systems, satellite communication links, and many other defence and aerospace applications.

1.5 Research Questions

Fibre optic transmission systems have great importance in the telecommunication world. Due to their high capabilities and efficiency, they have become a primary interest of the researchers in many commercial and defence fields. RoF is one of a unique transmission system that transmits radio frequencies through an optical fibre and then converts it back into its original form at the receiver side. The system being highly desirable also incurs a significant amount of signal impairments, which limits the signal transmission. These impairments are because of many reasons such as the nonlinearity in the material of components, and the signal losses due to the conversion of electrical to an optical domain and vice versa. These signal impairments such as signal losses, noises and distortion products pose a limit on the performance of the system. Typically, link gain, noise figure and dynamic range are a few metrics used to quantify the system performance. There are many techniques based on Dual-Parallel Mach Zehnder Modulator (DPMZM), which are most commonly being used for the suppression of IMD, which may also suppress one sideband to achieve optical single sideband (SSB). By using DPMZM, a system's transmitter can be optimised for the better spurious-free dynamic range, as it allows exceptional control over the harmonics at the modulator and by applying different phase shifting, the harmonics or intermodulation distortion can be controlled. The optical fibre also incurs some distortion like chromatic dispersion, which can be compensated by using techniques like Single Sideband modulation, and Dispersion compensating fibres. So, by tackling the nonlinearities at the transmitter and other optical links, the distortion can be suppressed, and the system's performance can be

significantly improved. The research aligns itself with the questions raised above, and the linearisation techniques proposed in this research involves the Mach Zehnder modulators (MZM), dual-parallel Mach Zehnder modulators (DPMZM) and Balanced Photodetectors to eliminate the distortion products. Thus, the transmitted radio frequencies are linearised, which overall improves system performance.

1.6 Major Contribution and Thesis Organisation

The objective of this research is to investigate the techniques to overcome the nonlinearities of the RoF system. As discussed earlier, nonlinearities of electro-optic (EO) modulator and optical fibre are the main reported concerns. This research includes an initial study about compensating the fibre dispersions, and then an in-depth study on the linearisation techniques for the modulators have been provided. The outcome of an initial literature review includes the proposed linearisation techniques for the Analogue Photonic Link (APL) to eliminate the distortion products (Harmonics, Intermodulation distortion). The proposed technique eliminates the even-order distortion products and suppresses the odd-order distortion products by utilising Double DPMZM and a Balanced Photodetector (BPD). This linearisation technique makes the APL a multi-octave system, and later the proposed configuration is optimised for dual RF channel transmission. The contribution of this research revolves around the linearisation of radio frequencies transmitting through an optical link.

Furthermore, the APL application is diversified to a Microwave Photonic Mixer, and a novel linearisation technique is proposed. In a Microwave Photonic Mixer, multiple radio signals are linearly down-converted or up-converted with a better dynamic range. In order to simplify the thesis for a reader, each chapter of this thesis is summarised below;

The first chapter of this thesis introduces the area of research, and a brief history of the area is provided. The background study includes the introduction of the Radio over Fibre system with its applications. The advantages and disadvantages of the RoF system have also been described. The motivation behind this area of research is mentioned in this chapter and based on this motivation; the research questions have been addressed. The chapter concludes with the description of contributions and summary of each chapter.

The second chapter of this thesis provides the background study and a review of existing linearisation techniques. At first, the contributing factors in the linearisation of RoF systems have been thoroughly discussed, and later the linearisation techniques for the suppression of nonlinear modulator distortion are reviewed and analysed by using a VPI photonic Simulation tool [24]. In order to fully understand the system nonlinearities, the dispersion in the optical fibre, and some dispersion compensation techniques are also reviewed and discussed. The reviewed linearisation techniques of the modulator are based on Single Mach Zehnder modulator (MZM), dual-electrode Mach Zehnder modulator (DEMZM), and dual-parallel Mach Zehnder modulator (DPMZM).

The third chapter of this thesis presents a proposed configuration for the linearisation of a multi-octave bandwidth analogue photonic link. The proposed configuration comprises two DPMZMs, two 180^{o} RF hybrid coupler, and a balanced photodetector (BPD). The configuration has been mathematically modelled to illustrate the elimination of distortion products such as second-order harmonic distortion (SHD), second-order Intermodulation distortion (IMD2). The experimental performance of the configuration has been presented and validated by comparing with the existing techniques. In this chapter, the proposed configuration has been validated for two different cases; a single RF channel AMPL, and dual RF channel AMPL. For a dual

RF channel AMPL, RF ports on $DPMZM_1$ are considered as first RF channel, and RF ports on $DPMZM_2$ are considered as the second RF channel.

The fourth chapter includes a novel configuration for the elimination of beat frequencies produced from multiple input RF signals in a Microwave Photonic Mixer. The design focuses on demonstrating the linearisation of the down-conversion and up-conversion process. The proposed configuration uses two independent Mach Zehnder Modulators, where first MZM carries input RF signals and the other MZM modulates the Local Oscillator (LO) signal. The fraction of the output from the first MZM is split into two optical paths, and one path combines with the output of the second MZM. Finally, the output of first MZM and the combined output from the first MZM and second MZM gets detected by a balanced photodetector BPD. Consequently, the common frequency components in both optical paths get cancelled out with a perfect intensity balancing. This helps clean the spectrum for a down-conversion/up-conversion process and linearised Intermediate frequencies can be achieved. The results were analysed by using a VPI Photonic simulation tool and the SFDR of the concerned distortions is plotted.

The fifth chapter is an extension of chapter 4, which includes some additional benefits with a novel design for a Microwave Photonics Mixer. In the previous chapter, only the beat frequencies (such as SHD, IMD2) of the two-tone RF signal were eliminated. However, in this proposed model, the second-order harmonic distortion of the local oscillator LO signal is also eliminated with the other beat frequencies mentioned in the previous chapter. This method includes an additional laser source of 1540nm wavelength, which is modulated by the LO signal at the MZM2. The purpose of using a different laser wavelength was to create another optical channel, which will carry similar distortion products related to the LO signal and gets eliminated over combining the detected electrical signals. A VPI model is designed, and the results are analysed in this chapter.

The sixth chapter concludes the research work completed. It also includes the future perspective of this research and discusses room for expansion or improvement. This chapter highlights the open research issues, which will guide any future research in this area.

Chapter 2

2 Background Theory and Linearisation Techniques for the RoF System

This chapter provides a general understanding of the RoF system, including various existing linearisation techniques. Initially, the RoF system was explored to provide a comprehensive background study of the Analogue Photonic Link (APL). Based on the undertaken research, necessary study on optical fibre, fibre dispersion, modulation techniques, system noises and noise parameters, and the intermodulation distortion, is explained in this chapter. Finally, the linearisation techniques for the APL system and Microwave Photonic Mixers are reviewed and critically analysed.

2.1 Optical Fibre and its Dispersions

Optical fibre is a flexible and transparent wire that has a core diameter slightly thicker than a human hair. Fibres are generally made of silica or plastic material, which is considered an ideal material due to its beneficial properties [25]. Optical fibre has almost overtaken the traditional coaxial cable because it possesses excellent benefits like reliability, large capacity, and low loss. The optical fibre consists of mainly two layers; core and cladding, which is then secured in a buffer coating. A core is the central passage that allows light to pass through by a total internal reflection method, and the cladding, due to its low refractive index, keeps the light waves inside the core as shown in Figure 2.1 [25]. Over a certain distance, the signal propagating through an optical fibre begins to lose power, which is due to a fibre attenuation. The attenuation, which is also known as transmission loss, depends on the material used in the manufacturing of the fibre and is measured as dB/km.

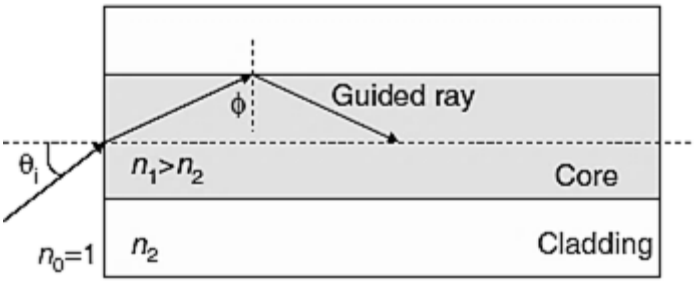

Figure 2.1: A total internal reflection in an optical fibre

The effective cross-sectional area of an optical fibre is an essential factor when considering the nonlinearities of an optical fibre. The nonlinearities in the fibre develops with an increasing optical intensity, and with a non-uniformly distribution of power in the cross-section of fibre. Therefore, it is necessary to consider an effective cross-sectional area (A_{eff}) of the fibre while implementing an optical system. It is related as follows; [26]

$$A_{eff} = \frac{\int_r^0 \int_\theta^0 r dr d\theta I(r,\theta)}{\int_r^0 \int_\theta^0 r dr d\theta I^2(r,\theta)} \tag{2.1}$$

where, I is the cross-sectional distribution of intensity, r and θ represent the polar coordinates.

Optical fibres have two types of index fibres; step-index and gradient-index fibre. Step-index fibre has constant refractive index throughout the entire cross-section, whereas in the gradient-index fibre, the refractive index of core decreases with the increase in the radial index. The light rays in the gradient-index fibre do not travel in a straight line, but instead, they continuously deflect towards the axis of the fibre. The refractive index of the core near the fibre axis is much higher than that of near to the cladding. Step-index is used in both single-mode and multimode fibre, however, gradient-index is only used in the multimode fibres. The two-modes of fibres are discussed in the following sections.

The losses in the fibre are called Attenuation, which reduces the power of the signal propagating in the fibre. The loss in a system can be expressed as [27];

$$Loss = \frac{P_{out}}{P_{in}} \tag{2.2}$$

Where P_{in} is the input power to the fibre and P_{out} is the power available at the output of the fibre. Also, the fibre loss is expressed in the decibels (dB), as it is mostly used as dB/km.

$$Loss_{dB} = 10 \log \frac{P_{out}}{P_{in}} \tag{2.3}$$

2.1.1 Fibre Dispersions

Dispersion is a broadening of signal in the optical fibre. This means that the signal travels at a different speed due to the nonlinearities or any other impairments in the fibre. These dispersions in the fibre can be compensated by using a Dispersion shifted fibre, dispersion compensating fibre (DCF) and by fibre Bragg gratings (FBG). The dispersions occur in the fibre are intermodal dispersion, chromatic dispersion, and Polarisation Mode Dispersion (PMD).

Intermodal dispersion occurs due to the different propagation velocity of the optical signal in the fibre, which means that if, for instance, two rays enter in the fibre at the same time, but one of the rays becomes slower than the other ray, and they exit the fibre with different velocities. However, this type of dispersion can be overcome by using Graded-index fibre. Another substantial dispersion in an optical fibre is chromatic dispersion. Chromatic dispersion is the change in the wavelength or the colour of the light beam. It causes the broadening of pulses and causes errors in the bits. It is commonly caused by non-linearity in the material used in the fibre that changes the refractive index. The other type of fibre dispersion is a Polarisation mode dispersion, where optical fibres have a different polarisation state at the propagation of light waves. This means that one pulse has two orthogonal polarisation modes and

when they travel through a fibre, due to impurities and nonlinearities, both modes acquire different arrival time as in Figure 2.2 [28]. The time difference between the two polarisation modes is called Differential Group Delay. Fibres with PMD are caused by Bi-refringence that is a default in fibre, where the refractive index of fibre changes with the polarisation state of light. In an ideal fibre, the two polarisation modes travel at the same speed but in reality, many nonlinearities cause PMD. This dispersion can also be caused by a bend in the fibre or any mechanical stress and by environmental behaviour such as temperature change.

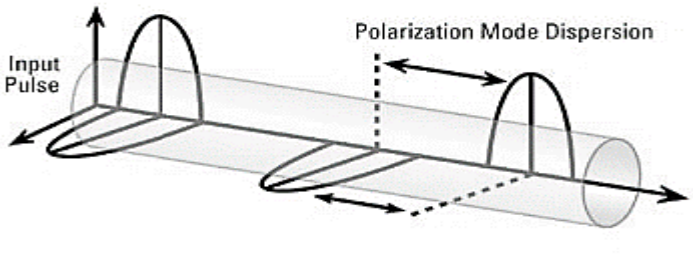

Figure 2.2: Polarisation mode dispersion in an optical fibre [28]

2.1.2 Dispersion compensation fibres

As the nonlinearities and different types of dispersion in the fibre causes a degradation in the quality of the signal and limits the transmission length. There are only a few dispersions like waveguide and modal dispersion that can be improved by only using the single mode fibre and by improving the fibre design. However, there is still a need for more sophisticated fibre techniques that can compensate the fibre in an efficient way. A few fibre dispersion compensation techniques are discussed below [29, 30].

2.1.2.1 Dispersion Shifted Fibre

Traditionally, the optical fibre communication systems were operated around a wavelength of 1310nm, which is now changed to 1550nm. As this wavelength is more desirable to the modest optical communication system and the losses in the

system are comparatively lower at this wavelength. Usually, the dispersion in the fibre is eliminated by a Single Mode Fibre (SMF) at a wavelength of 1310nm, which is at a zero-dispersion point. Though, using a standard SMF for a 1550nm wavelength exceeds the dispersion as compared to that of at 1310nm, which is why a Dispersion Shifted Fibre (DSF) is used to shift the zero-dispersion point from 1310nm to 1550nm, by manufacturing a single mode fibre with a triangular-shaped refractive index, instead of a step-index or graded-index [31]. The triangular shaped profile defines as the linear change of refractive index with increasing radial coordinate of optical fibre. As for step-index, the refractive index is constant in the core and it suddenly changes near the cladding. Dispersion Shifted Fibre performs better for single-channel as compared to WDM, due to four-wave mixing phenomenon in the Wavelength division multiplexing. However, this limitation of WDM was later overcome by cascading the Non-zero Dispersion Shifted Fibre (NZDSF) and standard single-mode fibre in the same link [29]. Non-zero dispersion shifted fibre is a fibre possessing a small non-zero dispersion at a wavelength of 1550nm.

2.1.2.2 Dispersion Compensation Fibre

Dispersion Compensating Fibre (DCF) is a new and vital way of compensating the dispersion from the fibre. The speciality of DCF is that it has a negative value of dispersion, which cancels the effect of chromatic dispersion. This technique is much more suitable for a single channel transmission as compared to multi-channels. The main reason behind this is the channel located further away from the centre wavelength receive less amount of dispersion compensating effect [29]. Regardless, it is still considered to have a remarkable impact on WDM. The design of DCF mainly depends on the core diameter of the fibre, and the less is the diameter the high is the negative dispersion. Due to its relatively small effective area, it is hard for DCF to handle high optical power, which increases nonlinear effects in the

transmission. While using DCF in the system, it is imperative to calculate the Group Velocity Dispersion (GVD) limited transmission distance for a given bit rate *B*. Equation (2.4), expresses the limited transmission distance for the DCF by using an external modulation process.

$$L = \frac{2\pi c}{16\lambda^2 |D| B^2} \tag{2.4}$$

where, *B* is represented as a bit rate, λ is the wavelength and *D* is the dispersion parameter.

In a standard SMF, the dispersion parameter is about 16ps/nm/km at a signal wavelength of 1550nm, whereas, in DCF the dispersion parameter could be from around -80ps/nm/km to -100ps/nm/km depending on the system requirement.

2.1.2.3 Fibre Bragg Grating

Fibre Bragg grating is an important tuneable technique for compensating the fibre dispersion. It is a section of fibre, where the refractive index inside the core varies periodically or aperiodically. The purpose of having a grated region in the core is to change the refractive index in a way that only beams with selected wavelength are reflected, and substantially all the reflected waves add up in phase. The reflected wavelengths from the grating are represented as [29];

$$\lambda_B = 2n_{eff} \Lambda_G \tag{2.5}$$

where, n_{eff} is the index of refraction that is seen by the light propagating in the fibre. Λ_G is the period of the refractive index modulation of the FBG.

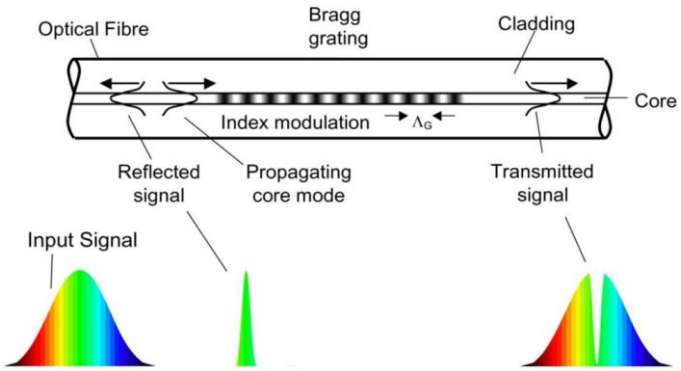

Figure 2.3: Illustration of Fibre Bragg grating [32]

The grated region in the fibre core is manufactured by photo-imprinting a hologram, and the material used for photo-imprinting is Germanium. Germanium is commonly used for the purpose of change in refractive index as it is highly susceptible to the high-intensity light, which effectively increases the refractive index of the fibre core. The diagram of the fibre Bragg grating is shown in Figure 2.3 [32]. As once the input spectrum transverse through the fibre, the grated region reflects some of the spectra with different wavelength. The transmitted signal received on the other side of the fibre is lacking the dispersive signals, as shown in Figure 2.3.

2.2 Optical Fibre Dispersions Compensation techniques

In this section, the techniques for the compensation of dispersion in the optical fibre are being discussed. The pulse broadening effect of the chromatics dispersion overlaps the signals in the adjacent bit periods, and this process is called intersymbol interference (ISI). Chromatic dispersion is reckoned a significant problem in the fibre, and there have been many techniques for compensating the dispersion such as Pre-, post-compensation, symmetrical compensation schemes using Dispersion Compensating Fibres (DCF).

In [33], few unique techniques for the compensation of chromatic dispersion, based on Distributed Feedback (DFB) laser have been discussed. Initially, a newly designed Nonlinearity group delay Chirped Fibre Bragg Grating (NLCFBG) is used

along with a single mode fibre and a tunable laser for the compensation of chromatic dispersion. NLCFBG can compensate the group delay on the upper and lower side RF carriers by adjusting the wavelength of the optical carrier. The second compensating technique includes single sideband modulation, where an optical carrier to sideband ratio can be controlled by using an ultra-strong optical injection-locked DFB laser. Where the power ratio of injected power and the power of DFB laser is controlled in order to achieve the desired side locked-mode, and when this signal is modulated with baseband signal, only a locked-mode signal would be modulated, and the rest will remain unaffected. Also, Optical Phase Conjugation (OPC) is proven to be a good scheme for dispersion compensation [33].

In [34], the three most common dispersion compensation schemes are presented and compared with each other for a Non-Return-to-Zero (NRZ) format. The comparison illustrates that the symmetrical compensation scheme performs better than pre and post compensation schemes at a bit rate of 10Gbit/s. This comparison was limited for a fixed data rate, whereas the performance of these dispersion compensation schemes depends on the bit rate and input power. It can also be seen in [35, 36], that the post-compensation and symmetrical compensation schemes result in minimum penalties as compared to pre-compensation. These schemes are based on a Dispersion Compensating Fibre (DCF), which have a negative dispersion. Negative dispersion helps the fibre to compensate for the positive dispersion in the SMF, but it also has a disadvantage in the system that is to exhibit a substantial attenuation in a signal power [37]. Subsequently, more optical amplifiers in the system are used, which makes the system more complicated and expensive.

Figure 2.4 illustrates the pre, post and symmetrical schemes, where pre-compensation is when a DCF is used before the SMF span to compensate for the dispersion in the fibre link. In the post-compensation scheme, DCF is used after the

SMF, whereas the symmetrical or mixed compensation scheme is a mixture of pre and post compensation schemes.

The pre-compensation scheme is primarily used for the compensation of dispersion by modifying the characteristics of the input signal from the transmitter, before transmitting it to the standard single mode fibre span.

The post-compensation scheme is used before the receiver end and after the SMF span. It compensates the Group Velocity Dispersion (GVD) from the fibre so that the fewer loss signals can be sent to the receiver for the demodulation process.

The symmetrical Compensation Scheme is a combination of pre and post schemes, which is also known as mixed-compensation or dual compensation scheme. It is used as two alternative combination of DCF and SMF, which are DCF-SMF-SMF-DCF, and the other is SMF-DCF-DCF-SMF.

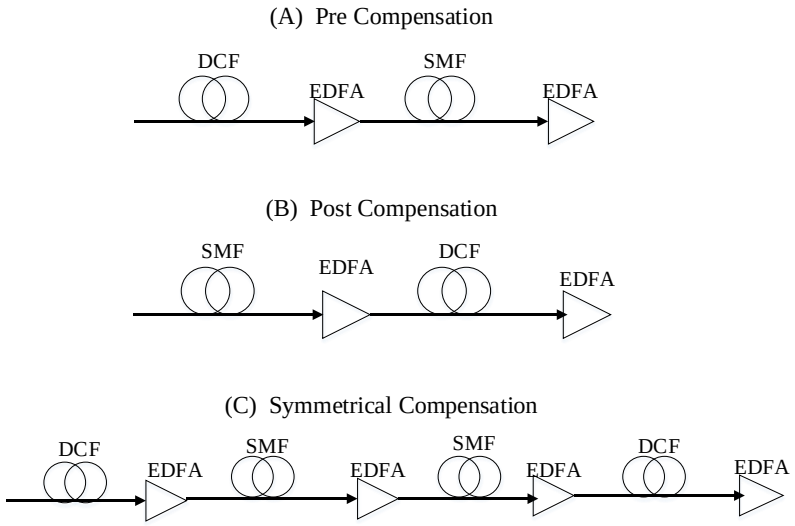

Figure 2.4: Fibre Dispersion Compensation Schemes

2.3 Modulation Process

The concept of modulation consists of transferring the data from electrical to the optical domain. There are mainly two strategies that can be used for modulation purpose; Direct Modulation and External Modulation [38].

In the direct modulation, the power of the light source is directly modulated by the RF signal and the data is impressed in the output intensity of the laser. The advantage of this technique is a simple architecture, and low in cost, whereas it is limited in frequency and response time.

External modulation is a technique that uses a continuous wave (CW) laser to emit light with constant power and time. Another external component called Optical modulator is used to modulate this light from the CW laser, with the RF signal, and an optical signal is achieved at the output. This method allows the use of high frequencies and high-performance applications efficiently. Due to this advantage, external modulation is the most popular method in RoF systems. Mach-Zehnder modulators are the most commonly used external modulators in the RoF systems currently.

External optical modulators are of two types. One is Electro-absorption modulator, and the other is Electro-optic modulator. Electro-absorption modulator (EAM) is based on modulating the number of photons absorbed in the semiconductor optical waveguide by changing the strength of the electrical field applied across the waveguide. Electro-optic modulators are the most commonly used external modulators due to their robustness against chirp as compared to direct modulation. The modulation process in the MZM is carried out by changing the voltage on each path of the MZ, which alters the path length by the electric field. The modulation in each path of MZM is referred to as phase modulation. By combining the phase modulation from two different paths, it is converted into intensity modulation.

A modulator can be chirp free if both branches of the MZ has an identical electric field which means that both paths have identical phase modulation, but they are different in signs. It is also known as a push-pull method [39]. Mach-Zehnder modulators are either single drive or dual drive, where a dual-drive generates an intensity modulation by using data and an inverted data on the arms of MZM.

External modulators are crucial in the high-speed communication systems, as it is difficult to directly modulate the signal at high speed using a direct laser. There are various types of external modulators, and Dual-electrode Mach-Zehnder (DEMZM) is one of the most important currently being used in the microwave photonics. Due to its flexible characteristics and many ways of providing the spectrally efficient optical signals, it can be used in different ways, such as balanced or unbalanced dual-drive and single drive. Dual-drive configuration uses data with alternative phases in order to generate an intensity modulation. In the dual-drive configuration, the chirp can also be removed by making the electric field on both branches identical [39]. A single drive modulator can be fabricated on all three crystal cuts; however, due to high chirp insertion, they are not commonly being used nowadays. Dual driven modulators are only z-cut, whereas single-drive modulators can be *x*- or *y-cut* and *z-cut* [40]. A schematic of a dual-electrode MZ modulator is shown in Figure 2.5. It shows that the optical signal passing through a waveguide under the influence of upper and lower electrodes, which are energised by an RF and DC voltage. The electric field generated from these electrodes modulates the optical signal in the waveguide according to the required baseband signal (RF). DC voltages are used to control the biasing in the modulator, as it changes the phase of sine waves in order to optimise the nonlinear modulation or to achieve different modulation conditions like Single sideband modulation.

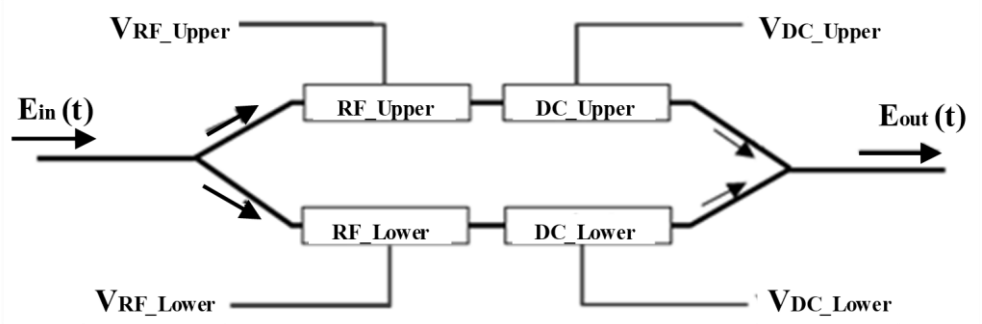

Figure 2.5: Dual Electrode Mach-Zehnder modulator

This modulator has upper and lower electrodes, where the RF and DC can be applied. When considering the design of an electro-optic modulator, it is essential to understand the materials in order to build a modulator suitable for a given wavelength and environment. Some of the materials have an undesirable resonant peak in the frequency response. The half-wave voltage is used to achieve the required degree of modulation for the selection of a crystal, and V_π needs to be small for a good modulation. It has great importance in designing the Electro-optic modulator (EOM), and the imperative factor of this design is a half-wave voltage length product $V_\pi L$. L is the length of the modulator electrode; it is defined as the product of the voltage, at which the phase difference between two electrodes of the modulator is 180^o and the length of the electrodes [41]. It can be mathematically expressed as follows;

$$V_\pi L = \frac{\pi V_o}{\Delta\beta}, \tag{2.6}$$

$$\Delta\beta = \beta_1 - \beta_0 \tag{2.7}$$

Where V_0 is the applied voltage, and β_1 and β_0 are the propagation constants of the fundamental modes of Mach-Zehnder arms with and without V_0 respectively [40].

2.3.1 Modulator's Operation

As the MZM can be configured in many ways. The bias voltages can control the operation of the modulator. When a voltage is applied on an electrode, the generated electric field alters the optical path length, and as a result, the optical signal in each path is phase modulated. The behaviour of the modulator can be observed by varying the modulation bias voltages.

The transfer function of a modulator is illustrated in Figure 2.6, where the operating points of a modulator can be identified based on a half-wave voltage and a bias voltage. A signal is modulated at a quadrature point, and in an ideal situation, no fluctuation in amplitude or frequency is seen. However, in real life, modulators tend

to drift their bias conditions due to environmental change or thermal state of the modulator, which effectively alters the amplitude and frequency of the modulated waveform [42]. When a phase difference is an integer multiple of 360°, a peak point occurs on the transfer function, and this process is called constructive interference. A peak operation in the modulator is achieved by setting bias to 0V as indicated in the transfer function plot.

When the phase difference is an odd integer multiple of 180°, a null point occurs on the transfer function, which represents a minimum transmission point. This configuration can be achieved by applying the bias on the modulator of Vπ or –Vπ. The transfer function of Mach-Zehnder modulator is expressed as;

$$E_o(t) = \alpha E_o cos2\left(\frac{V(t)\pi}{2V_\pi}\right) \tag{2.8}$$

Where, $E_o(t)$ is the transmitted intensity, α is the insertion loss, E_o is the input intensity from the laser diode, $V(t)$ is the applied voltage, V_π is the driving voltage.

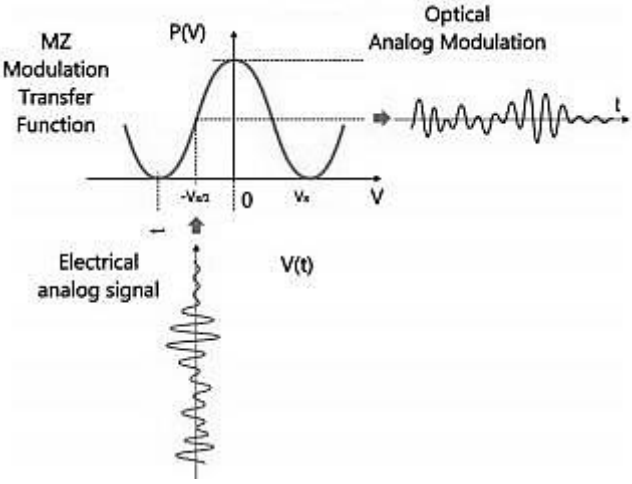

Figure 2.6: Transfer Function of MZM [42]

A modulator can be configured in many ways based on the normalised bias voltage and the operating points. A normalised bias voltage is represented as γ and defined

as V_{dc}/V_{π}, where V_{dc} is the DC bias voltage. A normalised amplitude of the drive modulating signal is represented as $\eta = V_m/V_{\pi}$, where V_{π} is the switching voltage of the modulator and V_m is the modulation voltage, also known as the drive voltage of the signal. By using the normalised modulation voltage, a modulation index of the RF signal can be calculated, which is expressed as $m = \pi\eta$. It can also be expressed as;

$$m = \pi \frac{V_m}{V_{\pi}} \tag{2.9}$$

The upper and lower electrodes of the DD-MZM can be controlled individually. The output optical field of DD-MZM can be written as [43];

$$E_{out}(t) = \frac{\alpha E_0}{2} e^{j2\pi f_0} \left\{ e^{j[\gamma\pi + \eta\pi \cos(2\pi f_m t)]} + e^{j[\eta\pi \cos(2\pi f_m t + \phi)]} \right\} \tag{2.10}$$

Where α is the optical power loss within the modulator, E_0 is the electric field of an optical carrier, and the exponential terms inside the curly brackets represents the field on the upper and lower electrodes of the modulator.

2.4 Sideband Modulations

A sideband is a band of frequencies lying on the upper and lower sides of the carrier signal. As a result of a modulation process, a sideband is produced, which contains all Fourier components of the modulated signals. Like an AM signal, along with upper and lower sideband, a carrier is present as well, which carries the message and transports it to the receiver. The purpose of a carrier signal in the modulation process is only to transport the data, and it carries no information, instead, it consumes about 50% of the power, which is why in most systems, the carrier is suppressed through the transmission, and it is brought back at the receiver to retrieve the information. In the sideband modulation, there are two main modulation techniques, such as double sideband modulation (DSB) and Single Sideband modulation (SSB). Figure 2.7 illustrates the modulation format, as it can be seen that the baseband signal modulates

with the carrier frequency to produce the two sideband spectrums, which is known as double sideband and then one of the sidebands can be eliminated in order to achieve the single sideband.

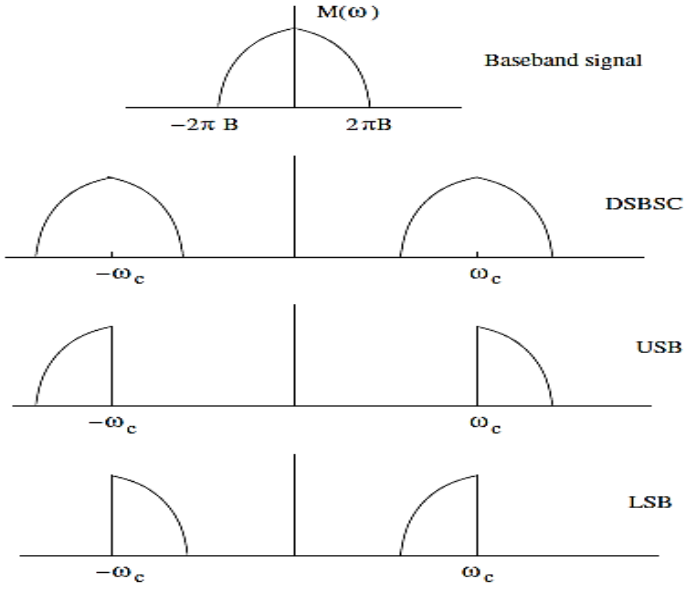

Figure 2.7: Diagram of DSB and SSB

2.4.1 Double Sideband Modulation (DSB)

As the name suggests that the double sidebands are involved in this modulation process. When a single frequency sinewave is modulated, then two sidebands are generated, and this process is called Double Sideband Modulation. In the modulation process, when a message signal is mixed with a carrier signal, an output signal consists of two sidebands on both sides of the carrier, comes out. There are two ways of using DSB, one with Full carrier and the other with a suppressed carrier, named as DSB-FC and DSB-SC respectively.

The basis of this modulation process depends on simple mathematics, as it is explained below. Suppose the baseband message signal is *m(t)*, and the waveform of the carrier signal is $m_c(t)$. Mathematical representation of these signals is [44];

$$m_c(t) = A_c \cos \omega_c t \tag{2.11}$$

After multiplying the carrier signal $m_c(t)$ with the baseband signal $m(t)$, the modulated signal $s(t)$ comes to this relation [44];

$$s(t) = A_c m(t) \cos \omega_c t \tag{2.12}$$

The Fourier transform of the baseband message $m(t)$ is $M(\omega)$, and that of the modulated signal can be represented as follows [44, 45];

$$S(\omega) = 0.5A_c M(\omega - \omega_c) + 0.5A_c M(\omega + \omega_c) \tag{2.13}$$

Figure 2.8 illustrates the modulation process of the double sideband, where it can be seen that a message signal and the carrier signal multiply and gives out a modulated DSB spectrum. The message signal is also referred to as a baseband signal and the spectral range that occupies it is called the baseband frequency range. Usually, in communication systems, the baseband has a limited (lower) frequency "ω", whereas a carrier signal has a high frequency "ω_c". As the baseband signal has typically positive and negative values, and the spectral component of a message signal on the positive side of the frequency spectrum ranges from $\omega_c \; to \; \omega_c + \omega$, which is called the upper sideband (USB). Likewise, the spectral components on the negative side of the frequency range from $\omega_c - \omega \; to \; \omega_c$, are called Lower sidebands (LSB). Thus, the bandwidth required for the transmission is twice the baseband frequency [45].

$$B_T = 2\omega \tag{2.14}$$

where, the B_T is the transmission bandwidth, ω is the baseband frequency.

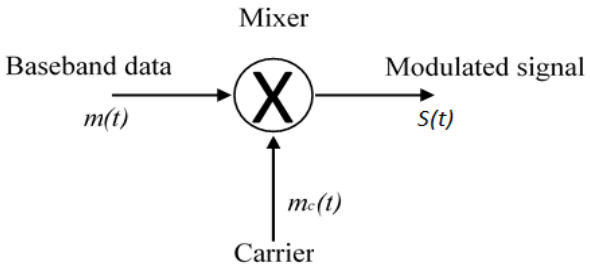

Figure: 2.8 Modulation format of DSB

In the radio over fibre system, the output amplitude of the double sideband modulation has a periodic fluctuation with the length of an optical fibre. Thus, the SSB modulation eliminates this effect of periodic fluctuations.

2.4.2 Single Sideband Modulation (SSB)

Single sideband modulation is a process in which one of the sidebands is eliminated or suppressed in order to utilise the bandwidth of the transmission system efficiently. In the frequency spectrum, the components of the spectrum are located equidistant from the carrier on the upper and lower side. The portion of frequency above the carrier is called Upper Sideband, and the portion below the carrier is named Lower sideband, as it is shown in Figure 2.7 [46]. Single sideband can also be used with or without the carrier signal, as carrier consumes much power, which can be saved by compressing the carrier and inserted it back at the receiver in order to retrieve the information from the signal. The reduction in power consumption and almost 50% of bandwidth reduction results in the improvement of the signal-to-noise ratio. The SSB with a full carrier is called SSBFC, and the single sideband with a suppressed carrier is referred to as SSBSC. The main advantage of using SSB is to improve the system's bandwidth and reduce the fibre dispersion. There are few different methods to achieve the SSB spectrum, the most used way is a Frequency discrimination method, and the other way is a Phase shift method. Frequency Discrimination method involves a bandpass filter, which is an easy way but comes at a high cost. Simply a lowpass filter can be used to suppress the upper sideband and a highpass

for lower sideband suppression. The block diagram of this simple modulation method is shown in Figure 2.9.

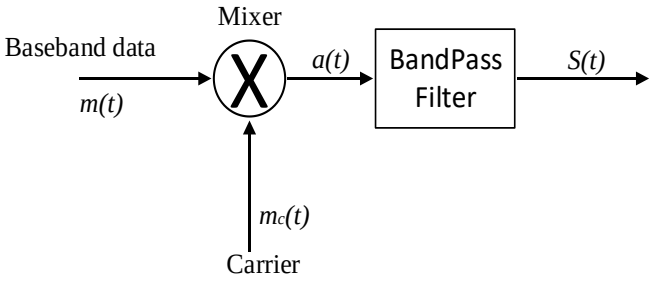

Figure 2.9: SSB modulation by using Filter

Mathematically, the modulation process can be calculated. Like the Double sideband modulation process, first, the message from a baseband signal *m(t)* is modulated with the carrier signal $m_c(t)$ from equation (2.12), and then a modulated signal *a(t)* is obtained. This double-sideband signal *a(t)* is shown as [46];

$$a(t) = A_c m(t) \cos \omega_c t \tag{2.15}$$

The Fourier transform of equation (2.15) is like equation (2.12). The double sideband spectrum is then passed through a Highpass or Lowpass filter, where the USB has a zero-valued spectrum for $|\omega| < \omega_c$ and the LSB has a zero-valued spectrum for $|\omega| > \omega_c$.

An SSB signal can be obtained by using the complex envelope as in equation (2.16), which results in the SSB signal waveform, as shown in equation (2.17) [46];

$$\tilde{s}(t) = 0.5A_c[m(t) \pm j\hat{m}(t)] \tag{2.16}$$

$$s(t) = 0.5A_c[m(t) \cos \omega_c t \pm \hat{m}(t) \sin \omega_c t] \tag{2.17}$$

Where, the baseband message is $m(t)$and its Hilbert Transform is $\hat{m}(t)$. The positive and negative signs in equation (2.17), are used according to the Single sideband requirement, such as for Lower sideband positive sign is used, and for Upper sideband, a negative sign is used.

The other modulation method for SSB is a phase-shifting method. The block diagram of this process can be seen in Figure 2.10 [46].

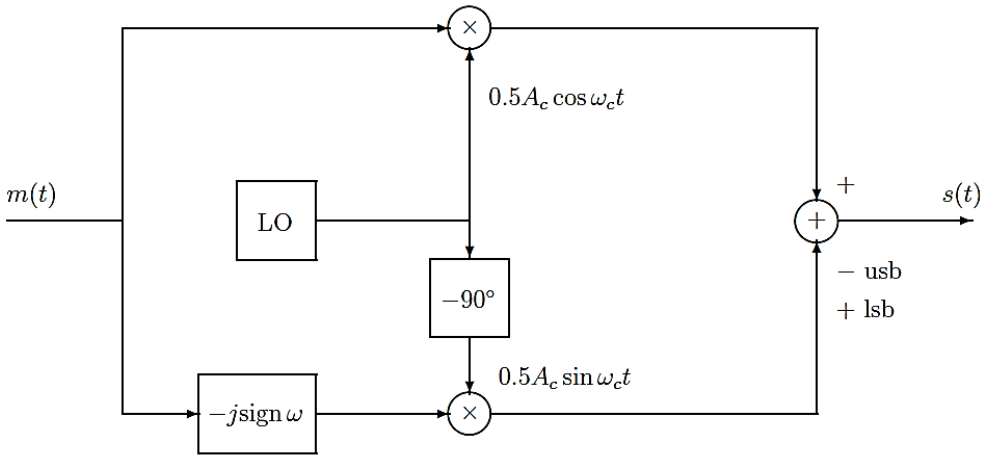

Figure 2.10: Phase Shifting method of SSB modulation [46]

2.5 Balanced Detection in Analogue Photonic Links

In a multi-octave bandwidth APL, high order distortion products are not dominant as compared to a sub-octave APL. Contemplating the modulators operating point, the distortion products produced from the nonlinear behaviour can either be controlled by biasing the modulator correctly or by applying the linearisation techniques to circumvent the distortion issues. In the APL systems, biasing modulator at quadrature has a significant advantage over second-order intermodulation distortion (IMD2) and $SFDR_2$ improvements. It is also true that biasing at high voltages contribute to high system noises, which is why, for some applications, low biasing the modulator is preferable [47]. Though low biasing reduces system noise, it contrarily generates second-order distortion products, which substantially limit the bandwidth of APL system. It is well known that the Laser RIN and Amplified Spontaneous Emission (ASE) noise from EDFA can be removed by using a balanced photodetector [48]. To overcome this limitation, a balanced detection method can be applied. In a balanced detection, two photodiodes are paired

together to form a differential configuration, as shown in Figure 2.11. Each photodiode has a set responsivity denoted as $\Re_1$ and $\Re_2$. Assuming the responsivity of both photodiodes is same, and an oppositely charged bias is applied on photodiodes. Consequently, common-mode signals can be cancelled out. The photocurrent at the output of balanced photodetector (BPD) can also be expressed as [49];

$$I_{BPD} = I_{PD1} - I_{PD2} \tag{2.18}$$

In equation (2.18), I_{PD1} and I_{PD2} are the photocurrents received at first photodiode and second photodiode, respectively. This phenomenon of cancelling the common-mode signal at the output of BPD is known as the common-mode rejection ratio (CMRR) [52].

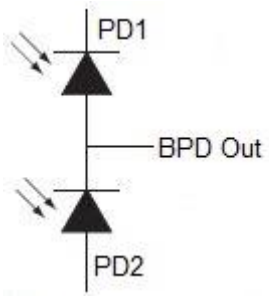

Figure 2.11: Schematic of a Balanced Photodetector [49]

2.6 Nonlinearities in Analogue Photonic Links

In APL, the modulation performance of multiple RF signals possesses some limitations due to the Intermodulation and Cross Modulation generated by the nonlinearities of Electro-optic Modulators [51, 52]. Among these nonlinearities is the nonlinearity of the intensity modulators, which generates multiple harmonic frequencies and distortion products. Second- and Third-order Harmonic Distortions (SHD and THD), and Second- and Third-order Intermodulation Distortions (IMD2 and IMD3) are the main limitations to the Spurious-free Dynamic Range (SFDR).

Intermodulation distortion (IMD) is an important frequency component in the signal analyser measurement, which assesses the linearity of the Microwave devices. [53, 54]. IMD can be defined as an amplitude modulation of two or more frequency signals caused by the nonlinearities in a system. The intermodulation between two or more fundamental frequency components produces an additional component at a frequency that is harmonic, sum and difference of the fundamental frequencies, and multiple of those sum/difference frequencies, which can be seen in Table 2.1. [55], where f_1 and f_2 are two fundamental frequencies.

The table clearly illustrates that the second harmonics occur at the multiple fundamental frequencies such as $2f_1$ and $2f_2$ and likewise, the third harmonics can be found at $3f_1$ and $3f_2$.

Table 2.1: List of 2nd and 3rd order spurs

Second-Order Distortions	**Third-Order Distortions**
$\boldsymbol{2f_1}$	$3f_1$
$\boldsymbol{2f_2}$	$3f_2$
$\boldsymbol{f_1 - f_2}$	$2f_1 + f_2$, $2f_2 + f_1$
$\boldsymbol{f_1 + f_2}$	$2f_1 - f_2$, $2f_2 - f_1$

The second-order products are the spurs, created due to the nonlinear interaction of two signals, which results as the sum and difference of the two fundamental frequencies, as it is shown in Figure 2.12 [53]. However, the most challenging intermodulation distortions are the third-order products that are caused by the interaction of the one fundamental frequency and the second harmonic of the other fundamental frequency.

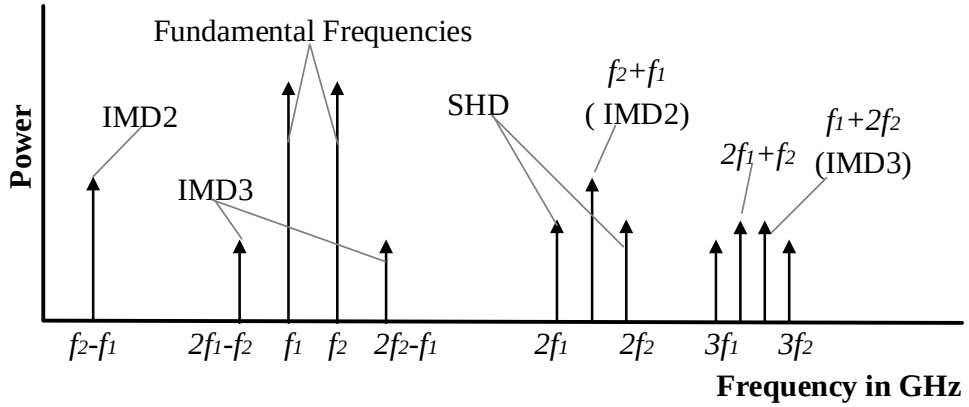

Figure 2.12: Intermodulation Distortion - Second-order and Third-order Products

Another aspect of nonlinearities has been explored here, and the intermodulation distortion along with cross-modulation distortions are illustrated in Figure 2.13. It depicts an output frequency spectrum of a frequency mixer. Usually, in a mixer, the reference frequencies (Two-Tone RF) are either down-converted or up-converted to the Intermediate Frequencies (IFs). In this process, the reference frequencies interfere with each other as well as with the local oscillator (f_{LO}) frequency, and as a result, multiple frequency components are generated. These additional frequency components are named as distortion products (shown in Figure 2.13 as Red Colour). The frequencies in red are generated from self-beating of reference frequencies (Two-Tone RF). Though, in a mixer, these components worsen the mixer performance and limit the bandwidth. In order to linearise a multi-tone RF mixer, the frequency components shown in RED must be removed. Also, the frequencies in BLUE must be suppressed to improve the dynamic range.

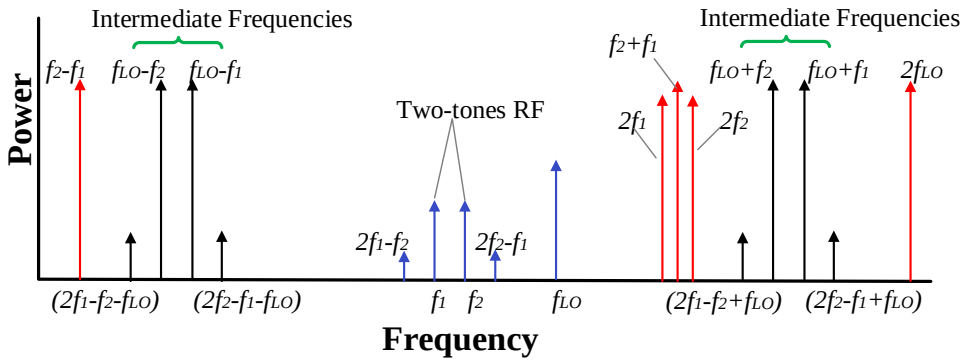

Figure 2.13: Intermodulation and Cross-modulation Distortions in a Frequency Mixer

2.6.1 Spurious-free Dynamic Range

Second-order Intermodulation distortion (IMD2) is of great concern in the wide bandwidth applications, whereas, the third-order intermodulation distortion (IMD3) is mainly considered in the narrow bandwidth applications, as IMD3 signal falls close to the fundamental signal frequencies [54,55]. The intermodulation distortion has a great dependence on the power level of the fundamental input tones, and it can be evaluated by the third-order intercept point (IP3) [54]. IP3 is defined as a power level intercept, at which the power level of third-order distortion products would be equal to the power of fundamental tones, as it is illustrated in Figure 2.14. This means that the first-order and third-order products are equal in power. IP3 can be extracted as shown in the equation below; [54]

$$IP3 = \frac{4}{\pi^2}\frac{V_\pi^2}{R_{MZ}} \tag{2.19}$$

Where, V_π is the half-wave voltage.

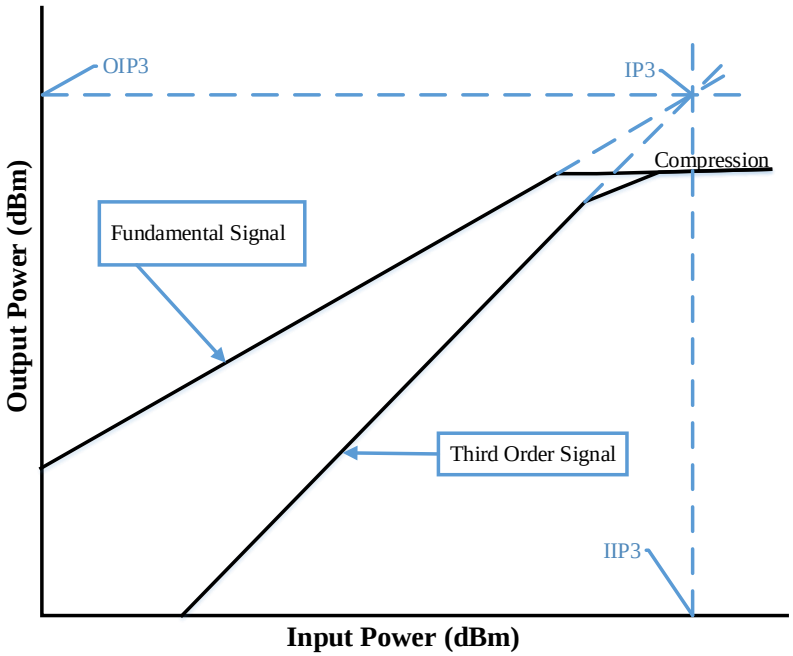

Figure 2.14: Third Order Intercept point power

Spurious-free dynamic range (SFDR) is an essential technique in communication systems, especially for the evaluation of the signal processing ability of microwave photonic links [54, 56]. This is defined as the range between a signal just above the noise floor and the largest undistorted signal introduced in the system, in other words, it is the ratio of the highest signal level a circuit can handle and the smallest signal a circuit can handle (usually equal to noise level), which can also be seen in the Figure 2.15 [57]. The noise floor is the noise level, and below this level, signals cannot be detected under the same measurement. For example, the SFDR can also be described as a power ratio between the output power of the fundamental frequencies and the third-order distortion products ($2f_1$-f_2 and $2f_2$-f_1).

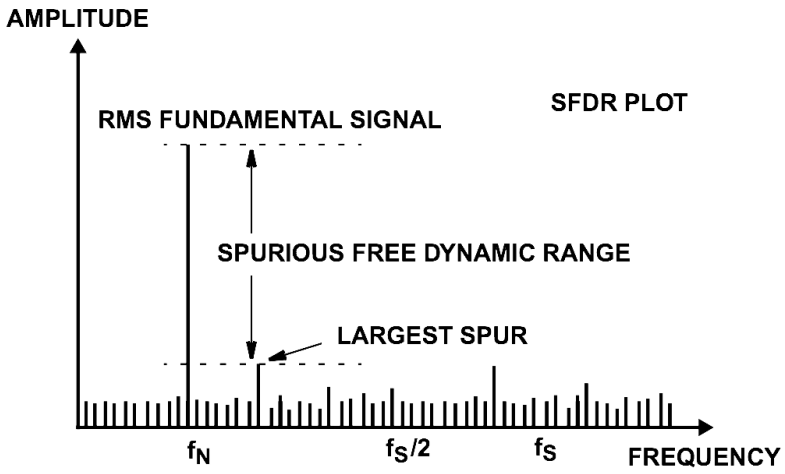

Figure 2.15: Measurement of Spurious free dynamic range [57]

In order to measure the SFDR in a Two-Tone APL, there are few essential factors that need to be considered.

- The output system noise level (OSNL) is a measurement of the output noise power per Hz.
- The input system noise level (ISNL) is the subtraction of system gain from the output noise power.
- Background noise level (BNL) is a usually -174dBm/Hz depending on the thermal noise under a room temperature of 290^o K.
- The noise figure (NF) equals to the input system noise level (ISNL) minus background noise level (BNL).

However, SFDR measurement for the high-end complex, and the third-order intercept point needs to be considered as it is represented in equation (2.22). To calculate the SFDR, noise figure in dB and BNL is subtracted from IP3 at a bandwidth of 1Hz. The conceptual plot of SFDR is shown in Figure 2.16. MDS is basically the minimum signal power that can be detected by a receiver to give an appropriate output.

Below are the representation of a Minimum detectable signal (MDS) and SFDR [54].

$$MDS = NF_{dB} + 10\log(BW) + BNL \tag{2.20}$$

$$SFDR = \frac{2}{3}[IP3 - MDS] \tag{2.21}$$

$$SFDR = \frac{2}{3}[-BNL + IP3_{dBm} - NF_{dB} - 10\log(BW)] \tag{2.22}$$

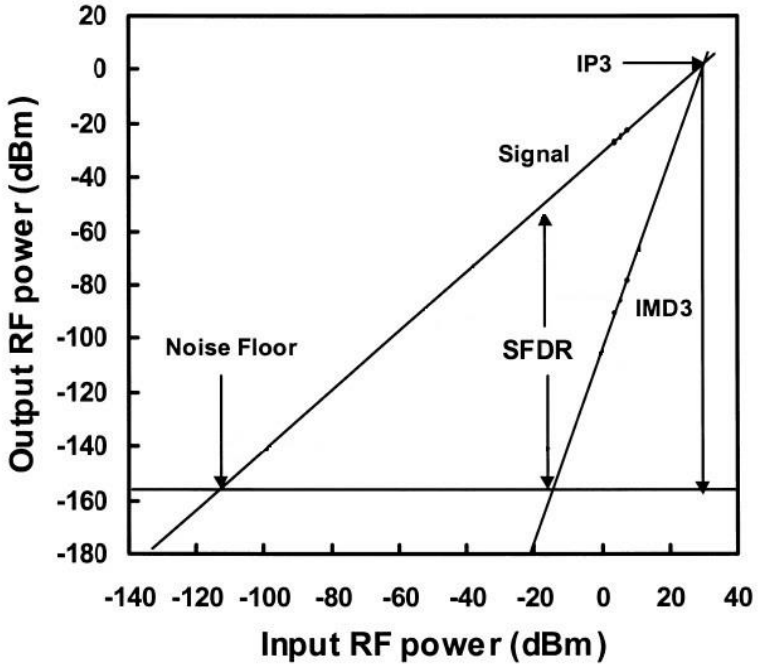

Figure 2.16: Graph of Spurious-free Dynamic Range

2.7 System Link Noise

In the radio over fibre link, many components introduce noise into the system and reduce the receiver sensitivity, and among them are intensity noise, phase noise, polarisation mismatch and fibre dispersion. This section illustrates the types of dominant noise in the APL, the sensitivity of the receiver, and techniques to measure and improve the performance of the link.

2.7.1 Thermal Noise

Thermal noise is a type of noise which arises from a fluctuation of voltage across a circuit such as a resistor. The thermal fluctuation happens due to thermal motion of charge carriers within a conductor [60]. Contemplating an example of a resistor, it

has a noise voltage (v_{th}) with a zero-mean Gaussian density function, and the power spectral density (PSD) at its open terminals can be expressed as below [61];

$$S_{\upsilon_{th}.\upsilon_{th}}(\omega) = \frac{Rh|\omega|}{\pi\left[\exp\left(\frac{h|\omega|}{2\pi kT}\right)-1\right]} \tag{2.23}$$

where, R is the resistance of the resistor, h is the Planck constant (6.63 x 10^{-34} Js), k is the Boltzmann constant (1.38 x 10^{-23} J/K), $\omega=2\pi f$ is the angular frequency, and T is an absolute temperature. Thermal noise is also known as a white noise, because it does not depend on the material of an electrical conductor, and it is constant at microwave frequencies. Equation (2.23) can be further simplified into;

$$S_{\upsilon_{th}.\upsilon_{th}}(\omega) = 2kTR \tag{2.24}$$

By using Wiener-Khinchin theorem, equation (2.24) can be expressed as a thermal noise voltage.

$$\left\langle \upsilon_{th}^2(t) \right\rangle = 4kTRB \tag{2.25}$$

The thermal noise voltage in equation (2.25) explains as twice the noise voltage multiples with an equivalent noise bandwidth B. the factor of two represents the involvement of positive and negative frequencies. Furthermore, the thermal current can be derived as;

$$\left\langle i_{th}^2(t) \right\rangle = \frac{4kTB}{R} \tag{2.26}$$

From equation (2.26), the power provided by thermal noise current to a load resistance R_L can be stated as;

$$p_{th} = \left\langle i_{th}^2(t) \right\rangle R_L \tag{2.27}$$

2.7.2 Shot Noise

Shot noise is a noise that is generated from the fluctuation of current in a photodetector. The fluctuation of photocurrent in a photodetector happens due to the appearance of photons at random times [3]. The power spectral density of the shot noise is flat, and it can be expressed as;

$$S_s(\omega) = qI_p \tag{2.28}$$

Where, $q = 1.6 \times 10^{-19} C$ is the electron charge, $I_p = R_d P_{in}$ is the average current with a resistance R_d and input optical power of P_{in}. Since, $S_s(\omega)$ is the spectral density for sidebands with positive and negative frequencies. Therefore, when considering only one-sided frequencies e.g positive frequencies, and by applying the Wiener-Kinchin Theorem, the shot noise current can be given as below;

$$\left\langle i_s^2(t) \right\rangle = 2qI_p B \tag{2.29}$$

From equation (2.29), the power provided by shot noise current to a load resistance R_L can be stated as;

$$p_{shot} = \left\langle i_s^2(t) \right\rangle R_L \tag{2.30}$$

2.7.3 Relative Intensity Noise

RIN is introduced due to the insertion of spontaneous emission into the coherent field of a laser [3]. This causes the fluctuation in the power of unmodulated optical carrier, which indeed becomes bigger noise at the receiver output. In order to evaluate RIN, firstly the optical power is measured by using the following equation.

$$P_o(t) = P_{av} + \Delta p(t) \tag{2.31}$$

where, $\Delta p(t)$ is the power fluctuation due to spontaneous emission. Due to these fluctuations in laser intensity at the laser output, the output of the photodiode after

conversion from optical to electrical gets affected, and the mean-squared noise current can be expressed as follow;

$$\langle i_{RIN}^2 \rangle = \frac{\langle I_d \rangle^2}{2} 10^{RIN/10} B \tag{2.32}$$

Here, I_d is the dark leakage current, and B is the noise bandwidth. RIN is mainly dominated over other noise in the link, in the directly modulated lasers.

2.7.4 Receiver Sensitivity

Receiver sensitivity is a minimum input signal (S_{min}) that is required to achieve a specific output signal with a particular signal-to-noise ratio (S/N). The minimum input signal is represented as a minimum signal-to-noise ratio times the mean noise power, shown in the equation below.

$$S_{min} = \left(\frac{S}{N}\right)_{min} kT_0 B(NF) \tag{2.33}$$

Where, $(S/N)_{min}$ is minimum signal to noise ratio for processing a signal, k is the Boltzmann constant that is 1.38 x 10^{-23} Joule/K, T_o is the absolute temperature of the receiver input, B is a receiver bandwidth in Hz, and NF is the noise figure/factor measured in dB. In case of a signal impinging on the antenna, the sensitivity is called minimum operational sensitivity (MOS), which is represented as;

$$MOS = \frac{\left(\frac{S}{N}\right)_{min} kT_0 B(NF)}{G} \tag{2.34}$$

Here, G is the gain of the antenna included with the transmission loss. MOS is used for system sensitivity. The sensitivity is usually measured in dBm, and it can be a negative number or a positive number. There are two different ways of defining the sensitivity, such as the ratio of response to input and input to the response. In the case of the ratio of response to input, the more negative the value is, the better is the

sensitivity, however in the case of input to response ratio, the more positive is the number, and the higher is the sensitivity [62].

2.7.5 Noise Figure

Noise figure is the ratio of signal to noise ratio at the input of the link to the signal to noise ratio at the output of the link at a standard temperature of 290K. It can be mathematically represented as below [62];

$$NF = 10\log\frac{S_{in}/n_{in}}{S_{out}/n_{out}} \tag{2.35}$$

It can also be expressed as;

$$NF = 10\log\frac{n_{out}}{g_{rf}n_{in}} \tag{2.36}$$

Here, n_{in} is the input noise which is also represented as thermal noise $n_{thermal\ noise}$, S_{in} and S_{out} are the RF input and output signal powers. The output signal power S_{out} and the output noise power n_{out} can be expressed mathematically as;

$$S_{out} = g_{rf}S_{in}, \tag{2.37}$$

$$n_{out} = g_{rf}\,n_{in} + n_{extra}, \tag{2.38}$$

Where,

$$NF = 10\log(1 + \frac{n_{out}}{g_{rf}n_{in}}), \tag{2.39}$$

2.7.6 Signal-to-Noise Ratio

Signal-to-noise ratio is directly connected with the Bit error rate (BER) of communication systems. It is defined as the ratio of signal power in the receiver to the mean noise power of the receiver. SNR is one of the many ways to measure the noise performance or sensitivity of the receiver. Electrical and optical SNR can be represented mathematically as;

$$SNR_E = \frac{S_E}{N_E} = \frac{v^2}{\sigma_v^2} = \frac{i^2 R}{\sigma_i^2 R} = \frac{i^2}{\sigma_i^2} \tag{2.40}$$

Where, S_E is representing the signal power, and the N_E is the noise power. The optical SNR can be represented as;

$$SNR_o = \frac{S_o}{N_0} = \frac{|\vec{E}|^2 \frac{1}{\eta}}{\sigma_o^2 \frac{1}{\eta}} = \frac{|\vec{E}|^2}{\sigma_o^2} \tag{2.41}$$

In the above equation, S_o and N_o is the optical signal power and the optical noise power respectively. η is the optical fibre impedance, σ_o^2 is the mean square average power and $|\vec{E}|^2$ is the optical current. The SNR is converted from optical to electrical at the receiver, and after conversion, it can be represented as the square root of the electrical SNR. By combining both electrical and optical SNR equations, a conversion can be achieved [63].

$$\sqrt{SNR_E} = \sqrt{\frac{S_E}{N_E}} = \frac{i_{signal}}{\sigma_i} = \frac{S_o R}{N_0 R} = SNR_o \tag{2.42}$$

At the receiver, the optical power is converted into an electrical current, and the ratio of electrical current and the incident optical power is called the responsivity, represented as $\Re$. The units are Ampere per Watt (A/W).

2.8 Linearisation techniques for Analogue Photonic link

A nonlinear transmitter can exhibit some limitation on the system, which can be linearised by optimising the components of the system. Microwave photonic Links have been of great importance because of their various applications like wireless communications, radars, and antenna remoting and warfare systems. MPLs also have many advantages over coaxial analogue links such as ultra-wide bandwidth, low transmission loss, low weight and immunity to the electromagnetic interference [14, 64]. There are two modulation techniques to impose a microwave signal on an optical carrier such as direct modulation and the external modulation. Direct

modulation uses the distributed feedback (DFB) laser diode, whereas, external modulation uses phase modulator, intensity modulators or polarisation modulators, which have been used previously for enhancing the SFDR and reducing the IMD [65, 66].

Previously, various techniques have been reported to improve the SFDR, which is directly linked with the intermodulation distortions produced by an external modulator. The linearisation techniques based on different modulators types, including pre- and post-compensations have been reviewed.

2.8.1 Schemes based on a Dual Electrode Mach Zehnder modulator

In [67], an optical single sideband (OSSB) modulation technique has been reported to compensate the distortions in the APL system. Similarly, in [68], OSSB has been built at the transmitter end. The configuration is achieved by using a dual-Electrode Mach-Zehnder modulator (DEMZM) that was driven from its upper and lower electrode, and the output at the receiver end is linearised by utilising two parallel Mach-Zehnder interferometers (MZI) and a Balanced Photodetector (BPD). The third-order intermodulation (IMD3) is suppressed by varying the differential delays of two MZI, and the fifth-order limited link response is achieved. This technique compensates the distortion in the system at the receiver side, which is known as the post-compensation scheme. This technique makes the architecture of the transmitter simple but makes the receiver complicated because two MZI and a fibre delay line are used to achieve the right phase shift for the cancellation of IMD3. This scheme does not suppress the even-order distortions, which can be a limiting factor on the system bandwidth. The architecture of the scheme is shown in Figure 2.17.

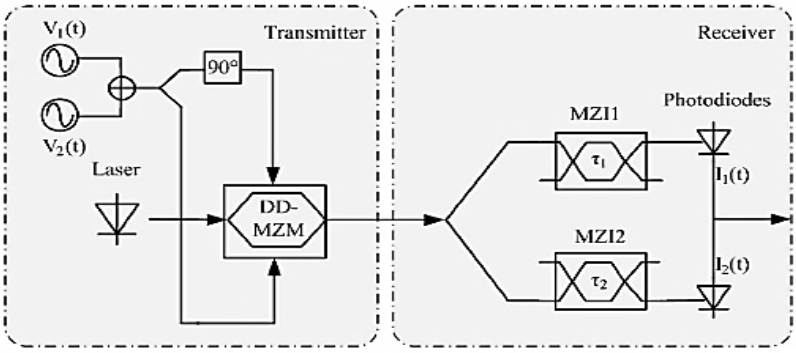

Figure 2.17: Linearised MPL proposed scheme based on two MZIs [67]

In [69], a technique based on a double sideband-suppressed carrier (DSBSC) and coherent, balanced detection, by using a dual-drive DEMZM is presented. The configuration uses two optical paths; one for a modulated optical signal and the other for an unmodulated optical carrier. A polarisation combiner combines both paths and then transmits through an optical wireless communication link towards the receiver. It is to be noted that both modulated and unmodulated signal is kept orthogonally polarised from each other. At the receiver, a balanced photodetector (BPD) is used that suppresses the IMD3 and the amplified spontaneous emission (ASE) noise. It reports suppression of IMD3 by up to approximately 46dB and a signal-to-noise ratio of 34.4dB. However, the system does not incorporate the even-order distortions, which can be a limiting factor of this system. An analogue photonic link uses addition polarisation devices (polarisation combiner, polarisation splitter and linear polarisers) that needs a precise alignment of the polarisation. It is complicated to align the polarisation states of the double sideband-suppress carrier signal (DSB-SC) and the unmodulated optical carrier (OC), especially when they are transmitting through an optical wireless link over a long distance. The architecture of the scheme is displayed in Figure 2.18.

In [70], an OSSB modulation link based on a DEMZM is reported, which reduced the effect of chromatic dispersion in the fibre and improved the system's dynamic range [71]. Like [69], a light beam is split into two optical paths; one gets modulated

by DEMZM and the other gets phase shifted by an optical phase shifter. Both beams are re-joined before detection to eliminate the IMD3, IMD2, and second-order harmonic (SHD). The reported Signal to interference ratio (S/I) is limited up to 55dB, and an SFDR for IMD3 is approximately 130dB at a bandwidth of 1Hz. Although the elimination of IMD2 was shown theoretically, the simulation or experimental performance analysis on IMD2 was missing in the article, which raises concern about it being sensitive to optical phase shift or modulation index.

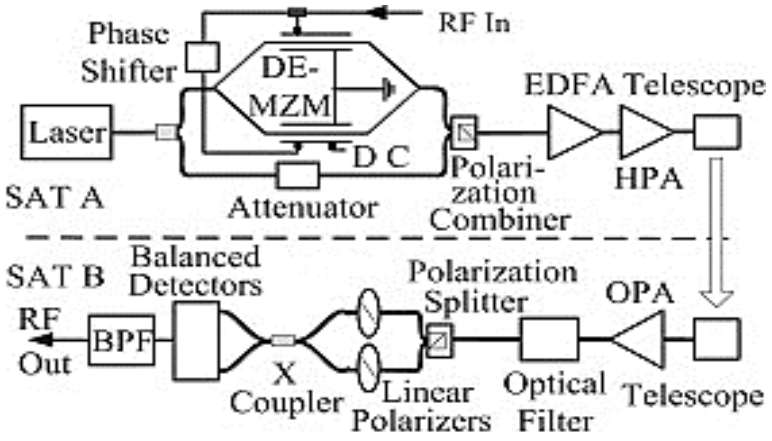

Figure 2.18: Linearised APL Architecture by using DD-MZM [69]

In [72], a single MZM is used to modulate an RF signal over a polarised optical beam. The MZM has two optical outputs, which are controlled individually by polarisers and then both beams are combined by a polarisation beam combiner, which effectively alter the angle of third-order intermodulation distortion, and upon detection, both polarisation states of IMD3 gets cancelled. Consequently, IMD3 is significantly suppressed. It is noticed that the suppression of IMD3 relies on very stable polarisation control, which is hard to achieve on a manual polarisation controller. The schematic of the linearisation technique is shown in Figure 2.19.

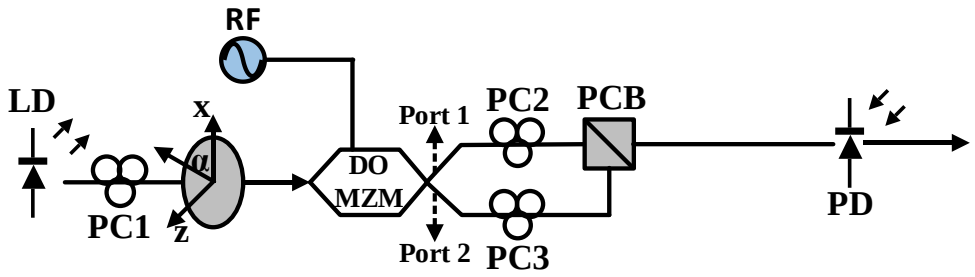

Figure 2.19: Linearised APL using Dual output MZM: LD, laser diode; PC, polarisation controller; PBC, Polarisation Beam combiner; PD, Photodiode [72]

In [73, 74], a sub-octave linearisation technique for the compensation of nonlinearities in the APL is reported. The configuration is based on a single DEMZM with an optical pulse shaper that acts as a compensation tool. Optical pulse shaper selectively modifies the phase and amplitude of the sidebands to effectively eliminates the IMD3 components. This compensation is named as a post-compensation technique, which optically processes the modulated signal for IMD suppression. The system reports a signal-to-interference ratio (S/I) of around 75dB, and SFDR of 124.8dB at 1Hz bandwidth. The technique being highly efficient also poses some limitations such as complexity due to the requirement for an optical pulse shaping technique, and the system is restricted to only sub-octave bandwidth.

Similarly, in [75], optical carrier band processing technique is analysed. It illustrates the suppression of the IMD3 by adjusting the phase of an optical carrier. The achieved fundamental to IMD ratio was 64.3dB, however this scheme is only limited to the sub-octave bandwidth systems.

2.8.2 Schemes based on Dual Parallel Mach Zehnder Modulator

A Dual-parallel Mach Zehnder (DPMZM) modulator has been built on a similar principle to an MZM. DPMZM comprises two parallel aligned MZMs integrated on a single chip [76]. This new configuration provides better control over the modulated frequency components compared to the MZM modulation. There have been various

linearisation techniques reported in the past, which are based on DPMZM. In [77], a Symmetrical Single Sideband (SSB) is realised by using multiple RF phase shifters and Dual-drive dual-parallel MZMs. The results show that the IMD3 is suppressed by approximately 30dB and the SFDR is improved by 12dB. However, in such systems, it is critical to realise the RF phase balance accurately, and any such imbalances would deteriorate the IMD3 cancellation. It is well known that the electrical phase shifters possess a huge phase imbalance at high frequencies. Hence, the system's best performance is limited to low frequencies. Similarly, in [78], a pre-compensation linearisation technique has been used, which deploys multiple RF phase shifters and a dual-drive DPMZM. The modulator is configured to achieve a switching voltage of π and $\pi/2$ at upper MZM and lower MZM, respectively. Third-order intermodulation distortion can be eliminated by using RF phase shifters and by controlling the bias voltages. An optical carrier suppression can be achieved on one of the sub-modulators without using any digital linearisation, optical processors and symmetrical single-sideband modulations. Quadrature modulation is achieved on the other sub-modulator by keeping the electrical signal on both electrodes the same. This technique measures the noise power density of -170 dBm/Hz, including both shot noise and thermal noise. An increase in SFDR of 11.2dB as compared to that of conventional techniques (single Intensity Modulation technique), which is $105.6\text{dB.Hz}^{2/3}$. Also, the IMD3 suppression is increased by 45dB. The block diagram of this model is shown in Figure 2.20.

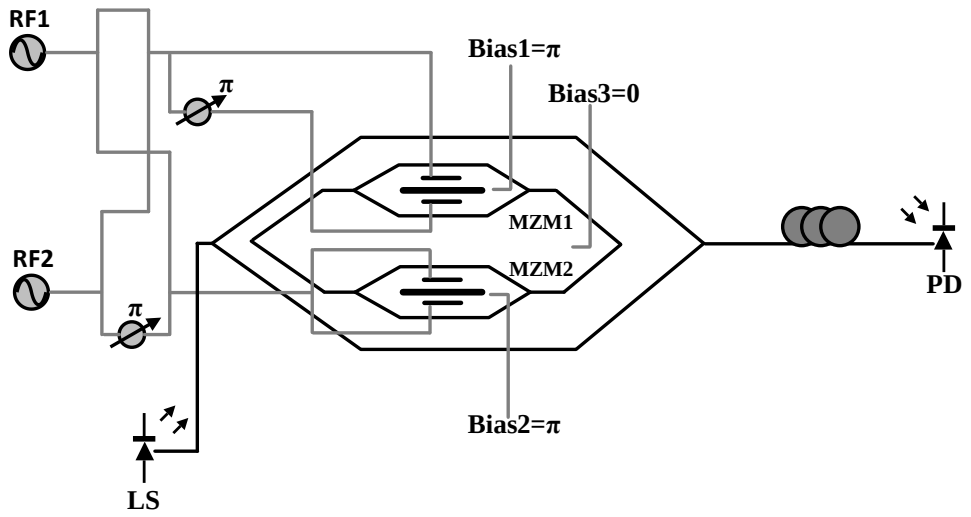

Figure 2.20: Architecture of a two-tone transmitter based on DP-MZM [78]

In [79], a theoretically proved scheme based on a dual-parallel Mach-Zehnder modulator and coherent detection is proposed. An arithmetical analysis of the design proves that the IMD3 can be suppressed and the SFDR for fifth-order of 144dB.$Hz^{4/5}$ can be predicted by simultaneously optimising the input optical power split ratio, output optical power split ratio and electrical signal power ratio. It limits the shot-noise, which makes it reliable. However, it is very complicated to realise accurate splitting ratios, as it needs a specific optical power splitting ratio combined with electrical splitting ratio. In [80], a linearised DP-MZM based on the electro-optic polymer is fabricated and used to suppress the third-order intermodulation distortion. This new DP-MZM is used with two parallel MZMs of unbalanced input and output couplers and a phase shifter on the output of one MZM. The optical power and a modulation depth of each MZMs are configured differently from each other, so that at the output when both have the same amplitude but one with an 180^{o} shift, are combined, a reduction of IMD3 below the noise floor is observed. The two-tones after modulation also incorporate a reduction in power of 10dB, also with the suppression of IMD3, IMD5 becomes a limiting product. The specific power splitting ratio combined with the electrical splitting ratio is difficult to achieve a

certain splitting ratio. This configuration is based on [79], and the structure is shown in Figure 2.21.

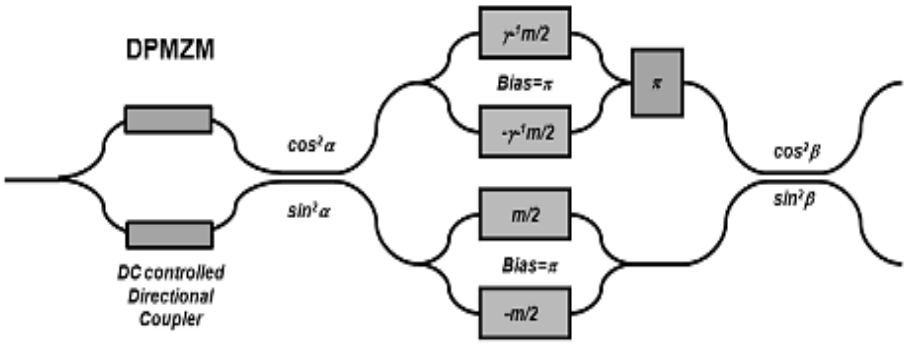

Figure 2.21: Linearised DPMZM with electro-optic polymer material [80]

In [81], a linearised radio over fibre system is proposed. This linearisation technique is based on a single-drive dual parallel Mach-Zehnder modulator, where RF signals are driven on only one sub-MZM of a DPMZM. On the other sub-MZM, no driving signal is applied, and the optical carrier is traversed unmodulated. The third-order intermodulation (IMD3) produced from the sub- modulators are opposite in phase and same in intensity that results in the cancellation of each other output and a highly suppressed IMD3 was achieved. An SFDR of 122.9dB.$Hz^{2/3}$ is achieved, which is 20dB more than a conventional MZM. However, the drawback of this schemes is that it is limited to low modulation depth, as for high RF modulation depth, the higher-order optical sidebands increase, which would also introduce IMD3. Also, not the all-optical sidebands are considered here, so the third-order intermodulation is limited. The design of this modulation scheme in the transmitter of the system can be seen in Figure 2.22.

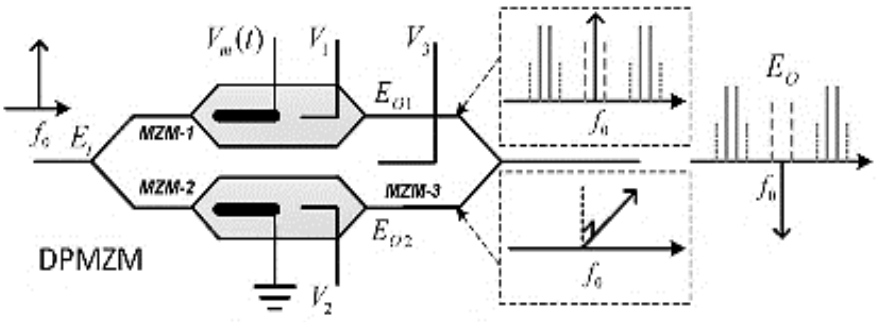

Figure 2.22: Design of linearised transmitter with single drive dual parallel MZM [81]

Unlike the former mentioned linearisation techniques, [82] is a multi-octave bandwidth APL system, which employs a pre-distortion compensation method. The configuration of the technique is based on a polarisation-multiplexing dual parallel Mach Zehnder modulator (PM-DPMZM) and a single photodetector. The operating conditions of the sub-MZM are altered to achieve a required modulation. Additionally, a polarisation rotator is integrated into an output arm of sub-DPMZM, which sets the modulated signal to the orthogonal state compared with the output signal of upper sub-DPMZM. Both optical outputs are combined and detected by a photodetector. Consequently, the second-order and third-order distortion products are suppressed effectively. The reported SFDR performance improves by 12dB, and the fundamental to interference ratio of up to 55dB was achieved. Similarly, in [83], an improvement in SFDR of ~18dB is shown. Considering it a simple technique, yet incur huge losses due to multiple DPMZM configuration, and maintaining the modulator bias condition and polarisation condition are difficult to realise. Hence, the linearisation technique is not very reliable for a harsh environment, such as military and defence applications. The schematic diagram of the model is illustrated in Figure 2.23.

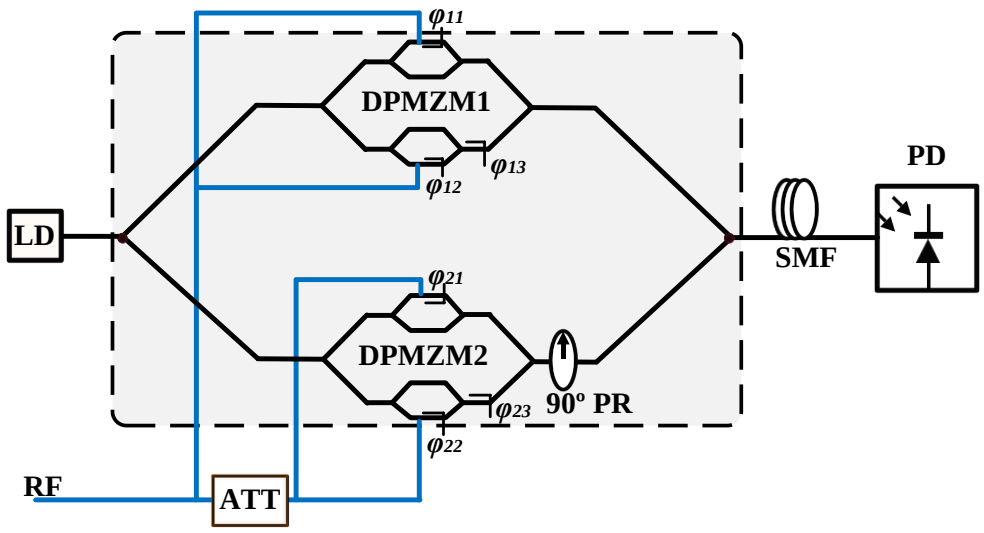

Figure 2.23: Schematic diagram of a linearisation technique based on PM-DPMZM [82]

In [84], a multi-octave linearized APL is based on a polarisation division multiplexing dual parallel Mach Zehnder modulator (PDM-DPMZM) and a balanced photodetector (BPD). The laser light is split into X- and Y-polarisation states inside a PDM-DPMZM, where upper sub-DPMZM modulates X-polarity and lower sub-DPMZM modulates Y-polarity. RF signals are modulated on both sub-DPMZMs and then at the output of PDM-DPMZM, a polarisation beam splitter is used to split apart the X- and Y-polarities. These orthogonal light beams are then detected by a BPD to cancel the second-order distortion products (SHD, IMD2). Subsequently, IMD3 is also significantly suppressed. Due to the balanced photodetector, the noise floor is lowered to -170dBm/Hz and the third-order SFDR is effectively improved to 123.9dB at 1Hz bandwidth. It is reported that system performance is frequency limited and at higher microwave signal the dynamic range starts to deteriorate. The block diagram is shown in Figure 2.24.

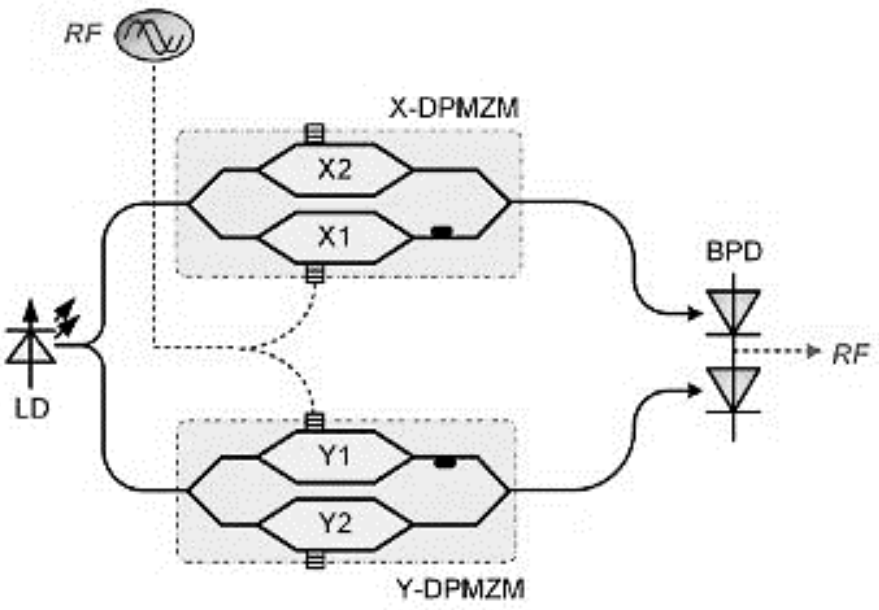

Figure 2.24: Linearisation technique based on a PDM-DPMZM and a balanced photodetector [84]

2.9 Linearisation techniques for Microwave Photonic Mixers

One of the key features of an analogue photonic link is frequency mixing for up-conversion or down-conversion. Since most of the RF antennas operate on microwave or millimetre wave frequencies, so these transmitted or received signals are processed digitally, and it needs an analogue-to-digital converter (ADC) [85-87]. Therefore, microwave photonic mixers are designed to down-convert or up-convert the signals. Mixers are generally restricted in terms of bandwidth such as for down-conversion normally the bandwidth is up to 2GHz. So, it is crucial to realise a linearised mixer for such a narrow bandwidth. Mixers have great use in the analogue photonic systems like mobile communication systems, phased array antennas and electronic warfare (EW) receivers [88-91]. Conventionally used electronic mixers are based on diodes or active transistors, and they require high power for a high SFDR. Electronic mixers are naturally lossy, and they have a poor RF-port to LO-port isolation, which effectively causes much interference in the baseband or

reference signal bandwidth. Microwave photonic mixers overcome the issues posed by a conventional electronic mixer. Previously the photonic mixing techniques were based on cascade modulation link [85, 92, 93], phase modulation link [94], and dual parallel modulation link. It has been observed that most of the techniques used for the suppression of XMD and IMD are based on a cascade link. The cascade links has been vigorously explored as compared to other links due its few advantages like infinite RF to LO port isolation and capability of remotely located LO link. However, the DPMZM links produces high conversion efficiency and low system noises. So far, the compensation techniques have only been developed to eliminate the third-order intermodulation distortions (produced from a beating between LO and an RF signal). However, to the best of our knowledge, not much literature has been published on the elimination of second-order intermodulation distortions (beating between two or more input RF signals, also known as Cross modulation distortion (XMD)) in a photonic mixer.

2.9.1 Scheme based on Cascade modulation link

The cascade modulation schemes for a photonic mixer was first proposed by using two Mach Zehnder Interferometric modulators in series [93, 95]. RF signal was modulated in one interferometric modulator, and the LO signal was modulated in another, which makes the RF to LO port isolation infinite. Further, the intermodulation distortions were removed by biasing the modulators at a quadrature operating point, but consequently, the IF becomes equal to the LO. Nevertheless, the dynamic range is entirely dependent on the modulator's bias condition, which is generally very unstable in Lithium niobite modulators. Therefore, the ratio of output Intermediate Frequency (IF) power to the input RF power is affected, which is also known as conversion efficiency. The schematic of the cascade structure is shown in Figure 2.25.

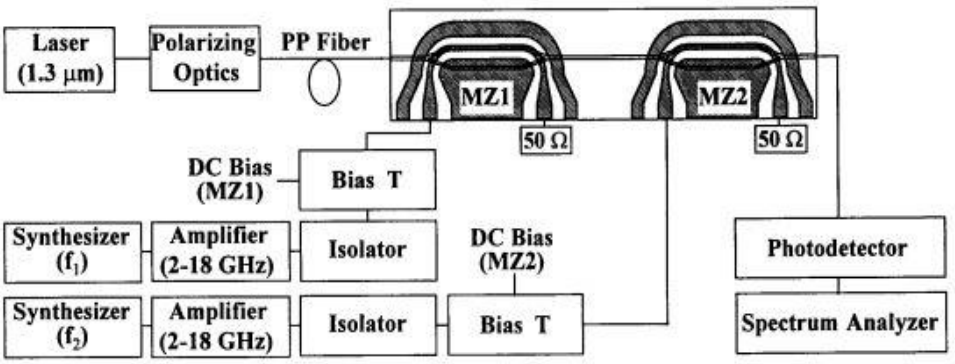

Figure 2.25: Microwave Photonic mixer based on a cascade modulation link [93]

Many techniques have been applied for the improvement of the conversion efficiency in the mixer based on a cascade electro-optic modulation. In [85, 96], an overdriven modulator is used in a series with another modulator to achieve a frequency mixing of conversion losses less than 5dB. Although it improves the conversion efficiency, it also increases the system nonlinearities. A mixer limited to system nonlinearities suffer from limited dynamic range and poor bandwidth efficiency. The modulator bias points were set to quadrature [85] and minimum [96]. Similarly, in [97], a cascade structure is used, but instead of operating the LO modulator at quadrature, it was biased at a maximum operating point. As a result, the LO frequency was eliminated, and twice the LO frequency (2LO) appears at the output, which is equal to the amplitude of IF. It is observed that all the techniques mentioned above for cascade photonic mixer are mainly focused on improving the conversion efficiency while ignoring the nonlinear distortions and the noise contributions. Therefore, a low biasing optical modulator technique is developed to circumvent the intermodulation distortion issue [98].

2.9.2 Scheme based on Dual Parallel modulation link

Microwave Photonic Mixers (MPM) has been developed based on various modulation techniques. Out of all, a mixer with dual parallel Mach Zehnder Modulator has been considered the most reliable and with better conversion

efficiency [99]. An additional feature of cascade mixers is that the modulators in series can easily be located remotely, whereas with parallel configured modulators it is difficult to locate each MZM remotely. In [100], two electro-optic modulators are placed in parallel, and the output from each modulator traversed to each diode of BPD. Note that the LO and RF signals are modulated at both modulators, and both modulators are set to bias at a minimum operating point. Consequently, the IMD3 terms are cancelled out at the output of BPD. The limitation of this scheme involves a precise RF and LO splitting ratio, which is difficult to achieve. Likewise, in [101], a dual parallel MZM structure with an additional integrated optical phase shifter is presented as shown in Figure 2.26. The optical phase shifter is configured to achieve a 180º, which subsequently, eliminates the optical carrier on combining the output of each MZM. Suppressing the optical carrier improves the conversion efficiency and the IF-to-RF suppression ratio and IF-to-LO suppression ratio can be maximised. The limitation to this model is that the dynamic range of IF is restricted by the intermodulation distortions, and in case of multiple input RF signals, the performance becomes worse due to IMDs and the Cross-modulation Distortions (XMD).

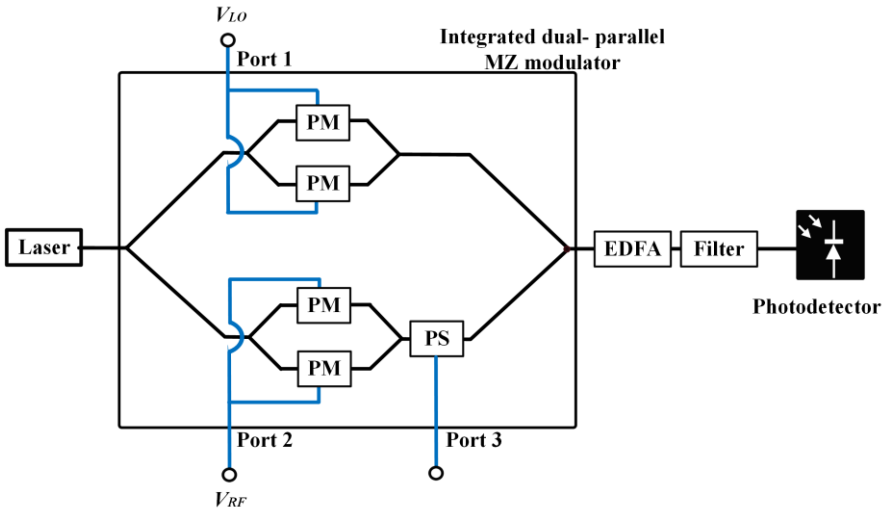

Figure 2.26: Schematic diagram of a photonic mixer based on DPMZM [101]

2.9.3 Scheme based on a single dual-drive MZM

The recent study includes the use of dual-drive Mach Zehnder modulators (DDMZM) for the down-conversion or up-conversion purpose. DDMZM uses two-phase modulators in parallel, where LO and RF signals can be independently modulated on each arm of DDMZM [102-104]. The advantage of this design over other designs is a compact size and low cost [95]. In [102], an Opto-electro oscillator is created from an inserted RF signal, and both RF signal and oscillator signal mix together to down-convert the RF to IF at the output. This configuration drives the modulator at a minimum operating point to suppress the optical carrier and enhance the conversion efficiency. Regardless, the suppression of an optical carrier in a single DDMZM is not great and limited due to extinction ratio mismatch of the upper and lower arm of the DDMZM. Another technique has been reported to suppress the optical carrier in a single DDMZM photonic mixer, which is by adopting an optical circulator and FBG in the system [103]. Mixing of multiple LO signals with the multiple Microwave signals for down-conversion has also been carried out on a single DDMZM, but it requires an additional bandpass filter (BPF) to pass only frequency band of 12 GHz to 25 GHz [104]. All the single DDMZM based techniques have one common drawback, which is the both LO and RF modulations happen at a single place, and both cannot be separated or remotely located. Additionally, these techniques report a high conversion loss compared to techniques based on a DPMZM.

2.9.4 Schemes for the suppression of cross-modulation and intermodulation distortions in a photonic mixer

In a photonic mixer, multiple RF tones are usually down-converted or up-converted simultaneously, which consequently, produces a lot of intermodulation distortion (IMD) and cross-modulation distortion (XMD). It is crucial for the mixer to minimise the distortions as much as possible so that the performance of an

Intermediate Frequency (IF) would not be affected while digitally processing it. Previous literature lacks in reporting linearisation techniques for the simultaneous suppression of XMD and IMD. Some techniques have been reported, but they rely on a post-compensation method, which means the nonlinear IF signal is linearized by using a digital linearisation algorithm [105-108]. It should be stated that utilising a digital method of linearising a mixer has many implications such as restricted bandwidth, and high losses. In [105], a cascade mixing technique is presented, where multiple RF signals are modulated at first Mach Zehnder modulator and the LO signal is modulated at the second Mach Zehnder modulator. After the detection of a down-converted signal, the IF signal is processed through an ADC and then a Digital Signal Processing (DSP) module. In the DSP module, an algorithm is first designed to eliminate the XMD and then the processed signal is compensated for IMD3. It is noted that the use of a DSP module in a photonic mixer makes the system complicated and limit the performance in a high-fidelity RF link. The block diagram of the DSP module can be seen in Figure 2.27. Another cascade mixer [109], reports two-tone down-conversion based on optical waveshaper and BPD. This model also relies on a DSP module for IMD3 removal, but it does not eliminate the beat frequencies from Two-tone RF signal.

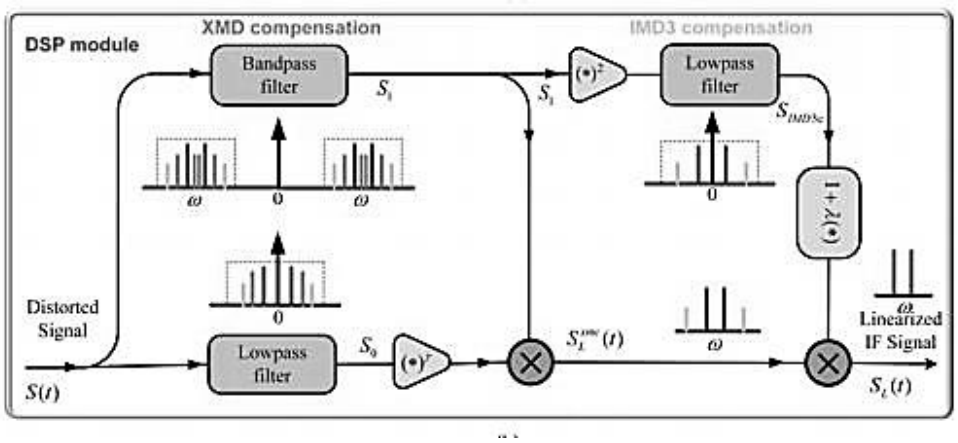

Figure 2.27: DSP module for the linearisation of a multi-tone Mixer [105]

Similarly, in [110], modulators in series are connected to multiply the modulated RF signals with the modulated LO signal. The resultant optical signal is transmitted through a circulator, which direct light-to-Fibre Bragg grating (FBG), and a reflected optical signal from FBG is directed to the lower input of a balanced photodetector (BPD). The reflected signal and the transmitted signal from FBG get detected by BPD. Hence the intermodulation distortions are removed, and the gain in IF power of around 13dB is reported. However, the scheme does not report elimination of XMD, which is critical for the linearisation of a multi-tone down-conversion. The schematic of the linearised mixer can be seen in Figure 2.28.

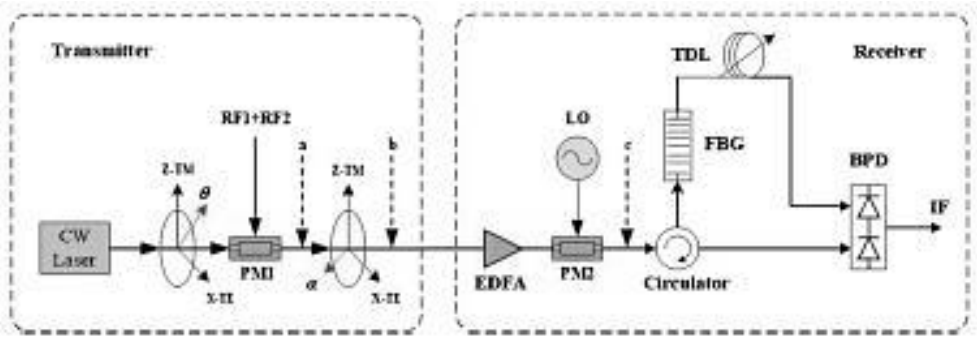

Figure 2.28: linearised cascade mixer based on FBG [110]

2.10 Summary

This chapter has presented a detailed overview of the research including the background of the radio over fibre (RoF) system, and the existing techniques for the linearisation of analogue photonic links. The cause of degradation in RoF system performance has been discussed, which includes the optical fibre dispersion, electro-optic modulator distortion. As discussed in the previous chapter, the focus of this research is to investigate the distortion products generated in the EO modulator. Hence, the existing linearisation techniques have been analysed and comprehensively discussed. It has been observed that most recent techniques involve

dual-parallel Mach Zehnder modulator and quad-parallel Mach Zehnder modulator, which gives a better control over the electro-optic modulation process and help reduce some of the distortion products. It has also been noticed that various linearisation techniques incorporate the balanced photodetector at the receiver end for the reduction of noise and even-order distortion products. Furthermore, the linearisation techniques for the microwave frequency mixer has also been explored. Understanding the importance of microwave frequency mixers in the RoF system, the linearisation techniques have also been discussed. A significant amount of work has been performed on microwave frequency mixers. Currently, electrical mixers have been used in the telecommunication sector. But electrical mixers have many limitations such as poor RF port to LO port isolation, limited bandwidth and IF-to-RF ratio. Conversely, Microwave photonic mixers (MPM) have a great potential to overcome these issues. The MPM techniques discussed in this chapter includes Cascade modulation link, dual-parallel modulation link, and single dual-drive Mach Zehnder modulator link. It has been shown that the techniques based on DPMZM have better conversion efficiency and dynamic range compared to the other reported techniques. Moreover, these techniques have also been explored for simultaneous multiple frequencies conversion, which results in large amount of distortion products with an IF signal.

Chapter 3

3. Proposed Analogue Microwave Photonic Link with Eliminated Even-Order Distortions

3.1 Introduction

This chapter presents a proposed linearisation technique for the optimisation of Signal to Interference Ratio (S/I) and spurious-free dynamic range (SFDR). The technique is mainly applicable in optical links like Receive Optical Links (ROL), which is why the configuration is implemented to demonstrate the performance for a single RF channel as well as dual-RF channels. Section 3.2 discusses the linearisation technique for single RF channel, whereas section 3.3, integrate the same linearisation technique for the Dual RF channel in an analogue microwave photonic link (AMPL). Analogue Microwave Photonic links (AMPLs) deploying external modulators offer great advantages for transmission of microwave signals due to their inherent high bandwidth, high dynamic range, reliability, and immunity to electromagnetic interference [111-113]. AMPLs have great importance in the telecommunication and defence sectors, where they are used for specific applications such as antenna remoting, radar detection, satellite communications, signal generation, and electronic warfare systems [19-21]. In such AMPLs, it is essential to channelise the Radio Frequencies (RF) in order to enable the high-resolution monitoring process [51]. Modulation performance of multiple RF signals over an optical carrier experience some limitations due to the Intermodulation and Cross Modulation generated by the nonlinearities occurring in optical devices such as Mach-Zehnder Modulator. Among these nonlinearities is the nonlinearity of the intensity modulators, which generates multiple harmonic frequencies and distortion

products. Second- and Third-order Harmonic Distortions (SHD and THD), and Second- and Third-order Intermodulation Distortions (IMD2 and IMD3) are the main limitations of the Spurious-free Dynamic Range (SFDR). The SFDR performance for second-order intermodulation distortion (SFDR2) and third-order intermodulation distortion (SFDR3) are presented in this chapter. To the best of our knowledge, few efforts have been carried out on the multi-octave APL systems as compared to the sub-octave systems. It should also be stated that dual RF channel APL links have not been previously fully explored for performance analysis. We believe that the dual RF channel would have major valuable applications, such as antenna remoting [114]. Antenna Remoting is highly desirable in the military applications, such as, one antenna is located at an avionic bay in the aircraft and other antenna is located at the wing of the aircraft. The modulation can happen at the antennas for better performance, instead of linking the antennas with the modulation unit through a cable.

3.2 Single RF Channel in AMPL

The proposed system configuration is based on two independent GaAs DPMZMs. GaAs modulators have many benefits over $LiNbO_3$ modulators, such as they are thermally stable and operate over a broad range of temperatures without causing any bias-point drift [115, 116]. These intrinsic properties of GaAs modulators make them highly suitable for the harsh operating environment in terms of thermal stability, power-handling, radiation resistance, and longevity for aerospace, defence, and satellite-to-ground downlink communication systems. Two microwave phase shifters are deployed to induce a phase difference of 180° between the electrical input of the two DPMZMs. By inducing RF phase difference and controlling DC bias of DPMZMs, the optical carrier is highly suppressed. The suppression of the optical carrier is a key to improve the system performance and to reduce the effect of the fibre nonlinearities [117]. It is also worth stating that the optical carrier plays a vital

role in the detection of fundamental RF signals. Therefore, an unmodulated optical carrier is transmitted through a polarisation maintained optical fibre, and then it is combined with the modulated signal by using a 50/50 coupler. The optical output fields from the coupler are detected by a BPD, which resulted in the elimination of even-order distortions due to the differential configuration of the BPD. The performance of our proposed system is compared with the previously reported work [82, 84], which is based on a Polarisation-multiplexing dual-parallel Mach-Zehnder modulator (PM-DPMZM). We have developed and demonstrated an APL experimentally with significant system performance, namely 115dB.Hz$^{1/2}$ and 127dB.Hz$^{2/3}$, compared to the APL system reported in [84], 95.5dB.Hz$^{1/2}$ and 123.9dB.Hz$^{2/3}$, respectively.

3.2.1 Mathematical model of distortion elimination

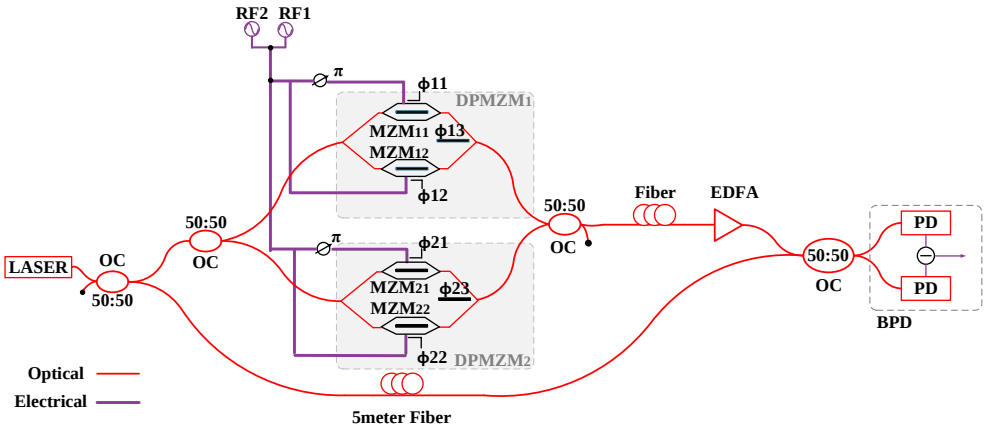

Figure 3.1: Schematic diagram of the proposed linearisation scheme with two input frequencies. OC: Optical Coupler; EDFA: Erbium-doped fibre amplifier; PD: Photodiode; BPD: Balanced Photodetector.

The schematic diagram of the proposed linearised multi-octave system is illustrated in Figure 3.1. The modulation section of the system comprises of two Dual-Parallel Mach Zehnder Modulators (DPMZM), which is named as Double Dual-Parallel Mach Zehnder Modulator (D-DPMZM). The transmitted light from the laser is equally (50:50) split into; 50% is fed to the inputs of D-DPMZM, and the other 50%

is transmitted to the receiver-end over an optical fibre, which is then coupled with a reference modulated signal before being detected by the BPD. E_c denotes the light beam, with its angular frequency of ω_c. Two input RF signals are combined and then equally split. Each DPMZM has two sub-MZMs that are fed with two-tone signals, and the input to both the sub-MZMs has a phase difference of 180°, as it is shown in Figure 3.1. A 180° phase shifter is used because both RF ports of the DPMZM are injected with the same signals, it would be logical to have those 180° out of phase so that the fundamental sidebands do not cancel out at the parent MZM (MZM_{13}, MZM_{23}) due to the destructive interference. RF1 and RF2 represent the two-tone RF signals, and their angular frequency is denoted as ω1 and ω2, respectively. The RF phase shift and the modulator's operating points contribute to suppressing the optical carrier. An external DC bias (V_{bias}) is used to control the operating points of each sub-MZM (MZM_{ij}; i =1, 2; j = 1, 2, 3) in order to achieve maximum suppression of an optical carrier and even-order distortions. The transfer function at the output of DPMZM1 and DPMZM2 can be expressed as [82];

$$E_{DPMZM_1}(t) = E_c e^{j\omega_c t}\left[\cos\left(\frac{\phi_{11}(t)}{2}\right) + e^{j\phi_{13}}\cos\left(\frac{\phi_{12}(t)}{2}\right)\right]. \tag{3.1}$$

$$E_{DPMZM_2}(t) = E_c e^{j\omega_c t}\left[\cos\left(\frac{\phi_{21}(t)}{2}\right) + e^{j\phi_{23}}\cos\left(\frac{\phi_{22}(t)}{2}\right)\right]. \tag{3.2}$$

The transfer function of a phase change $\phi_{ij}(t)$ in each MZM_{ij} can be further simplified by evaluating equation (3.1) and (3.2), which is caused by a modulating voltage of RF signal and a DC bias, can be represented as;

$$\left.\begin{aligned}
\phi_{11}(t) &= \phi_{m1}(t) + \phi_{11} \\
\phi_{12}(t) &= \phi'_{m1}(t) + \phi_{12} \\
\phi_{21}(t) &= \phi_{m2}(t) + \phi_{21} \\
\phi_{22}(t) &= \phi'_{m2}(t) + \phi_{22}
\end{aligned}\right\} \tag{3.3}$$

In equation (3.3), the phase difference caused by DC bias and the input RF signals

are described by $\phi_{ij} = \pi V_{biasij} / V_{\pi i}$, and $\phi_{mi}(t)$ (i = 1, 2; j = 1, 2, 3), respectively. Similarly, $\phi'_{mi}(t)$ it represents the input RF signals with a 180° of phase shift, which is induced by an external RF phase shifter. The transfer function of these phase change caused by modulating voltages can be expressed as below;

$$\left.\begin{aligned}
\phi_{m1}(t) &= m\left[\cos\left(\omega_{m1}t\right)+\cos\left(\omega_{m2}t\right)\right] \\
\phi'_{m1}(t) &= m\left[\cos\left(\omega_{m1}t+\pi\right)+\cos\left(\omega_{m2}t+\pi\right)\right] \\
\phi_{m2}(t) &= m\left[\cos\left(\omega_{m1}t\right)+\cos\left(\omega_{m2}t\right)\right] \\
\phi'_{m2}(t) &= m\left[\cos\left(\omega_{m1}t+\pi\right)+\cos\left(\omega_{m2}t+\pi\right)\right]
\end{aligned}\right\} \tag{3.4}$$

The optical fields of DPMZM1 and DPMZM2 are combined to obtain the transfer function of the D-DPMZM.

$$E_{D-DPMZM}(t) = E_{DPMZM1}(t) + E_{DPMZM2}(t). \tag{3.5}$$

Assuming $\phi_{ij} = \pi$; (i = 1, 2; j = 1, 2, 3), equation (3.5) can be further simplified to achieve an optical spectrum with carrier suppression. The carrier suppressed modulated signal is transmitted through an optical fibre to avoid power fading and fibre dispersions. However, later an optical carrier through another fibre cable is re-inserted at the receiver. The phase change ϕ_{13} and ϕ_{23} are set to π. Hence, equation (3.5) can be re-written as below;

$$E_{D-DPMZM} = E_c\left[\begin{Bmatrix}\cos\left(\dfrac{\phi_{m1}(t)+\pi}{2}\right)\\ -\cos\left(\dfrac{\phi'_{m1}(t)+\pi}{2}\right)\end{Bmatrix} + \begin{Bmatrix}\cos\left(\dfrac{\phi_{m2}(t)+\pi}{2}\right)\\ -\cos\left(\dfrac{\phi'_{m2}(t)+\pi}{2}\right)\end{Bmatrix}\right] \tag{3.6}$$

At the receiver, the optical carrier signal ($E_L(t) = E_L e^{j\omega_L t}$) is directly combined

with a carrier-suppressed modulated signal by using an optical coupler. A photodiode must have an optical carrier with its sideband signals to retrieve the fundamental frequencies (RF_1 and RF_2) [77]. The two output optical fields from the coupler and can be expressed [116];

$$\begin{bmatrix} E_1(t) \\ E_2(t) \end{bmatrix} = \frac{1}{\sqrt{2}} \begin{bmatrix} E_{D-DPMZM}(t) + E_L(t) \\ E_{D-DPMZM}(t) - E_L(t) \end{bmatrix}. \tag{3.7}$$

The photocurrent $I_{BPD}(t)$ of the balanced photodetector can be determined by substituting output fields of the coupler into the following:

$$I_{BPD}(t) = \Re\left[E_1(t).E_1^*(t) - E_2(t).E_2^*(t) \right] \tag{3.8}$$

Where, $\Re$ is the responsivity of the photodetector, $E^*_1(t)$ and $E^*_2(t)$ are the conjugates of the actual transfer functions, and both fields are subtracted due to a different configuration of the BPD. By substituting equations (3.4), (3.6) and (3.7), to equation (3.8), it can be rewritten as;

$$I_{BPD}(t) = 4E_C E_L \cos((\omega_C - \omega_L)t) \left\{ -4\sin\left(\frac{\phi_{m1}(t)}{2} \right) \right\} \tag{3.9}$$

The unmodulated carrier wavelength is represented as $\omega_{L,}$ and the modulated carrier wavelength is denoted as ω_C. Since a single wavelength laser source is used in the proposed system, ω_L and ω_C are equal (same wavelength). Also, by substituting $\phi_{m1}(t)$ into equation (3.9), the photocurrent can be expressed as;

$$I_{BPD}(t) = -4E_L E_C \left\{ \sin\left(\frac{m\cos(\omega_{m1}t) + m\cos(\omega_{m2}t)}{2} \right) \right\} \tag{3.10}$$

By applying the Jacobi-Anger Expansion in equation (3.10), the high order Bessel functions can be expanded to investigate the beating of different frequency components as shown below;

$$I_{BPD}(t) = -4E_L E_C \left\{ \sum_{p,q=-\infty}^{\infty} J_{p,q}\left(\frac{m}{2}\right) \sin\left(\begin{matrix} p\omega_{m1} + q\omega_{m2} \\ +(p+q)\left(\frac{\pi}{2}\right) \end{matrix} \right) \right\} \tag{3.11}$$

By expanding equation (3.11), and claiming that p≠q to satisfy the conditions for the elimination of IMD2 and SHD;

$$I_{BPD}(t) = -4\Re E_C E_L \left[\begin{matrix} J_{0,1}\left(\frac{m}{2}\right)\cos\left(\omega_{m2}t\right) \\ +J_{1,0}\left(\frac{m}{2}\right)\cos\left(\omega_{m1}t\right) \\ -J_{1,2}\left(\frac{m}{2}\right)\cos\left(\omega_{m1}+2\omega_{m2}\right)t \\ -J_{2,1}\left(\frac{m}{2}\right)\cos\left(2\omega_{m1}+\omega_{m2}\right)t \end{matrix} \right]. \tag{3.12}$$

In equation (3.12), the j^{th} order represents the higher order of frequencies. It can be observed that IMD2 and SHD do not exist and are eliminated at the Balanced Photodetector (BDP). However, theoretically, IMD3s still exist but are greatly suppressed, which results in a higher SFDR and Fundamental signal-to-interference ratio (S/I).

3.2.2 Experimental Results and Discussion

The proposed APL system configuration illustrated in Figure 3.1 is now implemented experimentally, as shown in Figure 3.2. The experimental setup of the proposed AMPL uses PM fibres and fibre-components, such as Laser source, EDFA, Optical couplers, Modulators**,** and Optical patch cables. The use of PM fibres in the set up contribute**s** to enhancing the system stability in contrast with the use of Single-mode (SM) fibres. A Distributed Feedback Laser source with the following specifications is used; (Gooch & Housego, EM650-193400-100-PM900-FCA-NA), centre wavelength 1550nm with an optical output power of 20dBm and Relative Intensity Noise (RIN) of -155dBm/Hz. The RF signals are modulated by two independent GaAs DPMZMs (Axenic, aXMD2050**,** and aXSD2125), which has an

RF half-wave voltage of 3V and 4.2V and a bandwidth of up to 50GHz. The two-tone RF signals (ω_1 = 5GHz and ω_2 = 5.0005GHz) at an amplitude of 6dBm are generated from the Signal Generators (R&S, SMA100A**,** and SMF100A). It should be stated that the RF signals are combined and split by power dividers (Marki Microwave, PD-0R618), and each electrical input of the DPMZM is phase-shifted at 180°, by using Microwave Hybrid couplers (RF Lambda, RFHB02G18GPI). After processing through these electrical components, the RF signals, become lossy and weak, and the actual incident power of RF signals on the modulator electrodes is measured to be around -2dBm. The optical output of both DPMZMs is coupled by using a 50:50 Polarisation Maintained (PM) optical coupler, where the resultant output is amplified by 20dB with an Erbium-doped fibre amplifier (EDFA) (Thorlabs, EDFA100P). The amplified optical field is finally coupled with an optical carrier from the original laser source. The optical carrier is transmitted through a 5-meter PM optical fibre, and then it is combined to an amplified modulated signal with a 50:50 optical coupler.

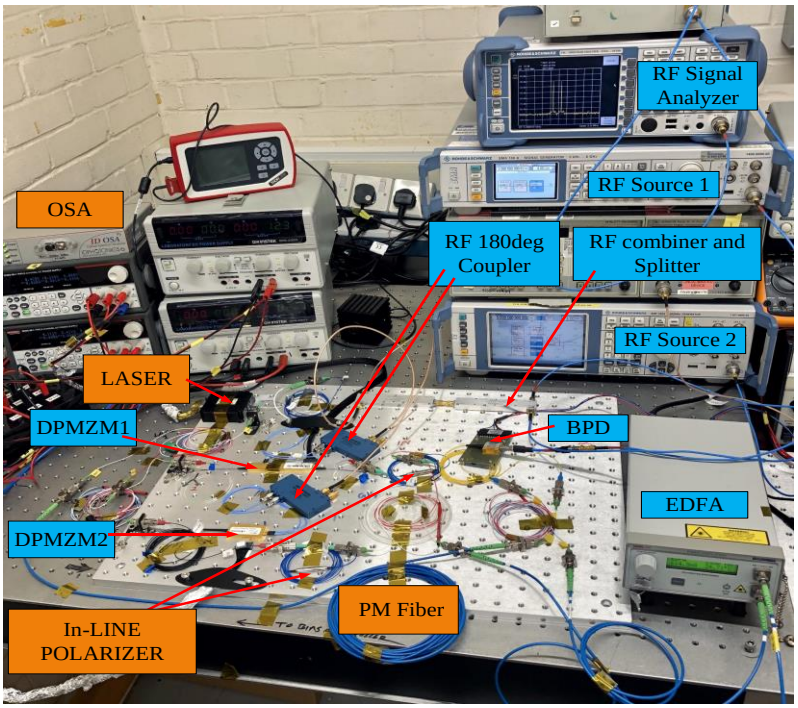

Figure 3.2: Experimental Setup of the proposed scheme in our Microwave Photonics lab.

The two optical fields from the coupler are then injected into the inputs of BPD (Finisar, BPDV2120R-VM-FP), where the detector is biased to function as a differential balanced detector. The first and second diodes of the BPD have a responsivity of 0.60A/W and 0.63A/W, respectively. It should be stated that the intrinsic property of BPD also helps in reducing the amplified spontaneous emission (ASE) and relative intensity noise (RIN) from the laser [119]. It is also well known that the increase in laser power increases the RIN, which results in the degradation of Signal-to-Noise Ratio (SNR). However, this degradation in SNR can be avoided by using the differential balanced detector. These benefits of the balanced detector over a single direct photodetector makes it suitable for the proposed scheme [120]. The electrical output of the BPD is analysed by an Electrical Spectrum Analyzer ESA (R&S, FSL 18). This experiment is developed by deploying components with Polarisation Maintained (PM) fibre pigtails and connectors, which obviate the need for any manually or electronically controlled polarisation controllers. It should also be stated that a perfect common-mode rejection ratio (CMRR) is achieved when both diodes of the BPD have identical responsivity. But, due to fabrication disorder, it is difficult to achieve ideal responsivity. Therefore, the effect of responsivity error between two diodes has been analysed in Figure 3.3, also the effect of optical attenuator has been observed on the correction of responsivity error. Responsivity Error is defined here as the difference between the responsivity value of both diodes. From Figure 3.3, the suppression of IMD2 is -86dBm at zero Responsivity Error (RE). On the other hand, an optical attenuator is used to overcome the RE, and it can be seen from the Figure 3.3 (grey line), that optical attenuation is linearly altered to with reference to the Responsivity Error. This change in optical attenuation with reference to RE, maintains the suppression of IMD2 to -86dBm.

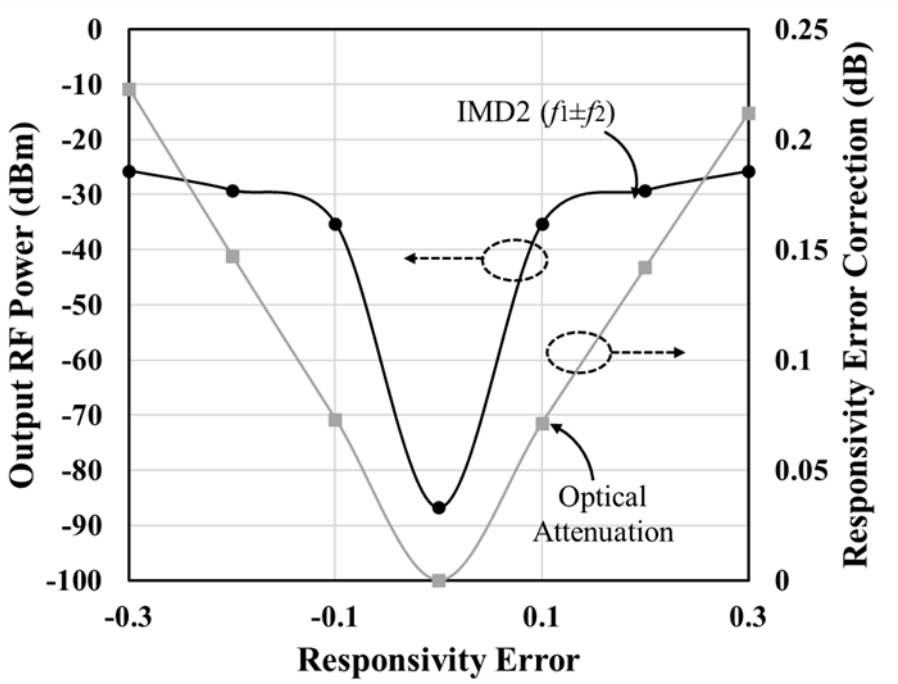

Figure 3.3: Effect of Responsivity Error on the suppression of IMD2 (Black Line) and its correction (Grey line)

Both independent DPMZMs are externally biased by DC supplies to suppress the optical carrier, as it is shown in Figure 3.4. The optical spectrum is observed by using an Optical spectrum Analyzer (ID Photonics OSA). The nulling of the optical carrier is achieved by biasing the sub-MZMs that include a parent sub-MZM of each DPMZM, to a Vπ, and by applying a 180° RF phase shifter to accomplish a phase difference of π between the two input electrical ports of each DPMZM. Figure 3.4 (a) shows an output of DPMZM1 with the maximum suppression of optical carrier at a level of -63dBm, whereas Figure 3.4 (b) shows the output spectrum of the DPMZM2, and it depicts the suppression of OC to -66dBm. The difference in the optical power of carrier from both the modulators is 3dB, which is because both devices are not 100% identical, and due to this reason, upon a combination of their output, an increment in the optical carrier peak power can be noticed as shown in Figure 3.4 (c). The Upper sidebands (USB) and Lower sidebands (LSB), shown in Figure 3.4, are the modulated RF signals, which are the addition and subtraction from the carrier frequency (ω_c). It should be stated that external DC bias sources are used

to control the modulators operating point, and it is observed that the bias-point of the modulators do not drift over a long period. This validates the properties of the GaAs, as mentioned in Walker's article [115]. As previously mentioned, the suppression of optical carrier helps in limiting the dispersions of an optical signal caused by the nonlinearity of fibre.

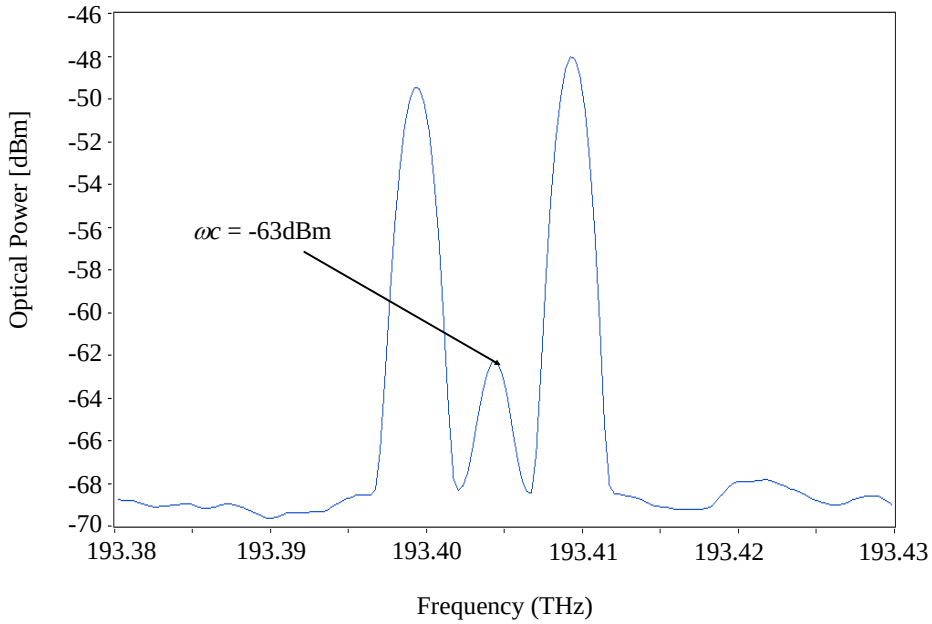

(a)

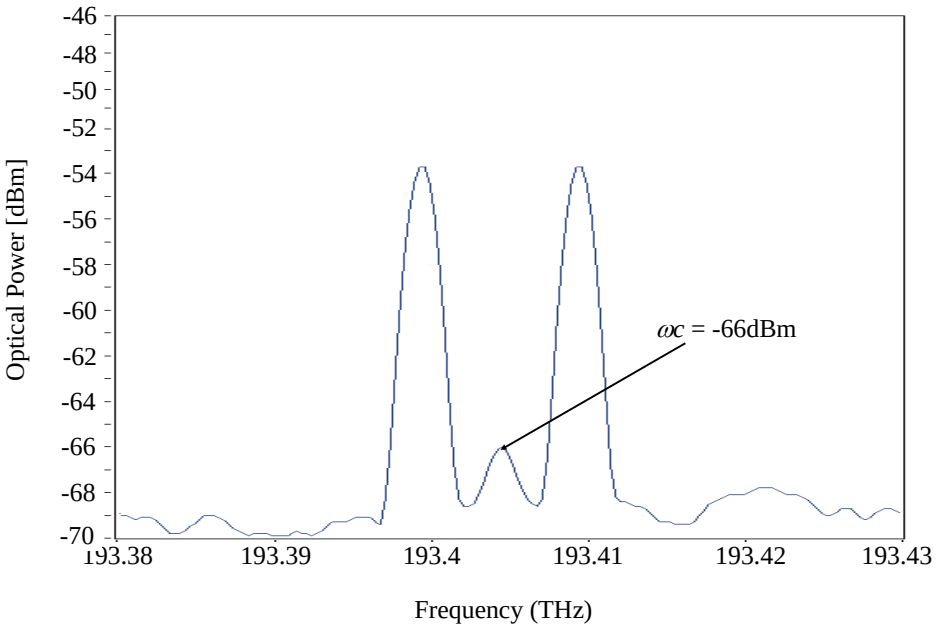

(b)

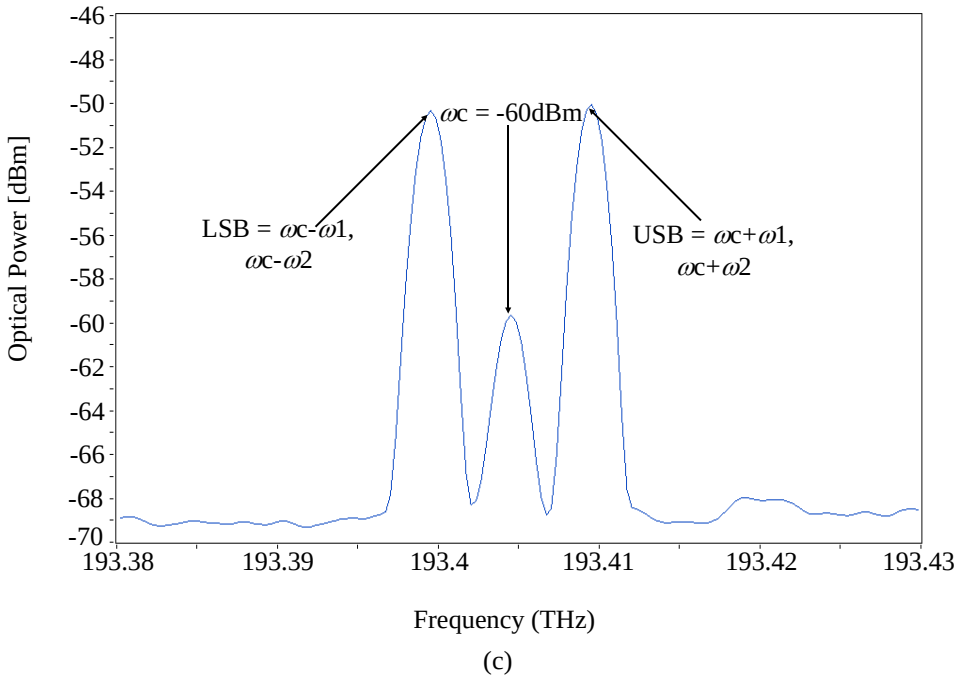

Figure 3.4: Measured Optical spectrum of the proposed structure illustrates the highly suppressed carrier (a) Optical spectrum from DPMZM1 (b) Optical Spectrum from DPMZM2 (c) Combined Optical Spectrum of DPMZM1 and DPMZM2.

3.2.2.1 Extinction Ratio Imbalance in a DPMZM

Throughout the experiment, it is noticed that the Extinction Ratio (ER) of each sub-MZM of the DPMZM is not identical, due to this difference in ER, the maximum suppression of optical carrier cannot be achieved. Therefore, we explored the sub-MZM imbalance in the DPMZM by using the VPI simulation model, where we found that the maximum suppression in the optical carrier and second-order distortions can only be achieved when the MZM imbalance is zero, as it is shown in Figure 3.5. It also illustrates that in a DPMZM, when sub-MZMs are biased to operate at a Null point, then the phase relation between the optical carrier and second-order harmonics (SHD) become identical, which is why in Figure 3.5, both OC and SHD varies uniformly to each other. In our study, the measured imbalance

in the ER of sub-MZMs is 3.3dB, which cannot be externally corrected, and it requires an internal monolithic optical attenuator.

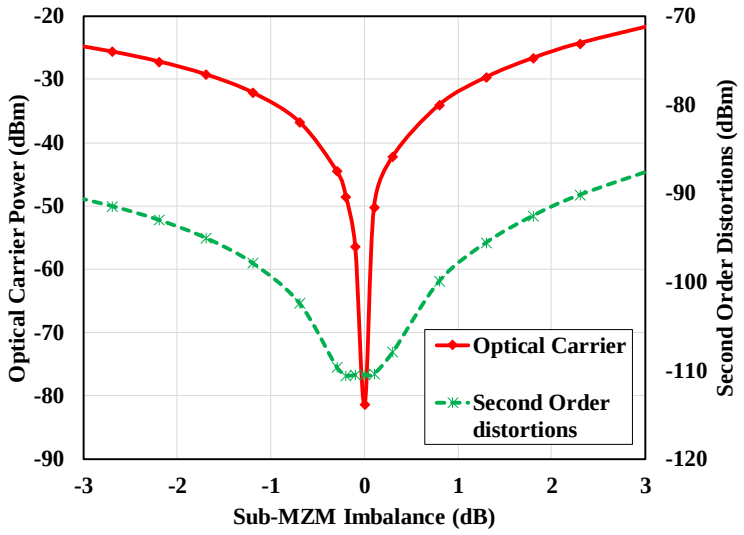

Figure 3.5: Sub-MZM imbalance analysis based on a simulation model

3.2.2.2 Signal to Interference Ratio analysis

The output of the modulator is amplified by using EDFA, and it is adjusted to limit the incident power on the photodiode to 8dBm. The light beam from the laser source is propagating through ~5 meters of PM optical fibre, and it is coupled with the reference modulated signal for the photodetector to retrieve the fundamental RF signals with high efficiency. Both optical fields from the coupler are detected at the BPD, where the differential configuration of the BPD cancels out the even-order distortions (SHD and IMD2). Nevertheless, it should be stated that due to the limitations posed by the components, a complete cancellation of the even-order harmonics is practically impossible. Hence, in Figure 3.6 (b) IMD2 (10.0005GHz) and SHD (10GHz & 10.001GHz) still exist, but their peak power is around 5dB lower compared to the performances reported in the literature [82].

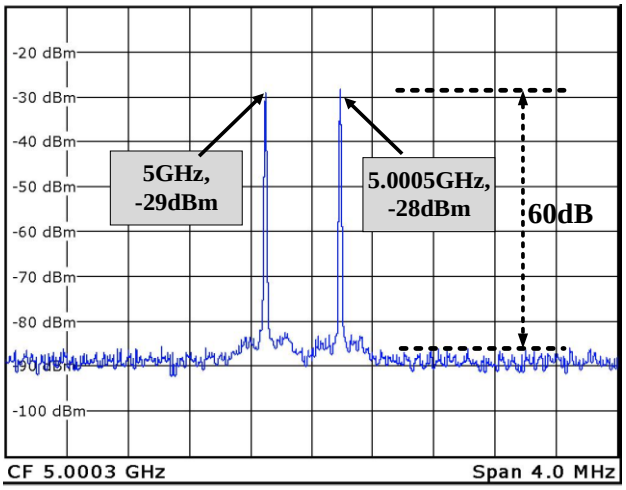

(a)

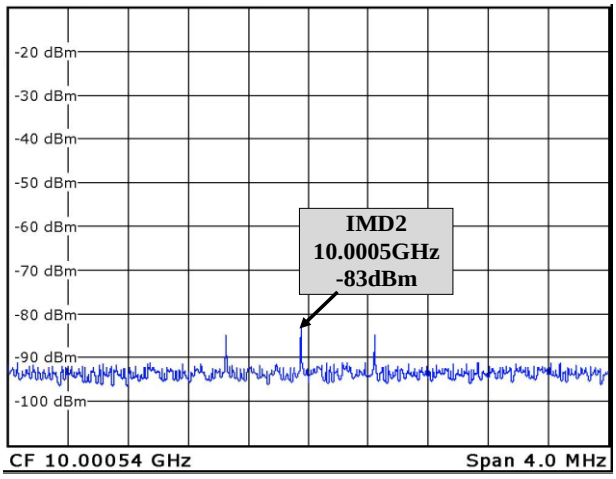

(b)

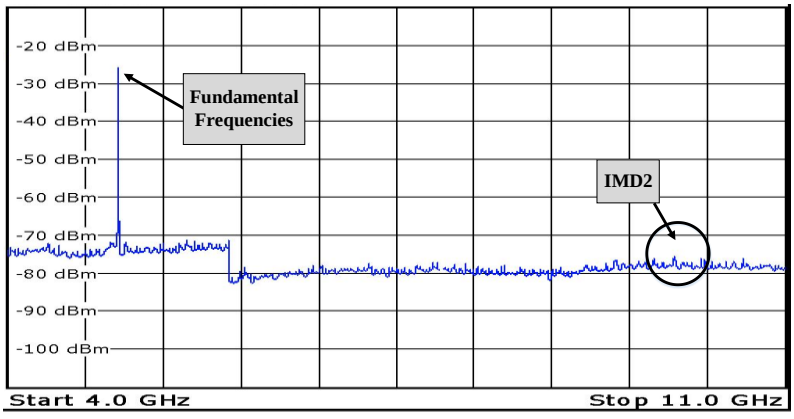

(c)

Figure 3.6: Measured Electrical Spectrum at the output of BPD (a) Spectrum with Fundamental frequencies and IMD3 (b) Spectrum with Even-Order Distortions (c) Spectrum showing fundamental signals and IMD2s.

Concurrently, improvements in the Fundamental Signal-to-interference ratio (S/I) are measured and illustrated in Figure 3.6 (a), which demonstrates that the IMD3s (4.9995GHz & 5.001GHz) are below the noise floor, at a level of -90dBm, with a measured S/I of 60dB. However, this performance can be further 10dB improved by increasing the input RF power.

Figure 3.6 (c) shows a multi-octave RF spectrum in a range of 4GHz to 11GHz, measured by ESA of a frequency range up to 18GHz. The notch in the spectrum on the surface of the noise floor at around 6GHz is due to an internal band filter of the ESA, which represents a particular band of the spectrum. Even-order distortions are also shown close to the level of the noise floor, which proves that intermodulation distortions are very low. Therefore, it means that a clean multi-octave spectrum can be achieved, and substantially a bandwidth of the AMPL can be maximised.

3.2.2.3 Modulation Index and SFDR analysis

The performance of the proposed AMPL was analysed at varying modulation indices from 0 to 1. The modulation index is a ratio of a drive voltage and a half-wave voltage of the modulator. It is an important performance indicator for every modulation link, which identifies a linear working region of any modulator, where distortion is minimised. In Figure 3.7, the modulation index is varied, and S/I is measured. It is then compared with the previously reported literature based on PM-DPMZM [82, 84]. It should be stated that the linear region of this system is between a modulation index of 0.05 and 0.2. After 0.2, the system performance starts to deteriorate and becomes limited by Intermodulation distortion. It is demonstrated that S/I of 75dB can be achieved at a modulation index of 0.12, which is 10dB higher than the PD-DPMZM based method, as shown in Figure 3.7. This performance factor indicates that our proposed and developed method is more robust to IMD3s and IMD2s and shows much better performances that any predecessor techniques reported in the literature, which makes it a highly efficient multi-octave system.

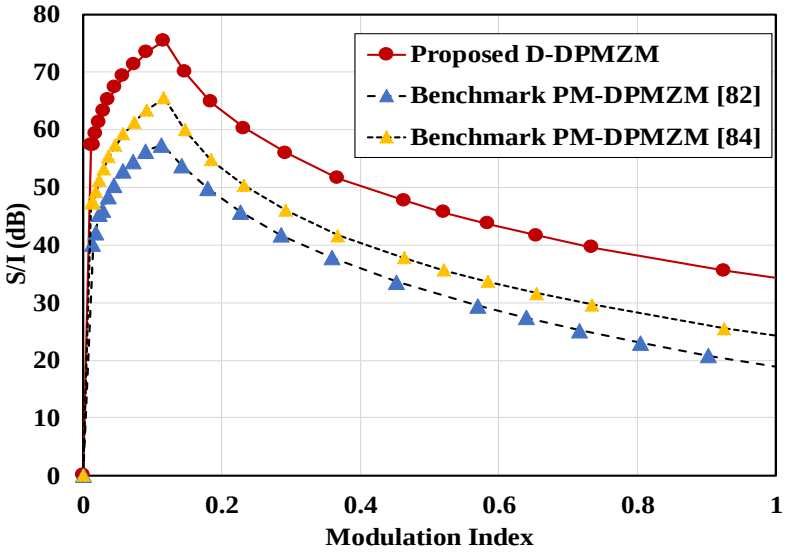

Figure 3.7: The Fundamental signal-to-interference ratio as a function of modulation index

The SFDR performances for IMD3 and IMD2 are analysed by increasing the input RF power and measuring the changes in the fundamental frequency amplitudes, including measuring the third and second-order intermodulation's amplitude at the output of the BPD. The noise level of the proposed system is mainly dependent on the shot noise and ASE noise contributions from the EDFA. However, the BPD reduces the RIN noise and ASE noise, which substantially decreases the noise floor to -170dBm/Hz. The path length of both the optical inputs of BPD is kept similar so that noise levels can be reduced, and SFDR performance can be enhanced [121]. The reported values of SFDR2 and SFDR3 in [84] are 95.5dB.$Hz^{1/2}$ and 123.9dB.$Hz^{2/3}$. From Figure 3.8, it can be seen that the IMD2 and IMD3 are increased by 19.5dB and 3.1dB, respectively. The performance of the proposed system is further analysed at different frequency ranges. In Figure 3.9, the Carrier-to-Interference Ratio (CIR) has been investigated at a frequency range of 0.5GHz to 20GHz. It is observed from the results that the performance of the system deteriorates at the higher frequencies.

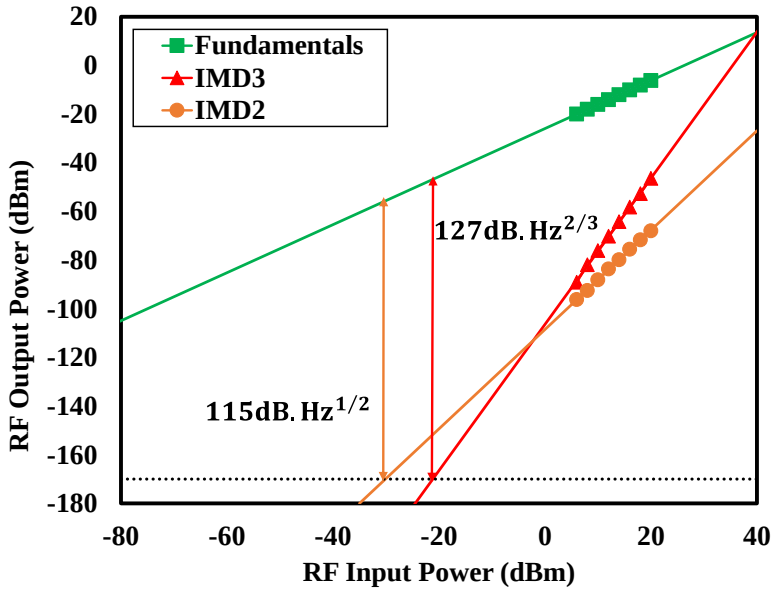

Figure 3.8: SFDR performance analysis of IMD3 and IMD2.

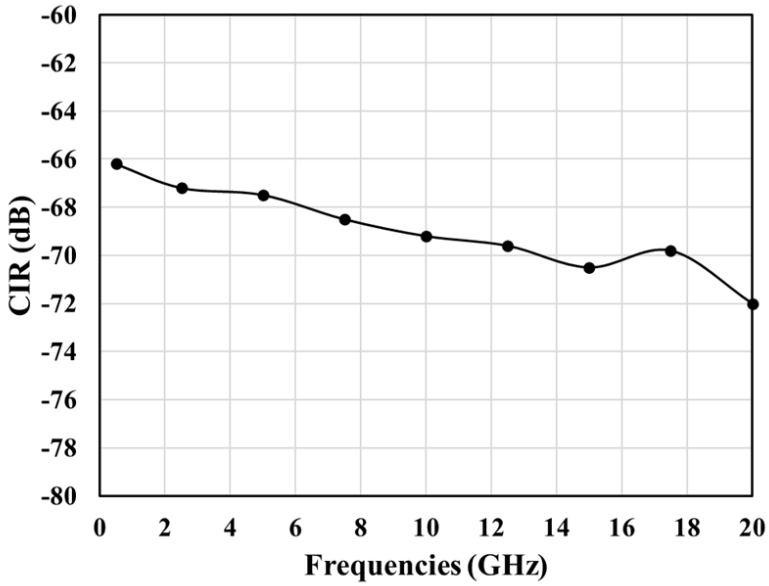

Figure 3.9: Performance of Single RF Channel AMPL at different frequencies.

3.3 Dual RF Channel AMPL

In this section, a linearised method for dual RF channels over a single optical wavelength has been proposed. The linearity of the proposed model is investigated by using two-tones in each RF channel, and the suppression of intermodulation distortion is demonstrated. In [108, 122], RF channelisation has been discussed by

using multiple input signals and reported a suppression in the cross-modulation distortion and intermodulation distortion. However, the proposed model does not contribute to the production of Cross Modulation distortion, which is why it is being benchmarked with a single channel modulation system to show a comparison in the suppression of intermodulation distortions and make the system multi-octave. The design is based on two independent GaAs dual-parallel Mach-Zehnder modulator (DPMZM) structure, which is used with microwave phase shifters to achieve the optical carrier suppression. GaAs modulators have many benefits over $LiNbO_3$ modulators, such as they are thermally stable and operate over a broad range of temperatures without causing any bias-point drift [115, 116]. These intrinsic properties of GaAs modulators make them highly suitable for the harsh operating environment in terms of thermal stability, power-handling, radiation resistance, and longevity for aerospace, defence, and satellite-to-ground downlink communication systems. The laser beam is split into two parallel polarisation-maintained paths; the first path includes the modulation link, and the second path consists of a Polarisation Maintained (PM) optical fibre. The modulated signal with a suppressed carrier is transmitted through the first path, and the optical carrier is traversed through the second path. Both paths are combined by using a 50/50 polarisation-maintained coupler. The resultant signal is converted by a balanced photodetector to recover the fundamental frequencies of both RF channels. The technique with suppressed optical carrier proves to be highly efficient as compared to the previously reported linearisation techniques, and consequently, a higher suppression of IMD3 is noticed. A Balanced Photodetector is configured to operate differentially, by applying oppositely charged voltage to each diode, and as a result, IMD2 and SHD are cancelled out. The use of two DPMZM in the proposed model offers an additional benefit of operating the link with remotely located RF antennas (RF Channels) [123]. Based on this proposed scheme, the nonlinearities of two RF channels are tested by

employing a two-tone test and compared the performance with a single RF channel scheme reported in [82].

3.3.1 Optical Carrier and Even order Harmonics Suppression

In this section, a mathematical model of a proposed system is presented, and it is shown that an optical carrier and even-order harmonics are theoretically eliminated. At first, a single-tone signal is used in each RF channel to demonstrate the optical carrier suppression, as it is shown in Figure 3.10. The D-DPMZM consists of two Dual-Parallel MZMs (DPMZM), and each DPMZM is comprised of two sub-MZMs. RF_1 in channel-1 and RF_2 in channel-2 are used as an input RF signals to the $DPMZM_1$ and $DPMZM_2$, respectively, which are denoted as ω_1 and ω_2, correspondingly.

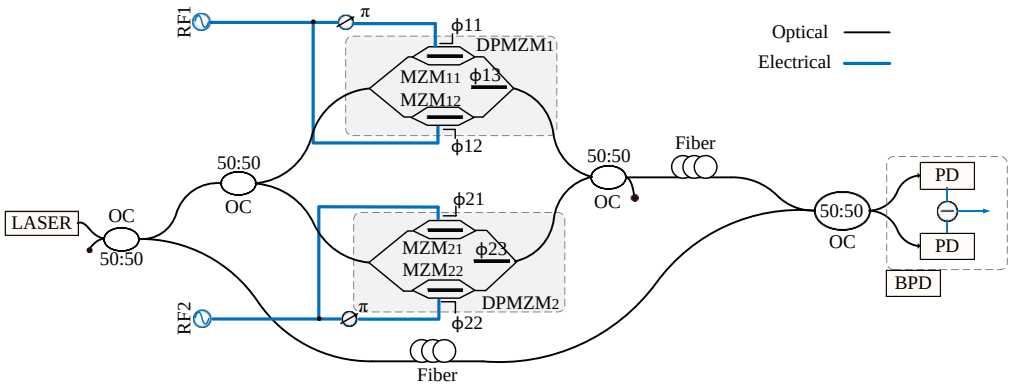

Figure 3.10: Schematic diagram of the proposed Dual RF channel linearisation scheme with two input frequencies.

The input RF signal to the upper and lower sub-MZMs of $DPMZM_i$ (i = 1, 2) has a phase difference of 180°, which is achieved by using an RF Phase Shifter. Each MZM_{ij} (i = 1, 2, j = 1, 2, 3) of $DPMZM_i$ (i = 1, 2) are bias controlled to set the operating point at NULL. It is well known that biasing the modulator electrodes to NULL operating point results in the suppression of optical carrier and even order harmonics. In our proposed model, the purpose of the RF phase shifters is to avoid the destructive interference of fundamental sidebands when $DPMZM_i$ (i = 1, 2) is

biased to Null. The transfer function of DPMZM$_i$ (i = 1, 2) is expressed in equations (3.1) and (3.2).

To further simplify equations (3.1) and (3.2), a phase difference between the two arms of each MZM$_{ij}$ is $\emptyset_{ij} = \pi V_{biasij}/V_{\pi i}$, which is controlled by the DC bias voltage V_{biasij} and the half-wave voltage $V_{\pi i}$. Each MZM$_{ij}$ is modulated by an RF signal ω_{mi}. The phase difference caused by a modulation voltage on MZM$_{i1}$ of i^{th}-DPMZM is $\emptyset_{m_i}(t) = \pi V_i \cos(\omega_{m_i})/V_{\pi i}$, and the phase difference on MZM$_{i2}$ with an additional RF phase shift of 180° is $\emptyset'_{m_i}(t) = m_i \cos(\omega_{m_i} t + \pi)$, where $m_i = \pi V_i/V_{\pi i}$, consequently, the total phase change of MZM$_{i1}$ can be expressed as;

$$\phi_{i1}(t) = \phi_{m_i}(t) + \phi_{i1} \tag{3.14}$$

Likewise, the phase change of MZM$_{i2}$ is shown as;

$$\phi_{i2}(t) = \phi'_{m_i}(t) + \phi_{i2} \tag{3.15}$$

After applying a Jacobi-Anger Expansion and using equations (3.14) and (3.15), the high-order Bessel functions can be analysed as below;

$$E_{DPMZM_i}(t) = E_c \begin{bmatrix} -2J_1 m_1 \cos(\omega_c t)\cos(\omega_{mi} t) \\ +2J_3 m_2 \cos(\omega_c t)\cos(3\omega_{m_i} t) \end{bmatrix}. \tag{3.16}$$

Where J_1 and J_3 are the first-order and third-order Bessel functions. The resultant electric field of the modulator shows that an optical carrier and even-order harmonics are eliminated, as in equation (3.17).

$$E_{DPMZM_i}(t) = E_c \begin{bmatrix} -J_1 m_1 \left\{\cos(\omega_c t + \omega_{m_i} t) + \cos(\omega_c t - \omega_{m_i} t)\right\} \\ +J_3 m_2 \left\{\cos(\omega_c t + 3\omega_{m_i} t) + \cos(\omega_c t - 3\omega_{m_i} t)\right\} \end{bmatrix}. \tag{3.17}$$

3.3.2 Second-order and Third-order Intermodulation Suppression

A further investigation is carried out by introducing two-tone frequencies at each RF channel in the first model (shown in Figure 3.10), which is a combination of two RF signals at each input of the DPMZM$_i$, as it is shown in Figure 3.11. The DC bias conditions are kept the same as the first model.

At each RF channel, two-tone frequencies are equally spaced from each other with a band of 10MHz. Like the first model, as in equations (3.14) and (3.15), the two-tones are modulated in each sub-MZM, and the phase difference caused by the modulating voltage is expressed in equation (3.18).

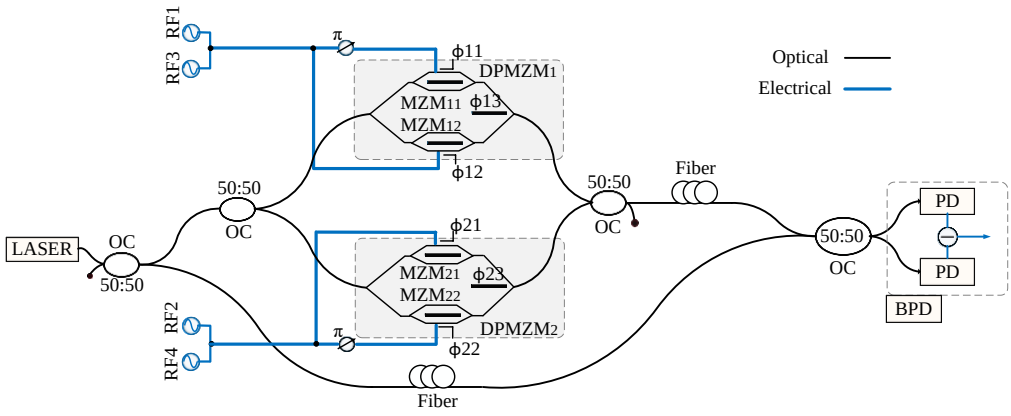

Figure 3.11: Schematic diagram of the proposed Dual RF channel Linearisation Scheme with four input frequencies.

$$\left.\begin{aligned}
\phi_{m1}(t) &= m_{11}\cos\left(\omega_{m11}t\right) + m_{12}\cos\left(\omega_{m12}t\right) \\
\phi'_{m1}(t) &= m_{11}\cos\left(\omega_{m11}t+\pi\right) + m_{12}\cos\left(\omega_{m12}t+\pi\right) \\
\phi_{m2}(t) &= m_{21}\cos\left(\omega_{m21}t\right) + m_{22}\cos\left(\omega_{m22}t\right) \\
\phi'_{m2}(t) &= m_{21}\cos\left(\omega_{m21}t+\pi\right) + m_{22}\cos\left(\omega_{m22}t+\pi\right)
\end{aligned}\right\} \qquad (3.18)$$

Where,$\emptyset_{m1}(t)$ and $\emptyset'_{m1}(t)$ are the phase changes occurred due to the RF modulation voltages at the sub-MZMs of DPMZM$_1$ for RF$_1$ and RF$_3$, and similarly, $\emptyset_{m2}(t)$ and $\emptyset'_{m2}(t)$ are the phase change at each sub-MZM of DPMZM$_2$ for RF$_2$ and RF$_4$, respectively. By using equation (3.18), this phase information can be substituted into equations (3.1) and (3.2) in order to obtain the transfer function of the D-DPMZM

with four input frequencies. Hence, the electric field of $DPMZM_1$ and $DPMZM_2$ is expressed in equation (3.19) and (3.20) as below;

$$E_{DPMZM1}(t) = E_c e^{j\omega_c t}\left[\begin{array}{l}\cos\left(\dfrac{\left[m_{11}\cos\left(\omega_{m11}t\right)+m_{12}\cos\left(\omega_{m12}t\right)\right]+\phi_{11}}{2}\right)+\\ e^{j\phi_{13}}\cos\left(\dfrac{\left[-m_{11}\cos\left(\omega_{m11}t\right)-m_{12}\cos\left(\omega_{m12}t\right)\right]+\phi_{12}}{2}\right)\end{array}\right]. \quad (3.19)$$

$$E_{DPMZM2}(t) = E_c e^{j\omega_c t}\left[\begin{array}{l}\cos\left(\dfrac{\left[m_{21}\cos\left(\omega_{m21}t\right)+m_{22}\cos\left(\omega_{m22}t\right)\right]+\phi_{21}}{2}\right)+\\ e^{j\phi_{13}}\cos\left(\dfrac{\left[-m_{21}\cos\left(\omega_{m21}t\right)-m_{22}\cos\left(\omega_{m22}t\right)\right]+\phi_{22}}{2}\right)\end{array}\right]. \quad (3.20)$$

The electric field of $DPMZM_1$ and $DPMZM_2$ can be combined to achieve a resultant D-DPMZM electric field, which is expressed as;

$$E_{D-DPMZM}(t) = E_{DPMZM1}(t) + E_{DPMZM2}(t). \quad (3.21)$$

Equation (3.21) can be further expanded by substituting equations (3.19) and (3.20) and it can be then expressed as below;

$$E_{D-DPMZM}(t) = E_c e^{j\omega_c t}\left[\begin{array}{l}\left\{\cos\left(\dfrac{\phi_{m1}(t)+\pi}{2}\right)+e^{j\phi_{13}}\cos\left(\dfrac{\phi'_{m1}(t)+\pi}{2}\right)\right\}\\ +\left\{\cos\left(\dfrac{\phi_{m2}(t)+\pi}{2}\right)+e^{j\phi_{23}}\cos\left(\dfrac{\phi'_{m2}(t)+\pi}{2}\right)\right\}\end{array}\right]. \quad (3.22)$$

Bias conditions for all the sub-MZMs are kept the same at a Null. Since the carrier is suppressed, a coherent receiver is needed to recover the signal in the RF domain [82]. An optical carrier is combined with the reference signal by using a directional coupler. The two output fields of the optical coupler are given in the equation (3.23), which is then detected by a balanced detector [79].

$$\begin{bmatrix} E_1(t) \\ E_2(t) \end{bmatrix} = \frac{1}{\sqrt{2}} \begin{bmatrix} E_{D-DPMZM}(t) + E_L(t) \\ E_{D-DPMZM}(t) - E_L(t) \end{bmatrix}. \tag{3.23}$$

The photocurrent $I_{BPD}(t)$ of the balanced detector can be determined by substituting output fields of the coupler into the following:

$$I_{BPD}(t) = \Re\left[E_1(t).E_1^*(t) - E_2(t).E_2^*(t) \right] \tag{3.24}$$

Where, $\Re$ is the responsivity of the photodetector, and $E_1(t)$ and $E_2(t)$ are the optical fields of an optical coupler. By substituting equations (3.23) and (3.24), and setting $\emptyset_{ij} = \pi$, equation (3.24) can be rewritten as;

$$I_{BPD}(t) = 4E_C E_L \left\{ -2\sin\left(\frac{\phi_{m1}(t)}{2} \right) - 2\sin\left(\frac{\phi_{m2}(t)}{2} \right) \right\} \cos((\omega_C - \omega_L)t) \tag{3.25}$$

As we know, the Optical carrier wavelength ω_C and local oscillator wavelength ω_L are the same. Also, by substituting $\emptyset_{m1}(t)$ and $\emptyset_{m2}(t)$ into equation (3.25). It can be expressed as;

$$I_{BPD}(t) = 4E_C E_L \begin{Bmatrix} -\sin\left(\frac{m_{11}\cos(\omega_{m11}t) + m_{12}\cos(\omega_{m12}t)}{2} \right) \\ -\sin\left(\frac{m_{21}\cos(\omega_{m21}t) + m_{22}\cos(\omega_{m22}t)}{2} \right) \end{Bmatrix} \tag{3.26}$$

Applying the Jacobi-Anger Expansion on to equation (3.26), the high order Bessel functions can be explored to see the beating of different frequency components, it can be expressed as shown below;

$$I_{BPD}(t) = -4E_C E_L \left\{ \sum_{n,m=-\infty}^{\infty} J_{n,m}\left(\frac{m_{11}}{2} \right)\left(\frac{m_{12}}{2} \right)\left(\frac{m_{21}}{2} \right)\left(\frac{m_{22}}{2} \right) \left[\begin{matrix} \sin\left(\begin{matrix} n\omega_{m11} + m\omega_{m12} \\ +(n+m)\left(\frac{\pi}{2} \right) \end{matrix} \right) \\ +\sin\left(\begin{matrix} n\omega_{m21} + m\omega_{m22} \\ +(n+m)\left(\frac{\pi}{2} \right) \end{matrix} \right) \end{matrix} \right] \right\}$$

(3.27)

By expanding equation (3.27), it can be said that n≠m to satisfy the conditions for the elimination of IMD2 and SHD.

$$I_{BPD}(t) = -4\Re E_C E_L \begin{bmatrix} J_{0,1}\left(\frac{m_{12}}{2}\right)\left(\frac{m_{22}}{2}\right)\left(\cos\left(\omega_{m12}t\right)+\cos\left(\omega_{m22}t\right)\right) \\ +J_{1,0}\left(\frac{m_{11}}{2}\right)\left(\frac{m_{21}}{2}\right)\left(\cos\left(\omega_{m11}t\right)+\cos\left(\omega_{m21}t\right)\right) \\ +J_{1,2}\left(\frac{m_{11}}{2}\right)\left(\frac{m_{12}}{2}\right)\left(\frac{m_{21}}{2}\right)\left(\frac{m_{22}}{2}\right)\begin{pmatrix}\cos\left(\omega_{m11}+2\omega_{m12}\right)t \\ +\cos\left(\omega_{m21}+2\omega_{m22}\right)t\end{pmatrix} \\ +J_{2,1}\left(\frac{m_{11}}{2}\right)\left(\frac{m_{12}}{2}\right)\left(\frac{m_{21}}{2}\right)\left(\frac{m_{22}}{2}\right)\begin{pmatrix}\cos\left(2\omega_{m11}+\omega_{m12}\right)t \\ +\cos\left(2\omega_{m21}+\omega_{m22}\right)t\end{pmatrix} \end{bmatrix}. \quad (3.28)$$

As from equation (3.28), it can be observed that IMD2 and SHD are eliminated. Although, the design persists a high dynamic range and low IMD3s that is extant when a modulator is driven at high RF power. $J_{0,1}$ and $J_{1,0}$ represent the first-order Bessel function, and it can be seen in equation (3.28) as fundamental RF signals. $J_{1,2}$ and $J_{2,1}$ represent the intermodulation signals produced due to interference between the first-order signals and the second-order signals, which is known as the third-order Intermodulation distortions.

3.3.3 Experimental Results and Discussion

The experimental setup can be seen in Figure 3.12. All-optical equipment used in the experiment have Polarisation Maintained (PM) fibre pigtails. The purpose of employing PM fibres in the system is to improve the signal stability transmitting through an optical link. A distributed feedback (DFB) laser (Gooch & Housego, EM650-193400-100-PM900-FCA-NA) of wavelength 1550nm with a maximum optical power of 20dBm, and Relative Intensity Noise (RIN) of -155dBm/Hz, is used as an optical source. The beam is split by a 49/51 polarisation-maintained optical coupler (Thorlabs, PN1550R5A2), and then the first half is transmitted through a

modulation link, and the other half traversed through a polarisation-maintained optical fibre. The modulation link is composed of two independent GaAs DPMZMs (Axenic, aXSD2050), which has a half-wave voltage of 4V and a bandwidth of 50GHz. The RF ports on each DPMZM are connected to a 180° hybrid coupler (RF Lambda, RFHB02G18GPI), which induces a phase difference of 180° between the two RF inputs. The input RF signals of frequencies, RF_1 = 6.0005GHz, RF_2 = 6.00328GHz, RF_3 = 6GHz, RF_4 = 6.00278GHz, were produced from the RF signal generators (R&S, SMA100A; R&S, SMF100A; Anritsu, 68369A/NV; Hewlett Packard, 8350B) at an amplitude of 6dBm. It should be stated that the RF signals are combined by two power dividers (Marki Microwave, PD-0R618). A 49/51 optical coupler joins both optical paths, and each output link of the coupler connects to the input link of a BPD (Finisar, BPDV2120R-VM-FP). The responsivity level of the balanced photodetector is defined as 0.6A/W and 0.63A/W. A BPD is configured to form a differential function by applying an oppositely charged bias on each diode. The length of both optical paths is kept the same, and a slight adjustment is made by using an optical delay line (Oz Optics, ODL-700-11-1550-9/125-S-60-3A3A-1-1), which can induce a delay of up to 18ps as it is shown in Figure 3.13. It should be stated that the intrinsic property of a balanced detector also helps in reducing the amplified spontaneous emission (ASE) and RIN from the laser [118]. In a proposed architecture, balanced detection is primarily being used to cancel out the SHD and IMD2. Due to the suppression of an optical carrier at the modulator, only sidebands are transmitted through the optical fibre, which requires a balanced detector to retrieve the transmitted signal. The phase information is not available at the direct detection, whereas balanced detection provides phase and amplitude information of the transmitted signal. As we know, the increase in laser power increases the RIN, which results in the degradation of the signal to noise ratio (SNR). However, this degradation in SNR can be avoided by using the coherent balanced detector. These benefits of a balanced detector over a single direct photodetector makes it suitable

for the proposed scheme [119]. The electrical output of the BPD is analysed by an Electrical Spectrum Analyzer ESA (Advantest, U3771).

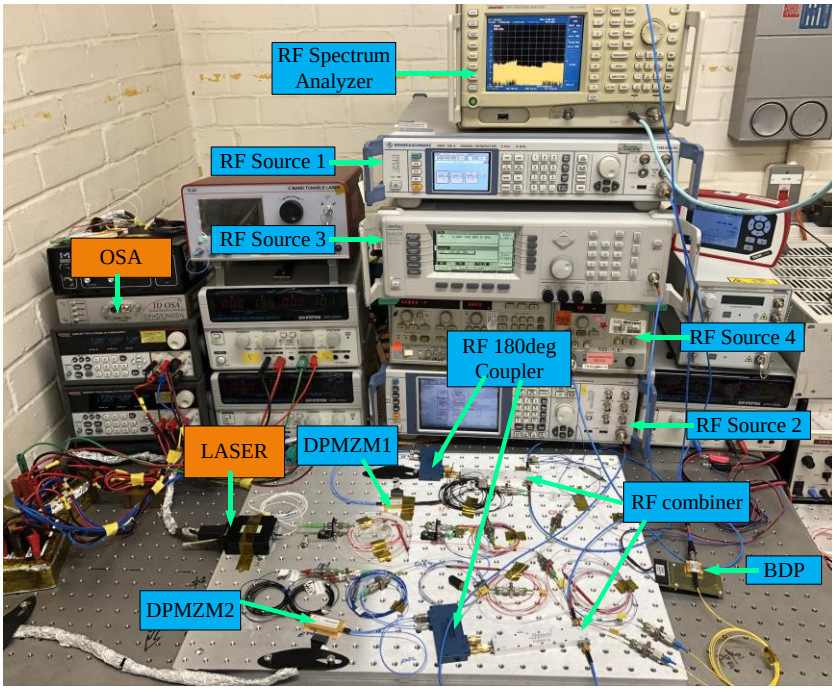

Figure 3.12: Experimental Setup of the proposed scheme in Royal Holloway University of London, Microwave Photonics and Sensors Lab.

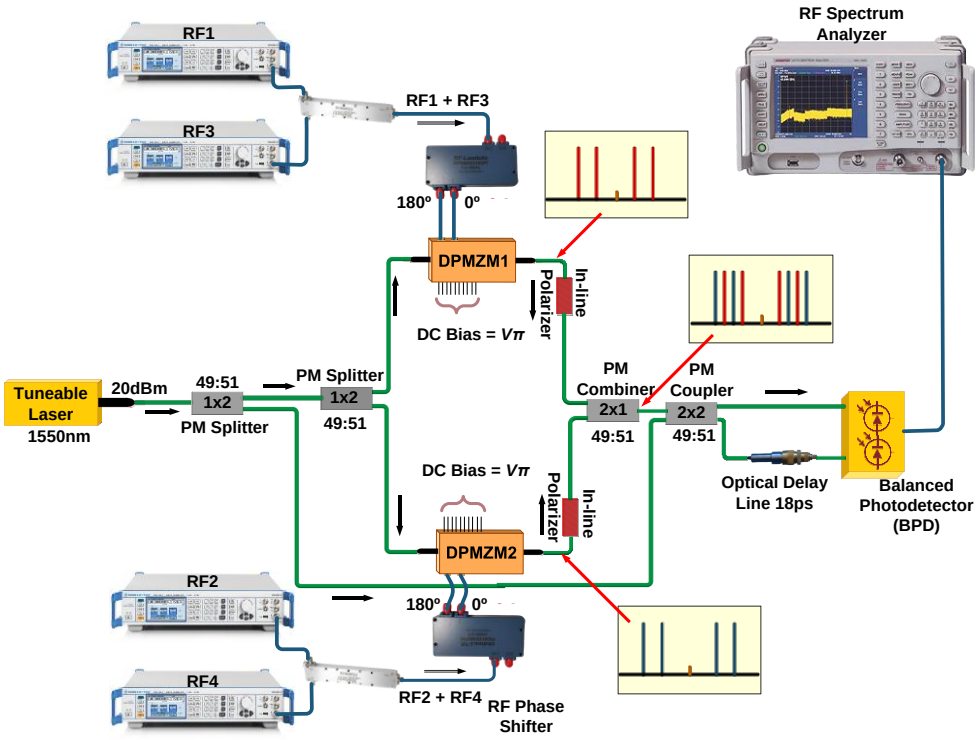

Figure 3.13: Schematic Diagram of the proposed experimental design

Both independent GaAs DPMZMs are bias controlled to achieve maximum suppression of optical carrier, as it is shown in Figure 3.14. The suppression is analysed by using an Optical Spectrum Analyzer (OSA), and the modulator's Null operating position was adjusted by gradually varying the DC voltage. However, the manual handling of DC voltages can be replaced by Automated Bias Controllers (ABC) in future work. In Figure 3.14, a suppressed carrier double sideband spectrum is illustrated, which is observed at the output of a coupler that joins the output fields of both DPMZMs. Experimentally, complete elimination of the optical carrier is not possible due to the intrinsic imbalance properties of the modulator. A suppressed carrier double sideband is then transmitted through an optical patch cable and then combined with a pilot optical carrier, which has traversed through an independent polarisation-maintained optical fibre. In Figure 3.14, upper sideband (USB) and lower sideband (LSB) represent the fundamental input frequencies (RF_1 = 6.0005GHz, RF_2 = 6.00328GHz, RF_3 = 6GHz, RF_4 = 6.00278GHz) of dual RF channel with respect to a central optical carrier frequency of 193.404THz (1550.084nm).

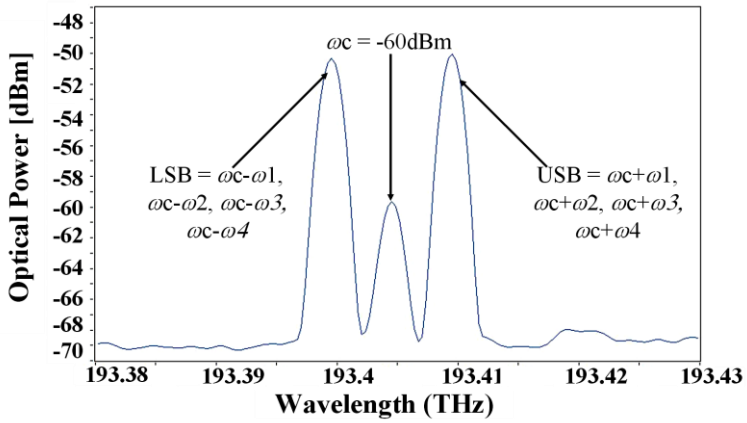

Figure 3.14: Measured Optical spectrum of a combined optical field from two DPMZMs

The combination of two optical paths is then fed to each input of BPD, which is then converted to an electrical signal. We have also analysed the electrical output signal with the help of a VPI simulation model, and then it was compared with the results achieved from an experiment. In Figure 3.15 (a), the fundamental single-tone signals of RF channel-1 and RF channel-2 are shown at a frequency of 6.0005GHz and 6.00328GHz. The IMD3 produced due to interference between the channels is below the noise floor when the modulation index is kept 0.28. Hence, the signal to interference (S/I) ratio of 71dB was observed. In Figure 3.15 (b), fundamental two-tone signals are modulated in each channel and transmitted through an APL. It is noticed that the S/I of 70dB can be achieved at a modulation index of 0.22. The two-tone signals used in RF channel-1 are 6GHz and 6.0005GHz, whereas, in RF channel-2, 6.00328GHz and 6.00278GHz are used.

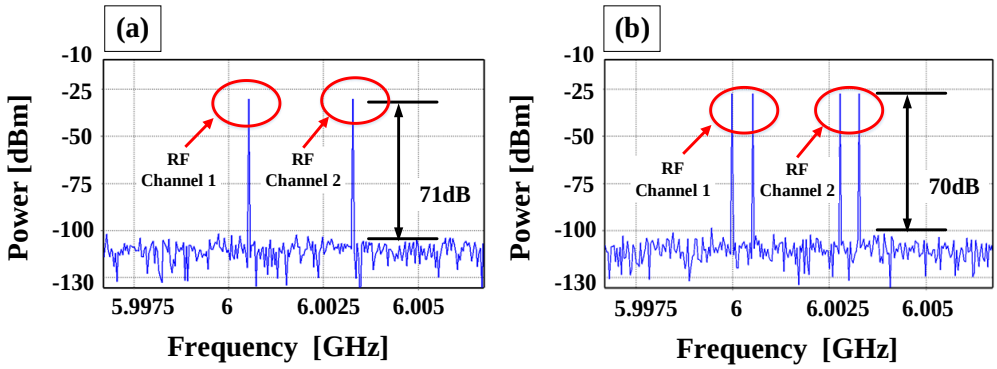

Figure 3.15: Simulated Electrical spectrum (a) Single-tone Dual RF channel (b) Two-tone Dual RF channel

Likewise, the electrical signals received at the BPD are analysed by an ESA, which itself has some restrictions such as the limited noise power density. However, the results shown in Figure 3.16, have a smaller S/I as compared to the simulated results. It can be clearly illustrated that the performance is mainly limited by the noise floor in the experimental results. Figure 3.16 (a) shows a single-tone spectrum of dual RF channel, and the measured S/I is 65dB. IMD3 component produced, in this case, are at 5.99772GHz, and 6.00606GHz, which has an amplitude of around -85dBm. The fundamental single-tones have a peak power of around -20dBm. It is to be noted that

the input RF power is kept at 6dBm for all tones, which gives a link gain of around -26dB. Figure 3.16 (b) shows a two-tone spectrum of dual RF channel with a measured S/I of 60dB. In this case, RF channel-1 demonstrates a link gain of around -38dB, whereas RF channel-2 shows a link gain of -36dB. The two-tone test is further explored in Figure 3.16 (c) for IMD2 and SHD, which do not appear above the noise floor. To observe the distortions, a wideband spectrum is shown in Figure 3.16 (d), which depicts the fundamental frequencies and suppressed intermodulation distortions. Different levels of noise floor are due to the internal band filter of the ESA.

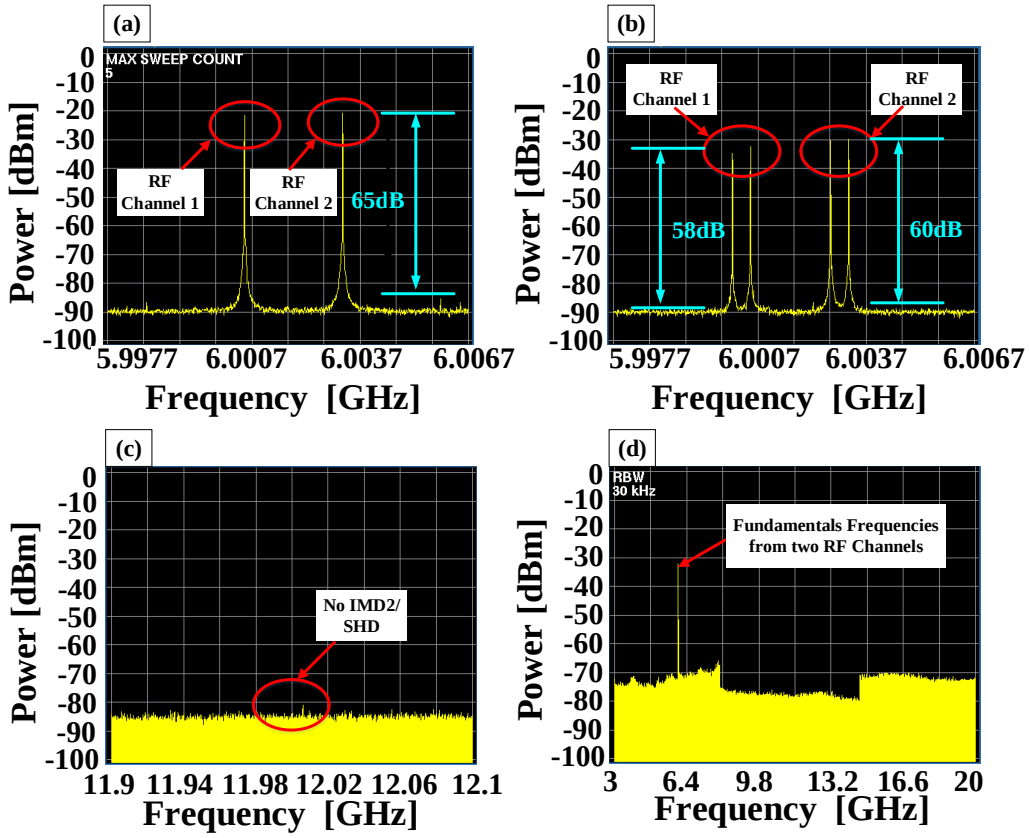

Figure 3.16: Measured Electrical Spectrum, (a) Single-tone dual RF channel (b) Two-tone dual RF channel (c) Second-order distortions for two-tone test (d) Wide spectrum for a two-tone dual RF channel.

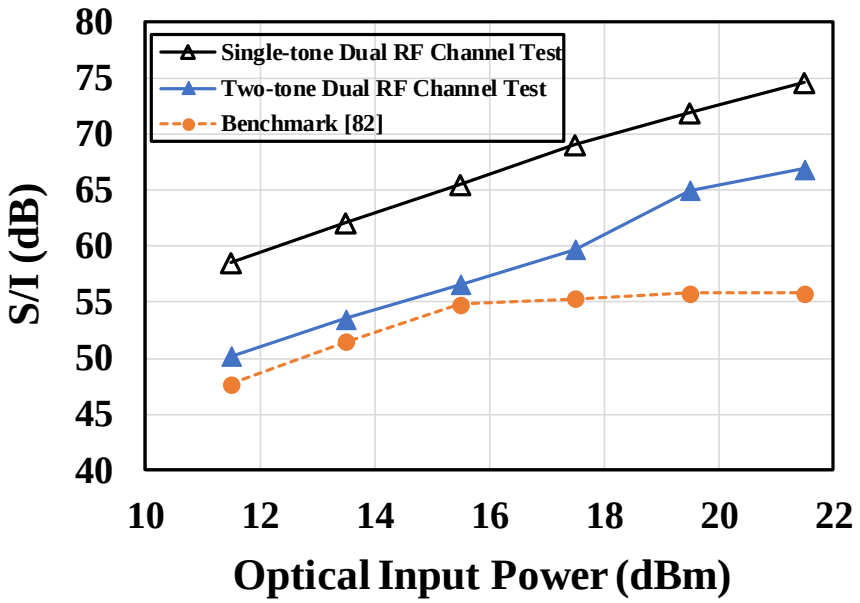

Figure 3.17: Performance analysis of a proposed model and the benchmark model, as a reference of Optical input power.

After the demodulation process of the transmitted signal, the S/I is calculated with reference to optical input power and compared with the benchmarked results, as shown in Figure 3.17. It should be noted that the benchmark method reported in [82] has limited S/I due to the existence of high IMD3, whereas the proposed method is much more robust and has a potential to achieve S/I of up to ~75dB considering the power limitation posed by the optical devices. However, the S/I for benchmarked PM-DPMZM method reported in [82] is nearly constant at 15.5dBm. This illustration provides a foreseen optimised performance of the proposed link when the optical source power is increased. The components used in the existing infrastructure of APL are power limited, and high optical power would either deteriorate the performance or damage the component. So, if this limitation posed by the components can be overcome, then the performance of the APL can be further improved by a great margin.

3.3.3.1 Signal to Interference ratio and SFDR Analysis

We present a linear modulation range of the modulator by observing the modulation index. At a small modulation index, the system generally has a higher Signal to

interference ratio, and by plotting the data, the linear region of a modulator can be observed. In our proposed model, the modulation index is optimised to achieve the maximum dynamic range. For a Single-tone test, the S/I is maximum at a modulation index of 0.57. However, for the Two-Tone linearisation test, the S/I of ~65dB is achievable at a modulation index of 0.14 (as shown in Figure 3.18). The performance of the model deteriorates at a high modulation index, which means the modulator is being overdriven.

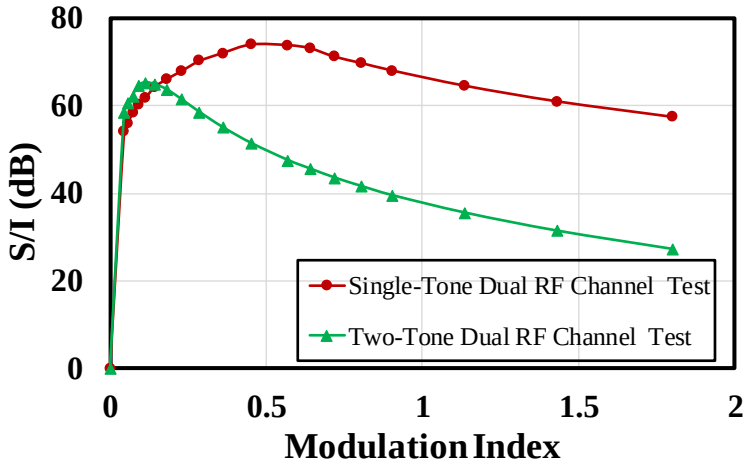

Figure 3.18: Signal to Interference ratio as a function of Modulation index

The SFDR performance of the proposed scheme, based on the linearisation tests for the Dual RF channel, is illustrated in Figure 3.19. The output RF power of fundamental frequencies and IMD3 as a function of the input RF power is plotted for both Single-tone and two-tone tests. The noise floor based on the system RIN is set to -160dBm/Hz, considering the thermal noise of 3.163e-10A/√Hz at the detector. However, the measured noise floor from the ESA is -140dBm/Hz, which is restricted by ESA specifications. In the SFDR measurements, the calculated noise floor of -160dBm/Hz is used. All the fundamental frequencies and their IMD3s have an equal output power as the input RF powers for each tone is kept similar, which is then varied to calculate the performance of SFDR. As can be seen from our proposed Single-tone linearisation test, we have achieved an SFDR of 116dB.$Hz^{2/3,}$ and it is of

110dB.Hz$^{2/3}$ for the two-tone linearisation test of a dual RF channel. Figure 3.19 (a) shows the measured SFDR performance of the proposed model with a Single-tone input frequency at each RF channel. The SFDR2 and SFDR3 for a single-tone test are 109dB.Hz$^{1/2}$ and 116dB.Hz$^{2/3}$ respectively. Whereas, for a two-tone test, as shown in Figure 3.19 (b), the SFDR2 and SFDR3 are 108.5dB.Hz$^{1/2}$ and 110dB.Hz$^{2/3}$ respectively. It is to be noted that in both cases, the SFDR2 is comparatively high, which illustrates that IMD2s has been highly suppressed.

The proposed linearised scheme realises a highly efficient multi-tone dual-channel system. However, biasing the multiple modulators to a desired operating point can be a bit tricky, which can be omitted by using Automated Bias Controllers (ABC) in a real experiment. The performance can be further improved by using Amplified Spontaneous Emission (ASE) filters to reduce the noise level after the amplification of an optical signal.

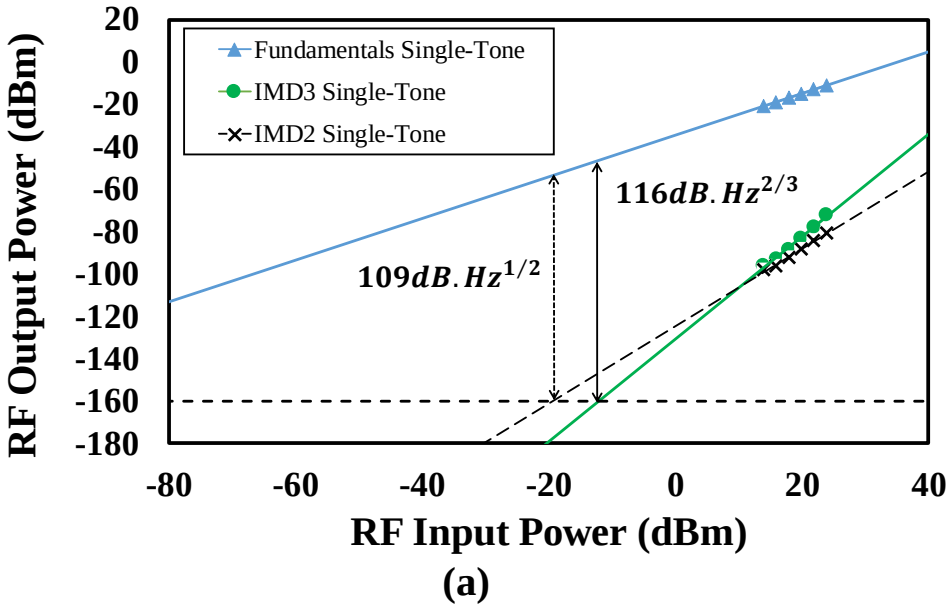

(a)

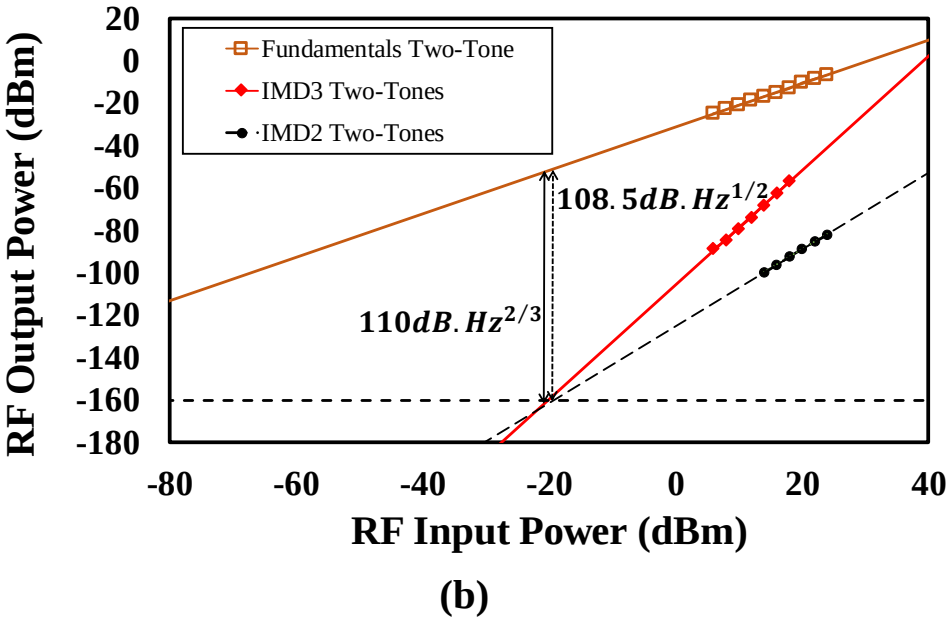

(b)

Figure 3.19: SFDR performance of a proposed D-DPMZM scheme for the linearisation of (a) Single-Tone, (b) Two-Tone Dual RF channel.

3.4 Summary

In this chapter, a linearisation technique for the multi-octave AMPL has been discussed. The configuration emphasis on the transmission of a suppressed carrier double sideband signal and an additional polarisation maintained optical link is provided to transmit an unmodulated optical carrier. Both modulated link and unmodulated link are coupled and detected by the balanced photodetector (BPD). The purpose of achieving two parallel optical links was to reduce the effect of optical fibre nonlinearities on the modulated signal. Hence a suppressed carrier and low-power optical signal have been transmitted through the link. At the receiver end, a BPD has been used to eliminate the second-order distortion products as well as the RIN noise from the laser source. The model was designed to function for a dual RF channel as well as a single RF channel. The performances of both scenarios have been analysed. The signal to interference ratio (S/I) and spurious-free dynamic range (SFDR) for IMD2 and IMD3 have been presented. It was proven that the configuration retains the S/I of above 60dB for single RF channel and dual RF

channel. The above-presented work has been submitted for two different journal articles and it is in under review state.

Chapter 4

4. Proposed Two-tone Photonic Mixer with IMD cancellation

4.1 Introduction

As previously discussed, the suppression and elimination of different distortion products in the APL, which are mainly caused by the nonlinear behaviour of the modulator and occasionally due to a chromatic dispersion of an optical fibre. In this chapter, a linearisation technique for the down-conversion of multiple input RF signals is discussed. When modulating more than one RF signals (Two-tones) simultaneously for down-conversion or up-conversion, it produces unwanted intermodulation distortions as well as high-order harmonics. A novel method of overcoming this issue will be presented and discussed thoroughly in this chapter.

Presented is the proposed Two-tone photonic mixer with IMD cancellation. This model contributes to the elimination of Intermodulation Distortions produced due to a nonlinear mixing of multiple input RF signals (referred to as Two-tone-IMD2). It should also be stated that the proposed model has an additional capability of removing the second-order harmonics of input RF signals (2RF). However, it retains the Intermediate Frequencies (IF), also known as IMD2 in the APL systems, which are produced due to interference between the multiple inputs RF signals and a Local Oscillator (LO) signal. The reason for retaining the IF is to validate the down-conversion process of a Photonic Mixer.

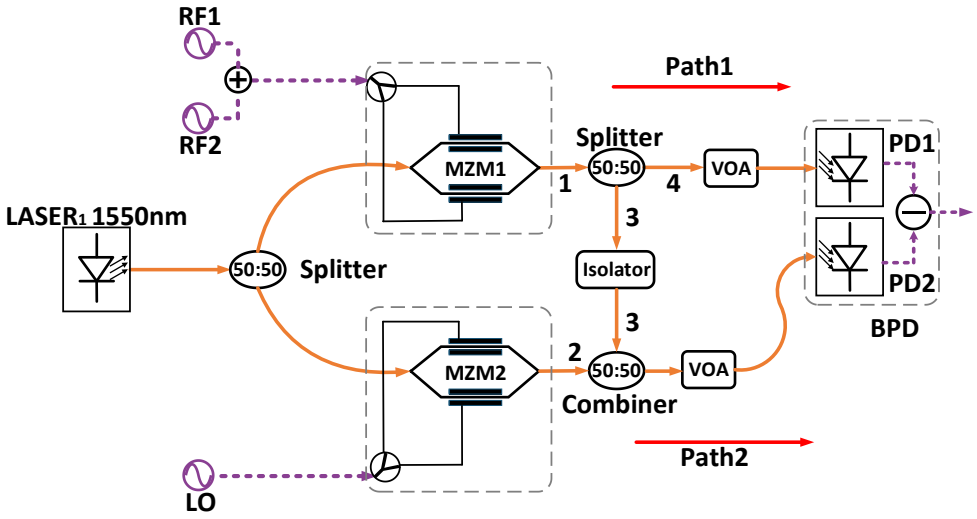

Figure 4.1: Schematic Diagram of a novel Two-tone Photonic Mixer

A schematic diagram of the proposed linearized photonic mixer is shown in Figure 4.1. The composition of the model includes two independent MZM modulators, optical splitters, optical combiners and a Balanced Photodetector (BPD). A first MZM is adapted to impose RF signals received through an input of the RF mixer onto a first optical beam and a second MZM is adapted to impose a LO signal from a LO signal source onto a second optical beam. Then, an optical splitter arranged to split the first optical beam outputted from the first MZM to provide a third optical beam and a fourth optical beam, as it is shown in Figure 4.1. The third optical beam is combined with the second optical beam by an optical combiner, then the combined optical beam is received by the second photodiode (PD2) of BPD, and this optical path is labelled as Path 2. The fourth optical beam is directly transmitted to the first Photodiode (PD1) of a BPD circuit, which is labelled as a Path 1. The BPD circuitry is arranged to provide an electrical output signal corresponding to a difference between the electrical responses of PD1 and PD2. Because the unwanted beat frequencies (IMD2s) derived from interference between received RF signals will be present on both inputs to the balanced photodetector circuitry they will be substantially eliminated by the balanced photodetector differential circuit and thus

absent from its output. The beat frequencies (IFs) derived from interference between the LO signal and received RF signals, which are only present at one input to the balanced photodetector circuitry will still be present in the photodetector circuit's output.

However, when implemented in a receiver system, this allows for undesired beating to be removed from the received signal before being passed to the DSP. In the case of a transmitter system arranged to transmit two RF signals simultaneously, the proposed model similarly allows for the removal of unwanted beat frequencies from the input to the antenna. In addition to providing the function mentioned above, the balanced photodetector can also provide its conventional function of balancing fluctuations in the optical power of the two beams received by the photodetector circuitry resulting from temporal changes in the output power of a single laser source from which the beams originate.

The RF mixer may comprise one or more intensity controllers arranged to alter the intensity of one or more of the: first, second, third and fourth optical beams, in order to substantially match the optical intensity of the Path 2 (combined second and third beam), and a Path 1 (fourth beam) at the electro-optic transducer.

4.2 Theoretical model of a Proposed Photonic Mixer

In this section, a mathematical model of a novel design for the cancellation of beat frequencies (Two-tone-IMD2) from the input RF signals is presented. The proposed photonic mixer is mathematically investigated for two different scenarios. Firstly, a single-tone input RF signal is modulated and mixed with a LO signal to down-convert, and at the receiver, an Intermediate Frequency of a single-tone is presented. Secondly, two-tone input RF signals are modulated and mixed with a LO signal to generate Intermediate Frequencies of the input RF tones.

4.2.1 Elimination of Second-order Harmonics in a Single-Tone Mixer

A single-tone mixer is a mixer which down-converts or up-converts a single RF signal to an IF signal by mixing it with a LO signal. Here, a model is presented, which eliminates the second-order harmonic of input RF signals. At first, an optical light beam is propagated from a laser source, which is expressed as $E_c(t) = E_c e^{j\omega_c t}$. The light beam is equally divided into two optical beams and fed to each MZMs. First MZM modulates a single-tone signal (ω_1), whereas the second MZM modulates a LO signal (ω_{LO}). The output electric field of first and second MZM can be represented as $E_{out1}(t)$ and $E_{out2}(t)$, respectively, which is expressed as below;

$$E_{outi}(t) = E_C e^{j\omega_C t}[e^{jV_{i1}(t)} + e^{-jV_{i2}(t)}], \text{ (where } i = 1, 2) \tag{4.1}$$

Each MZM has upper and lower electrodes, which generates the electric field around the waveguide to modulate the optical carrier with an input electrical signal. The voltages produced on each electrode are expressed as below;

$$\left.\begin{aligned} V_{11}(t) &= m[\cos(\omega_1 t)] + \pi \\ V_{12}(t) &= m[\cos(\omega_1 t)] \\ V_{21}(t) &= m[\cos(\omega_{LO} t)] + \pi \\ V_{22}(t) &= m[\cos(\omega_{LO} t)] \end{aligned}\right\} \tag{4.2}$$

In equation (4.2), $V_{11}(t)$ and $V_{12}(t)$ represent the voltages applied on upper and lower arms of the first MZM, correspondingly. Whereas, $V_{21}(t)$ and $V_{22}(t)$ represents the voltages for second MZM. However, the DC bias voltages for $V_{11}(t)$ and $V_{21}(t)$ are represented by π, because MZM is being operated at a NULL operating point, which essentially suppresses the optical carrier. The modulation index of the modulating signal is the ratio of RF voltage (V_{RF}) and half-wave voltage(V_π). Assuming the input RF and LO signals have the same amplitude, then it can be expressed as $m = \pi\, {V_{RF}}/{V_\pi}$. By substituting the equation (4.2) into equation

(4.1), and then applying Taylor series, the output electric field of first MZM and second MZM can be expressed as below;

$$E_{out1}(t) = jE_C\left[-2m\cos\left(\omega_1 t\right) + m^3\left(\frac{\cos\left(3\omega_1\right)}{12} + \frac{\cos\left(\omega_1\right)}{4}\right)\right] \tag{4.3}$$

$$E_{out2}(t) = jE_C\left[-2m\cos\left(\omega_{LO} t\right) + m^3\left(\frac{\cos\left(3\omega_{LO}\right)}{12} + \frac{\cos\left(\omega_{LO}\right)}{4}\right)\right] \tag{4.4}$$

A combined optical beam from the second and third optical beams can be mathematically expressed by using equations (4.3) and (4.4). The output field is stated in equation (4.5).

$$E_{out12}(t) = jE_C\left[\begin{array}{l} m^3\left(\begin{array}{l}\frac{\cos\left(3\omega_1\right)t}{12} + \frac{\cos\left(3\omega_{LO}\right)t}{12} \\ + \frac{\cos\left(\omega_1\right)t}{4} + \frac{\cos\left(\omega_{LO}\right)t}{4}\end{array}\right) \\ -m\left(2\cos\left(\omega_1 t\right) + 2\cos\left(\omega_{LO} t\right)\right)\end{array}\right] \tag{4.5}$$

The fourth optical beam (as shown in Figure 4.1) propagates to the PD1 of the BPD circuit and gets demodulated to a photocurrent of $I_{PD1}(t)$. The combined optical beam from second and third beams is travelled to the PD2 of the BPD, and the photocurrent $I_{PD2}(t)$ is generated. Both the photocurrents can be expressed as below;

$$I_{PD1}(t) = 2m^2\Re_1 P_C\left[\cos\left(\omega_1 t\right) + 1\right] \tag{4.6}$$

$$I_{PD2}(t) = 2m^2\Re_2 P_C\left[\begin{array}{l} 2\cos\left(\omega_1 - \omega_{LO}\right)t + \cos\left(2\omega_1 t\right) \\ + \cos\left(2\omega_{LO} t\right) + 2\cos\left(\omega_1 + \omega_{LO}\right)t + 2\end{array}\right] \tag{4.7}$$

From equation (4.6) and (4.7), $\Re_1$ and $\Re_2$ are the responsivities of PD1 and PD2 of the BPD circuitry, respectively. P_C is the optical power fed to the inputs of MZM_1 and MZM_2. Considering the circuitry of BPD, both diodes are oppositely biased to realise a differential configuration. It can be stated as below;

$$I_{out}(t) = I_{PD1}(t) - I_{PD2}(t) \tag{4.8}$$

By substituting equations (4.6) and (4.7) into equation (4.8), the final output of the mixer can be achieved. The resultant electrical signal includes the IFs and 2LO only as the other frequencies gets eliminated as it is shown in equation (4.9).

$$I_{out}(t) = -2m^2\Re_1\Re_2 P_C \begin{bmatrix} 2\cos\left(\omega_1 - \omega_{LO}\right)t + \cos\left(2\omega_{LO}t\right) \\ +2\cos\left(\omega_1 + \omega_{LO}\right)t + 1 \end{bmatrix} \tag{4.9}$$

4.2.2 Elimination of Intermodulation Distortion in a Two-Tone Mixer

The proposed model is primarily designed for the down-conversion or up-conversion of two-tone RF signals as it is shown in Figure 4.1. Although the model has been tested for single-tone RF signal in section 4.2.1, the advantages of down-converting two-tones using this model are far greater than single-tone mixing. Modulating multiple frequencies means there will be more distortion products, and it will make the system difficult to filter out the unwanted distortion products from the required frequencies. In this section, a mathematical model is presented, which illustrates the electric fields of the optical signals and the photocurrent received at the output of the BPD. The two-tone input signals used in the system are symbolised as (ω_1) and (ω_2), whereas the LO signal is represented as (ω_{LO}). It is to be noted that the upper electrode of first MZM and second MZM are DC biased with a "π" so that an optical carrier can be suppressed in each MZM.

$$\left.\begin{aligned} V_{11}(t) &= m[\cos(\omega_1 t) + \cos(\omega_2 t)] + \pi \\ V_{12}(t) &= m[\cos(\omega_1 t) + \cos(\omega_2 t)] \\ V_{21}(t) &= m[\cos(\omega_{LO} t)] + \pi \\ V_{22}(t) &= m[\cos(\omega_{LO} t)] \end{aligned}\right\} \tag{4.10}$$

The output field of the MZM can be investigated by substituting equation (4.10) into equation (4.1) and then a Taylor series is applied to express the output of first MZM and second MZM as below;

$$E_{out1}(t) = jE_C\left[\begin{array}{l} m^3\left(\begin{array}{l}\dfrac{\cos(\omega_1-2\omega_2)t}{4}+\dfrac{\cos(\omega_1+2\omega_2)t}{4} \\ +\dfrac{\cos(2\omega_1+\omega_2)t}{4}+\dfrac{\cos(3\omega_1)t}{12}+\dfrac{\cos(3\omega_2)t}{12} \\ +\dfrac{\cos(2\omega_1-\omega_2)t}{4}+\dfrac{3\cos(\omega_1)t}{4}+\dfrac{3\cos(\omega_2)t}{4}\end{array}\right) \\ -m\left(2\cos(\omega_1 t)+2\cos(\omega_2 t)\right)\end{array}\right] \quad (4.11)$$

$$E_{out2}(t) = jE_C\left[-2m\cos(\omega_{LO}t)+m^3\left(\frac{\cos(3\omega_{LO})}{12}+\frac{\cos(\omega_{LO})}{4}\right)\right] \quad (4.12)$$

As discussed earlier, that second optical beam and third optical beam are combined to generate a mixed optical beam so that a LO signal can down-convert two-tones. The transfer function of the combined optical output is expressed as below;

$$E_{out12}(t) = jE_C\left[\begin{array}{l} m^3\left(\begin{array}{l}\dfrac{\cos(\omega_1-2\omega_2)t}{4}+\dfrac{\cos(\omega_1+2\omega_2)t}{4} \\ +\dfrac{\cos(2\omega_1+\omega_2)t}{4}+\dfrac{\cos(3\omega_1)t}{12}+\dfrac{\cos(3\omega_2)t}{12} \\ +\dfrac{\cos(3\omega_{LO})t}{12}+\dfrac{\cos(2\omega_1-\omega_2)t}{4} \\ +\dfrac{3\cos(\omega_1)t}{4}+\dfrac{3\cos(\omega_2)t}{4}+\dfrac{3\cos(\omega_{LO})t}{4}\end{array}\right) \\ -m\left(2\cos(\omega_1 t)+2\cos(\omega_2 t)+2\cos(\omega_{LO}t)\right)\end{array}\right] \quad (4.13)$$

Equation (4.13) depicts the theoretical representation of an actual combined signal, which includes the fundamental signals and the third-order signals expressed as m and m^3, respectively. The optical electric field is then converted into a photocurrent by squaring the field. Hence, the photocurrent of the PD1 and PD2 is expressed below as $I_{PD1}(t)$ and $I_{PD2}(t)$, respectively.

$$I_{PD1}(t) = 2m^2\Re_1 P_C \begin{bmatrix} 2\cos(\omega_1 - \omega_2)t + \cos(2\omega_1 t) \\ +\cos(2\omega_2 t) + 2\cos(\omega_1 + \omega_2)t + 2 \end{bmatrix} \quad (4.14)$$

$$I_{PD2}(t) = 2m^2\Re_2 P_C \begin{bmatrix} 2\cos(\omega_1 - \omega_2)t + 2\cos(\omega_1 - \omega_{LO})t \\ +2\cos(\omega_2 - \omega_{LO})t + \cos(2\omega_1 t) \\ +\cos(2\omega_2 t) + \cos(2\omega_{LO} t) \\ +2\cos(\omega_1 + \omega_2)t + 2\cos(\omega_1 + \omega_{LO})t \\ +2\cos(\omega_2 + \omega_{LO})t + 3 \end{bmatrix} \quad (4.15)$$

As we know, the BPD circuitry is configured to execute a differential function at the final output of the BPD. Thus, the photocurrents of both photodiodes are subtracted as shown below;

$$I_{out}(t) = I_{PD1}(t) - I_{PD2}(t) \quad (4.16)$$

By substituting equations (4.14) and (4.15) into equation (4.16), the outcome can be achieved. It can be noticed from the equation (4.17) that the beat frequencies of Two-Tone signals ($\omega_1 \pm \omega_2$) are eliminated, and only the beat frequencies of input Two-Tones and LO signal ($\omega_1 \pm \omega_{LO}$; $\omega_2 \pm \omega_{LO}$) remain.

$$I_{out}(t) = -2m^2\Re_1\Re_2 P_C \begin{bmatrix} 2\cos(\omega_1 - \omega_{LO})t + 2\cos(\omega_2 - \omega_{LO})t \\ +2\cos(\omega_1 + \omega_{LO})t + 2\cos(\omega_2 + \omega_{LO})t \\ +\cos(2\omega_{LO} t) + 1 \end{bmatrix} \quad (4.17)$$

4.3 Simulation Modelling and Results Analysis

Initially, the proposed novel model is mathematically developed to validate the distortion frequency cancellations in the system. Later, the model is simulated in a VPI Photonic simulation software, to visualise the implementation of the proposed photonic mixer. VPI software provides an image of the proposed model closest to the reality, and it helps to identify the real-life implications on the system. We shall discuss the VPI implemented design in this section and the results recorded from this software.

Table 4.1: Parameters of GaAs Mach Zehnder Modulator

Parameters	MZM1	MZM2
RF Vπ (V)	3.1	3
DC Vπ (V)	10.3	10.4
Extinction Ratio (dB)	29.9	36.1
Insertion loss (dB)	9.2	9.3

As shown in Figure 4.1, two RF signals are combined and modulated on a first independent Mach Zehnder modulator (MZM), and a LO signal is modulated on a second MZM. The parameters used in the simulation model for the MZM are based on a real GaAs device which is listed in Table 4.1. The half-wave voltage for the RF electrode and DC electrodes are represented as RF Vπ and DC Vπ, respectively. Both MZMs have slightly different parameters, which is usually due to a fabrication default. A Continuous Wave (CW) laser is set to a wavelength of 1550nm with a linewidth of 170kHz, relative intensity noise (RIN) of -155dB/Hz, and the output power of 100mW (20dBm). The laser parameters are taken from the Gooch & Housego laser module, EM650-193400-100-PM900-FCA-NA. The laser beam is equally divided into two paths by using an optical 50:50 polarisation-maintained coupler, and each path is traversed to each MZM link. The output of the first MZM is similarly split by another 50:50 optical coupler, where the one output beam travels toward the PD1 (PD1) via a variable optical attenuator (VOA). The second output beam from split coupler is combined with the output optical beam from the second MZM. An optical coupler combines both fields. This combined beam is transmitted to the PD2 of a BPD. The optical input of the PD1 is attenuated by a VOA to adjust the optical intensity because by equalising the optical intensity, the oppositely phased distortion products get cancelled out by a BPD. The parameters of balanced

photodetector (BPD) used in the simulation model are taken from a BPD manufactured by Finisar (BPDV2120R-VM-FP).

4.3.1 Analysis of IMD cancellation in a Two-Tone Mixer

The results achieved from the proposed photonic mixer are analysed and compared with the results obtained without linearisation technique. In the proposed photonic mixer, the distortion of interest is the Intermodulation Distortion (IMD) produced due to an interference of the input two-tone radio frequencies, which are being addressed as Two-Tone IMD2 and SHD of the Two-Tone signal. The input Two-Tones used in the simulation model are 9GHz and 9.2GHz, whereas the Local Oscillator signal used is 11GHz. The amplitude of both input tones is set to 10dBm, and that of LO is set to 24dBm.

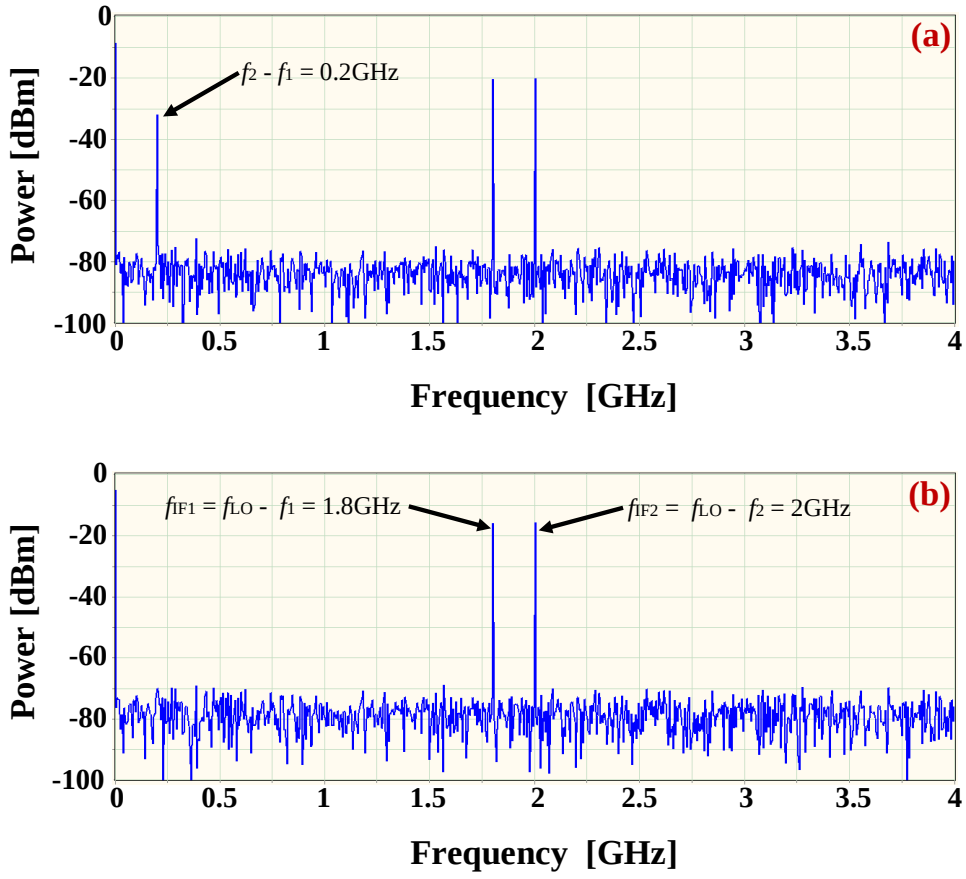

Figure 4.2: Electrical Spectrum at the output of BPD; (a) Mixer without Linearisation; (b) Mixer with Linearisation

Figure 4.2 illustrates the existence of Intermediate Frequencies and the Two-Tone IMDs at the output of the BPD. Two-Tones 9GHz and 9.2GHz are down-converted to produce 1.8GHz and 2GHz, which are the beating between LO and RF, as shown in Figure 4.2. An ideal mixer should only down-convert or up-convert the input RF signals with respect to a LO signal, and no other beat frequencies should exist in the spectrum. However, the beat frequencies between the input RF signals are also nonlinearly generated at a frequency of 0.2GHz (200MHz), as are shown in Figure 4.2(a), and at 18.2GHz as shown in Figure 4.3(a). These frequencies can limit the mixer performance and can interfere with the required signal in the ADC circuit. Therefore, the proposed method eliminates these beat frequencies (Two-Tone-IMD2) and makes the system highly efficient by down-converting multiple RF signals simultaneously, as shown in Figure 4.2(b).

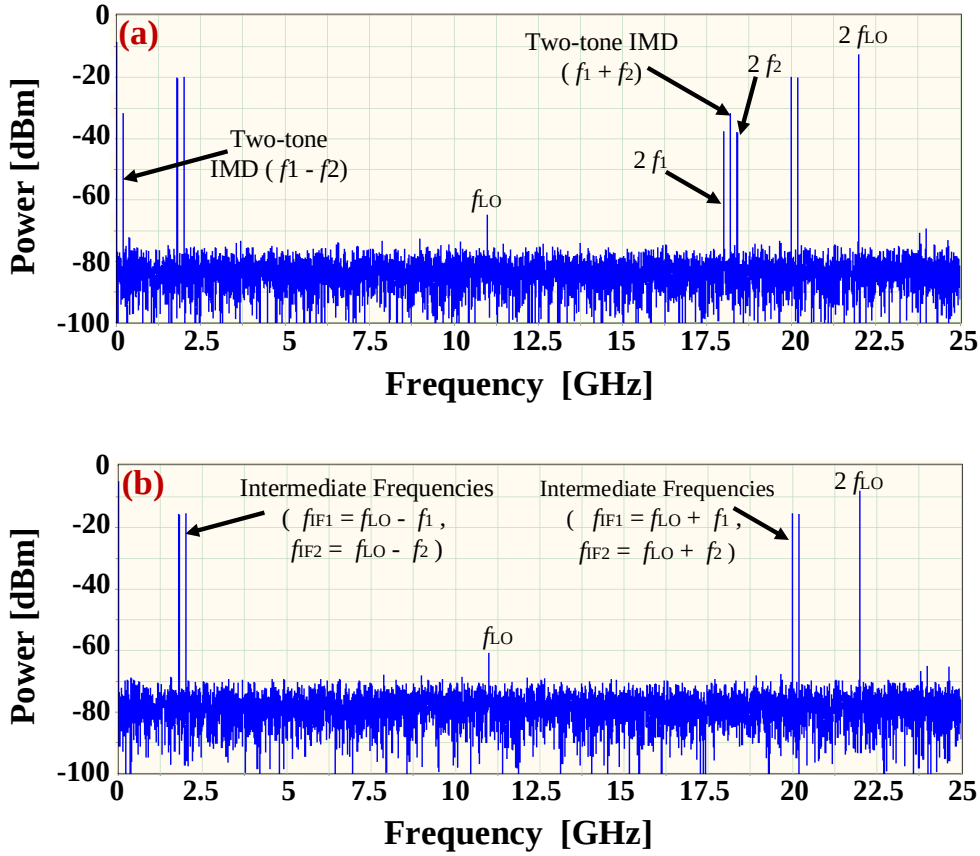

Figure 4.3: Full RF spectrum at the BPD; (a) without Linearisation technique; (b) with Linearisation technique

From Figure 4.3, the upper side of the electrical spectrum can be observed, and the second-order distortion products generated from the interference of Two-Tones are eliminated by the proposed method. In Figure 4.3 (a), dual parallel MZM structure is used with two input RF signals and one LO signal [101]. However, the beat between the input RF signals is eliminated; also, the second-order of the input RF signals have been removed simultaneously.

4.3.2 Adjustment of Optical Intensity in Path 1

The cancellation of distortion products at the BPD is sensitive to optical intensity mismatch between the fourth optical beam path and the combined beam path of the second and third optical beam. A variable optical attenuator is used to adjust the intensity in path 1 by Δα slightly. In Figure 4.4, the effect on the amplitude of output frequencies is noticed by varying the optical attenuation. In the simulation model, maximum suppression of Two-Tone-IMD was achieved at an attenuation in each optical path of 3.2dB. By shifting the attenuation away from the set point that causes an increase in the amplitude of the Two-Tone-IMD as can be seen from Figure 4.4.

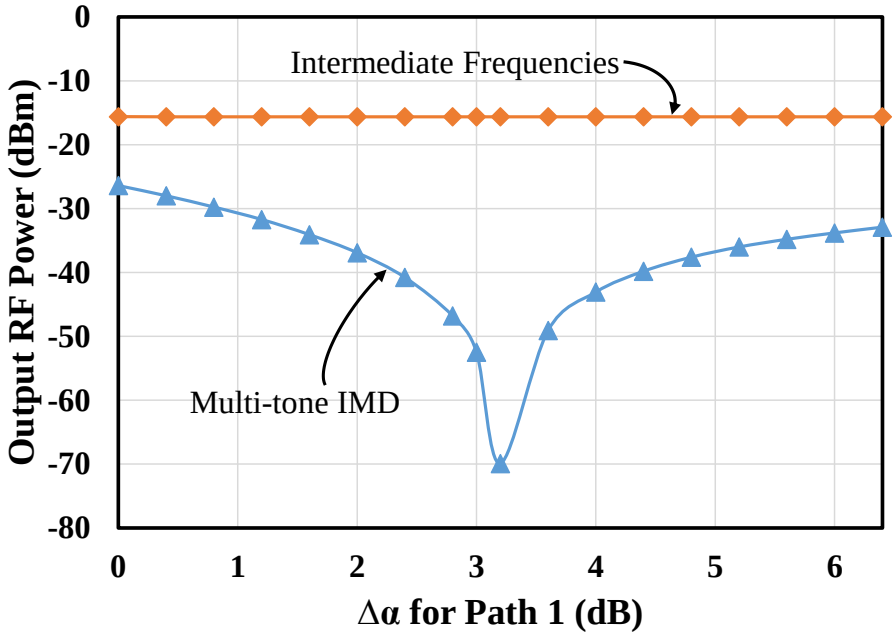

Figure 4.4: Elimination of Two-Tone IMDs with reference to optical path intensity mismatch

4.3.3 Spurious-free Dynamic Range Analysis

The spurious-free dynamic range is the primary measuring technique for the linearisation of an optical link. By plotting this graph, the performance of the intermodulation distortions can be predicted at various RF power ranges that are sometimes not physically possible. In the proposed model, the intermodulation distortion is being suppressed, which are labelled as Two-Tone-IMD2 and IMD3-IF in the Figure. 4.5. The Two-Tone-IMD2 is the second-order intermodulation distortion produced by nonlinear interaction of Two-Tone input RF signals (f_1, f_2), and this can interfere with the actual IF signals ($f_{IF1} = f_{LO} - f_1$, $f_{IF2} = f_{LO} - f_2$). IMD3-IF is the third-order intermodulation distortion, which is generated by the input RF signals and the LO signal. They generally lie close to the IF signals and they are represented as $2f_2$-f_1-f_{LO} and $2f_1$-f_2-f_{LO}.

Figure 4.5 presents the performance of IMD3-IF and Two-Tone-IMD2, and at a noise floor of -170dBm/Hz, IMD3-IF and Two-Tone-IMD2 of 114.2dB.Hz$^{2/3}$ and 89dB.Hz$^{1/2}$ are achieved, respectively. However, the noise floor level is generally higher than -170dBm/Hz, which is because EDFAs and high-power input RF signals are used. As we know, to get a high conversion efficiency, the EDFA amplification may be compensated by high input RF signal power. It should also be stated that increasing input RF power also has complications on the system, as it may over-modulate the signal and nonlinearities become active. So, the solution to these bottlenecks is to use an amplified spontaneous emission (ASE) filter with an EDFA, and this way the need for high input RF power can be obviated and the noise floor can be reduced. It is to be noted that the slope for each entity changed linearly with a change of input RF power. The output power of fundamental signal changes with a factor of one, and that of third-order and second-order changes by a factor of three and two, respectively.

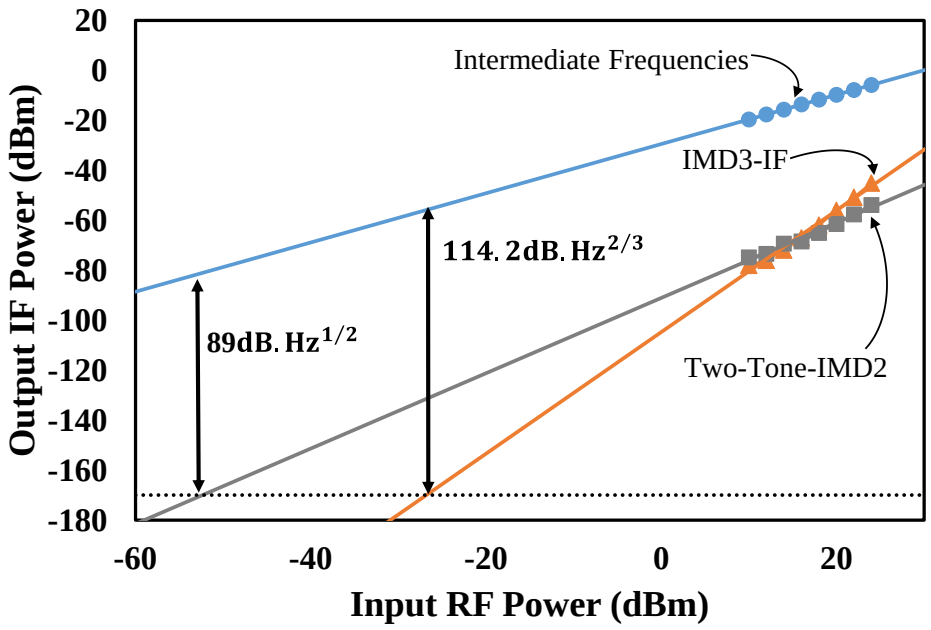

Figure 4.5: The SFDR performance of a Two-Tone photonic mixer

4.4 Summary

In this chapter, a novel method of linearising a Two-Tone photonic mixer has been demonstrated. It was shown that the beat frequencies, which are generated due to nonlinear interference of input Two-Tone RF signals, can be eliminated. In a Two-Tone Mixer, this interference is very problematic, and limits the mixer's performance while digitally processing the down-converted signal. The proposed design of mixer involves a balanced photodetector, which is connected to the two intensity-controlled optical paths (path 1 and path 2). To achieve a perfect cancellation of Two-Tone-IMDs, the optical intensity in Path 1 needs to be attenuated by ~3.2dB. However, the mathematical model shows an ideal cancellation of IMDs based on the phase relation of the frequency components. The model was simulated in a VPI photonics software, and the results were analysed. It was discovered that the Two-Tone photonic mixer could also down-convert a single-tone RF signal and the second harmonics generated from a single-tone was eliminated. In a case of Two-Tone input signals, the results were analysed and the SFDR performance for the IMD3-IF and Two-Tone-IMD2 of 114.2dB.$Hz^{2/3}$ and 89dB.$Hz^{1/2}$

were achieved, respectively. The above-presented work has been filed for Patent by the Leonardo UK Ltd, under an IP agreement, with a patent application number of GB1900552.9.

Chapter 5

5. Proposed Two-Tone Photonic Mixer with Additional Control Over Second-order Harmonics of LO Signal

5.1 Introduction

The linearisation of a Two-Tone photonic mixer was discussed in Chapter 4, and it was noted that Second-order Intermodulation Distortion of Two-Tone Signals (Two-Tone IMD2) could be eliminated by precisely balancing the optical path intensities. However, the model is incapable of eliminating the second-order harmonics Distortion (SHD) of a Local Oscillator signal (2LO), which consumes system bandwidth, and it can be problematic in an up-conversion process, as it lies close to the Intermediate Frequencies. In this chapter, a new design will be discussed for the elimination of Two-Tone IMD2 as well as SHD of the LO signal. Considering the applications of a mixer in aerospace or electronic warfare (EW) systems, where the incoming frequencies are usually unknown. So, a mixer must be capable of handling multiple incoming frequencies, and the interference generated from incoming frequencies must be minimised or removed to process the down-converted signal by the electronic devices.

A newly proposed method of eliminating Two-Tone IMD2 and 2LO, in the photonic mixer is mainly influenced by the design of a novel photonic mixer discussed in the previous chapter. However, this model holds an additional advantage of cancelling out 2LO from the output RF spectrum. This novelty is achieved by incorporating an additional laser beam of wavelength 1540nm and multiplexed with the laser beam of wavelength (1550nm). The multiplexed optical beam is only processed through the second MZM, where a LO signal is being modulated over both optical carrier

wavelengths (1550nm and 1540nm). The output from the second MZM is referred to as a second optical beam comprises two optical wavelengths, as shown in Figure 5.1. A first MZM is adapted to modulate the input Two-Tone signals over a laser wavelength of 1550nm, and the output beam of first MZM is referred to as a first optical beam. An optical splitter is then arranged to split the first optical beam to third and fourth optical beams. The fourth optical beam is sent to the first photodiode (PD1) of a BPD via a variable optical attenuator (VOA), which adjusts the optical intensity of the optical path, named as Path 1. A third optical beam is combined with a second optical beam, and then the combined beam faces a demultiplexer (De-MUX), which splits the two optical wavelengths apart into two optical paths, named as Path 2 and Path 3. Path 2 comprises of a combined second optical beam and third optical beam over an optical wavelength of 1550nm. The second photodiode (PD2) of a BPD is arranged to receive the optical beam from Path 2. The differential circuitry of the BPD combines the received beams at both PD1 and PD2 to form a final electrical signal.

After demultiplexing of the optical signal, path 3 receives an optical beam of wavelength 1540nm, which has been modulated by a LO signal. An additional photodetector (PD3) is arranged to form an opto-electric conversion of an optical signal received from path 3. The output electrical signal representative of the LO signal becomes the first input of subtractor circuitry e.g. implemented by a differential amplifier, the output of the balanced photodetector (BPD) forms a second input of the subtractor circuitry. It is to be noted that the subtractor circuitry must include an additional 180^{o} phase shifter at either input to form an additional function. The subtractor circuitry or a differential amplifier is arranged to provide an electrical signal at its output, corresponding to the addition between the signals received at its inputs. The output of the subtractor circuitry may form an input to the ADC.

The advantage of using the second laser wavelength (1540nm) is to modulate the LO signal in a second MZM, which as a result generates a SHD of LO (2LO) at the first input of subtractor circuitry. Identical SHD of LO (2LO) exists in the second input of subtractor circuitry, which gets eliminated as a result of the subtraction process. It is to be noted that the second modulator is arranged to modulate the LO signal over both transmitted wavelengths (1550nm and 1540nm) simultaneously.

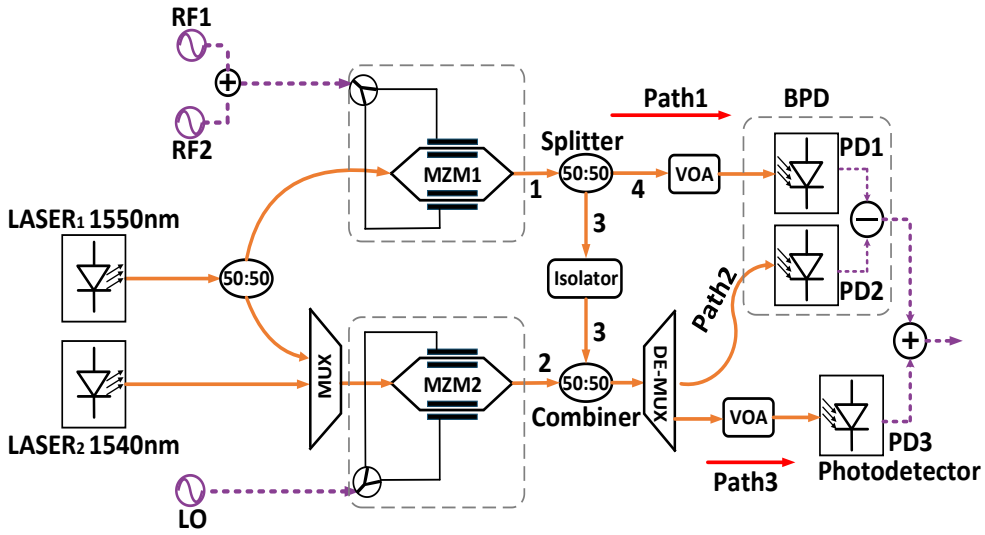

Figure 5.1: Schematic Diagram of a novel Two-Tone Photonic Mixer with 2LO suppression.

5.2Analysis of a Two-Tone Mixer

In this section, the proposed model is theoretically explained, and the cancellation of Two-Tone IMD2 and SHD of LO (2LO) are mathematically validated. In the model, two laser sources of different wavelengths are used, and the electric field of laser with 1550nm wavelength is represented as $E_c(t) = E_c e^{j\omega_c t}$, whereas the second laser of 1540nm wavelength is mathematically expressed as $E_c'(t) = E_c' e^{j\omega'_c t}$. The light beam from the first laser is split equally to feed the first half to the first MZM (MZM_1) and the other half to the second MZM (MZM_2) through a multiplexer (MUX). A MUX also receives the laser beam from second laser, and then a combined output from the MUX is processed by the MZM_2. The Two-Tone input

RF signals (represented as ω_1 and ω_2) are used to modulate the $E_c(t)$ at MZM$_1$. In a second MZM (MZM$_2$), the LO signal of frequency ω_{LO} is modulated over the two multiplexed wavelengths (ω_c and ω'_c). The modulated signals in each MZM are further optimised by applying an appropriate DC bias voltage to achieve maximum suppression of the optical carrier. The bias conditions of the first and second MZM are set to NULL, which is equivalent to a half-wave voltage (V_π) of the DC electrode. The modulation index of the modulating signal is the ratio of RF voltage (V_{RF}) and half-wave voltage (V_π). Assuming the input RF and LO signals have the same amplitude, then it can be expressed as $m = \pi\, {V_{RF}}/{V_\pi}$. The applied voltages on each electrode of the MZM$_1$ and MZM$_2$ are expressed below;

$$\left.\begin{aligned} V_{11}(t) &= m[\cos(\omega_1 t) + \cos(\omega_2 t)] + \pi \\ V_{12}(t) &= m[\cos(\omega_1 t) + \cos(\omega_2 t)] \\ V_{21}(t) &= m[\cos(\omega_{LO} t)] + \pi \\ V_{22}(t) &= m[\cos(\omega_{LO} t)] \end{aligned}\right\} \tag{5.1}$$

In equation (5.1), $V_{11}(t)$ and $V_{12}(t)$ represents the voltages applied on upper and lower arms of the MZM$_1$, correspondingly. Whereas, $V_{21}(t)$ and $V_{22}(t)$ represents the voltages for MZM$_2$. However, the DC bias voltages for $V_{11}(t)$ and $V_{21}(t)$ are set to π, which represents the phase difference between the MZM electrodes, occurred by applying a DC voltage equivalent to Vπ. The output field of MZM$_i$ (i = 1, 2) are generally expressed as $E_{out\,i}(t) = E_c e^{j\omega_c t}\left[e^{-jV_{i1}t} + e^{-jV_{i2}t}\right];\ (i = 1, 2)$, whereas for the second laser of wavelength ω'_c, the output beam from the MZM$_2$ can be expressed as $E'_{out\,2}(t) = E'_c(t)\left[e^{-jV_{21}t} + e^{-jV_{22}t}\right]$. These electric fields can be further simplified by substituting equation (5.1), and after applying the Taylor series, the transfer function for each MZM can be expressed as below;

$$E_{out1}(t) = jE_C \left[\begin{array}{l} m^3 \left(\begin{array}{l} \frac{\cos(\omega_1 - 2\omega_2)t}{4} + \frac{\cos(\omega_1 + 2\omega_2)t}{4} \\ + \frac{\cos(2\omega_1 + \omega_2)t}{4} + \frac{\cos(3\omega_1)t}{12} \\ + \frac{\cos(3\omega_2)t}{12} + \frac{\cos(2\omega_1 - \omega_2)t}{4} \\ + \frac{3\cos(\omega_1)t}{4} + \frac{3\cos(\omega_2)t}{4} \end{array} \right) \\ -m\left(2\cos(\omega_1 t) + 2\cos(\omega_2 t)\right) \end{array} \right] \quad (5.2)$$

Equation (5.2) shows the output electric field of MZM_1, where the Two-Tone signals and their third-order intermodulation distortions (IMD3) and third-order harmonic (THD) can be observed. Even-order products have been eliminated due to the DC bias condition being at Vπ. However, in a case of MZM_2, two different wavelengths are being modulated with the LO signal, and the output electric field is being expressed based on different carrier wavelength, as below;

$$E_{out2}(t) = jE_C \left\{ \begin{array}{l} -m\left(2cos(\omega_{LO}t)\right) \\ +m^3\left(\frac{\cos(3\omega_{LO}t)}{12} + \frac{\cos(\omega_{LO}t)}{4}\right) \end{array} \right\} \quad (5.3)$$

$$E'_{out2}(t) = jE'_C \left\{ \begin{array}{l} -m\left(2cos(\omega_{LO}t)\right) \\ +m^3\left(\frac{\cos(3\omega_{LO}t)}{12} + \frac{\cos(\omega_{LO}t)}{4}\right) \end{array} \right\} \quad (5.4)$$

Similarly, in equation (5.3) and equation (5.4), the modulation of the LO signal can be seen. Equation (5.3) depicts the modulation of LO signal over an optical carrier of function $E_C(t)$, whereas the equation (5.4) shows the modulation of LO over a second wavelength of a transfer function $E'_C(t)$. From equation (5.2, (5.3) and (5.4), it can be observed that a NULL condition has eliminated the optical carrier and even-order distortions. A combined second optical beam and the third optical

beam is propagated through the Path 2, and the transfer function can be expressed as;

$$E_{out12}(t) = jE_C \begin{bmatrix} m^3 \left(\begin{array}{l} \frac{\cos(\omega_1 - 2\omega_2)t}{4} + \frac{\cos(\omega_1 + 2\omega_2)t}{4} \\ + \frac{\cos(2\omega_1 + \omega_2)t}{4} + \frac{\cos(3\omega_1)t}{12} \\ + \frac{\cos(3\omega_2)t}{12} + \frac{\cos(3\omega_{LO})t}{12} \\ + \frac{\cos(2\omega_1 - \omega_2)t}{4} + \frac{3\cos(\omega_1)t}{4} \\ + \frac{3\cos(\omega_2)t}{4} + \frac{3\cos(\omega_{LO})t}{4} \end{array} \right) \\ -m\left(2\cos(\omega_1 t) + 2\cos(\omega_2 t) + 2\cos(\omega_3 t)\right) \end{bmatrix} \quad (5.5)$$

From equation (5.5), the intermodulation of Two-Tones with the LO signal can be achieved. This electric field is then received by the PD2 of the BPD, and a photocurrent of $I_{PD2}(t)$ is produced. Similarly, the electric field of MZM_1 is detected by the PD1 of the BPD, and a photocurrent $I_{PD1}(t)$ is generated, which can be expressed as below;

$$I_{PD1}(t) = 2m^2 \Re_1 P_C \begin{bmatrix} 2\cos(\omega_1 - \omega_2)t + \cos(2\omega_1 t) \\ +\cos(2\omega_2 t) + 2\cos(\omega_1 + \omega_2)t + 2 \end{bmatrix} \quad (5.6)$$

$\Re_1$ is the responsivity of the PD1 of BPD circuitry. P_C is the optical power from the first laser input to the MZM_1 and MZM_2. The photocurrent at the PD2 of BPD is expressed as;

$$I_{PD2}(t) = 2m^2 \Re_2 P_C \begin{bmatrix} 2\cos(\omega_1 - \omega_2)t + 2\cos(\omega_1 - \omega_{LO})t \\ +2\cos(\omega_2 - \omega_{LO})t + \cos(2\omega_1 t) + \cos(2\omega_2 t) \\ +\cos(2\omega_{LO} t) + 2\cos(\omega_1 + \omega_2)t + 2\cos(\omega_1 + \omega_{LO})t \\ +2\cos(\omega_2 + \omega_{LO})t + 3 \end{bmatrix} \quad (5.7)$$

$\Re_2$ is the responsivity of the PD2 of BPD circuitry The BPD adapts a differential functionality to subtract the photocurrents received at PD1 and PD2. Equation (5.6) and (5.7) are substituted into the following equation to form a differential photocurrent at the output of the BPD.

$$I_{PD12}(t) = I_{PD1}(t) - I_{PD2}(t) \tag{5.8}$$

$$I_{PD12}(t) = -2m^2\Re_1\Re_2 P_C \begin{bmatrix} 2\cos(\omega_1 - \omega_{LO})t + 2\cos(\omega_2 - \omega_{LO})t \\ +\cos(2\omega_{LO}t) + 2\cos(\omega_1 + \omega_{LO})t \\ +2\cos(\omega_2 + \omega_{LO})t + 1 \end{bmatrix} \tag{5.9}$$

As it was discussed in the previous chapter that the output of the BPD includes IF_1, IF_2 and 2LO, and it eliminates the Two-Tone IMD2 and second-order of Two-Tones. Similarly, it can also be achieved in this model as expressed in equation (5.9). The optical Path 3 comprising an optical field $E'_c(t)$ and the LO signal ω_{LO}, which is detected by an independent single diode PD3. The photocurrent produced can be expressed as;

$$I_{PD3}(t) = 2m^2\Re_3 P'_C\left[\cos(2\omega_{LO}t) + 1\right] \tag{5.10}$$

$\Re_3$ is the responsivity of a separate PD3 used for the LO signal detection. P'_C is the optical power from second laser input to the MZM_2. The photocurrent from a PD3 is combined with the resultant output photocurrent of the BPD. The summation is expressed in equation (5.11).

$$I_{out}(t) = I_{PD12}(t) + I_{PD3}(t) \tag{5.11}$$

Equation (5.9) and (5.10) are substituting into equation (5.11) to express the resultant photocurrent as below;

$$I_{out}(t) = -2m^2\Re_1\Re_2\Re_3 P_C P'_C \begin{bmatrix} 2\cos(\omega_1 - \omega_{LO})t + 2\cos(\omega_2 - \omega_{LO})t \\ +2\cos(\omega_1 + \omega_{LO})t + 2\cos(\omega_2 + \omega_{LO})t \end{bmatrix} \tag{5.12}$$

The combined photocurrent $I_{out}(t)$ from equation (5.12) shows that the second-order harmonic of the LO signal $\cos(2\omega_{LO}t)$ has been eliminated, and only the downconverted or upconverted signals are left behind in the electrical spectrum.

5.3 Simulation Results and Analysis

As shown in Figure 5.1, two different laser sources of different wavelengths are used to form a dual multiplexed channel link. The sole purpose of the dual multiplexed channel is to optimise the system for the additional functionality of eliminating 2LO at the receiver. As theoretically discussed in the previous section, the model was then designed in a VPI simulation software to visualise the performance of the proposed model. The results produced from the VPI simulation modelling are known to be close to reality, as demonstrated in the previous chapters. The components used for the implementation of a simulation model are listed in Table 5.1 with their parameters. These parameters are taken from the real devices to envisage the results as it would have taken from an experiment. The components used, other than those listed in Table. 5.1 are Variable Optical Attenuator (VOA), optical splitter/combiners, MUX and De-MUX. The model includes laser λ_1 and λ_2, which has a set RIN of -155dBm/Hz. The modulator MZM_1 is driven by RF signals f_1 and f_2 over a wavelength λ_1, whereas MZM_2 is driven by the LO signal over two wavelengths λ_1 and λ_2. Both modulators are DC biased at V_π to achieve an optical phase variation of π. The optical couplers used in the simulation model has a 50:50 coupling ratio, however, these may be adjusted to optimise the optical intensity match for a perfect distortion cancellation. The optical paths received by the photodiodes are intensity-controlled, which means that the Path 1, Path 2, and Path3 may need to be adjusted by varying attenuation $\Delta\alpha$ to achieve maximum suppression of the desired frequency components.

Table 5.1: Parameters of a Simulation Model

First Laser wavelength		λ_1	1550 nm
Second Laser wavelength		λ_2	1540 nm
Optical Power of both lasers		P_o	20 dBm
RF1 frequency		f_1	9 GHz
RF2 frequency		f_2	9.2 GHz
LO frequency		f_{LO}	11 GHz
MZM1	**RF Half-wave voltage**	$V_{\pi\text{-RF}}$	3.1V
	DC Half-wave voltage	$V_{\pi\text{-DC}}$	10.3V
	Extinction Ratio	ER_1	29.9dB
	Insertion loss	η_1	9.2dB
MZM2	**RF Half-wave voltage**	$V_{\pi\text{-LO}}$	3.2V
	DC Half-wave voltage	$V_{\pi\text{-DC}}$	10.4V
	Extinction Ratio	ER_2	36.1dB
	Insertion loss	η_2	9.3dB
Balanced Photodetector	**Responsivity of first photodiode**	$\Re_1$	0.6A/W
	Responsivity of second photodiode	$\Re_2$	0.63A/W
Responsivity of a single Photodetector		$\Re_3$	0.7A/W

5.3.1 Analysis of 2LO and IMD2 cancellation in a Two-Tone Mixer

Here the results achieved in Chapter 4 for the cancellation of beat frequencies of input RF signals are further investigated. It was noticed in the previous results that 2LO cannot be eliminated, which led to an optimisation in the configuration of a Two-Tone photonic mixer. In the proposed photonic mixer, the distortion of interest is the Intermodulation Distortion (IMD) produced due to an interference of the input

Two-Tone radio frequencies, which are being addressed as Two-Tone-IMD2, SHD of the input Two-Tone signal and SHD of the LO signal. The input Two-Tones used in the simulation model are 9GHz and 9.2GHz, whereas the Local Oscillator signal is 11GHz. The amplitude of both RF input tones is set to 10dBm, and that of LO is set to 24dBm.

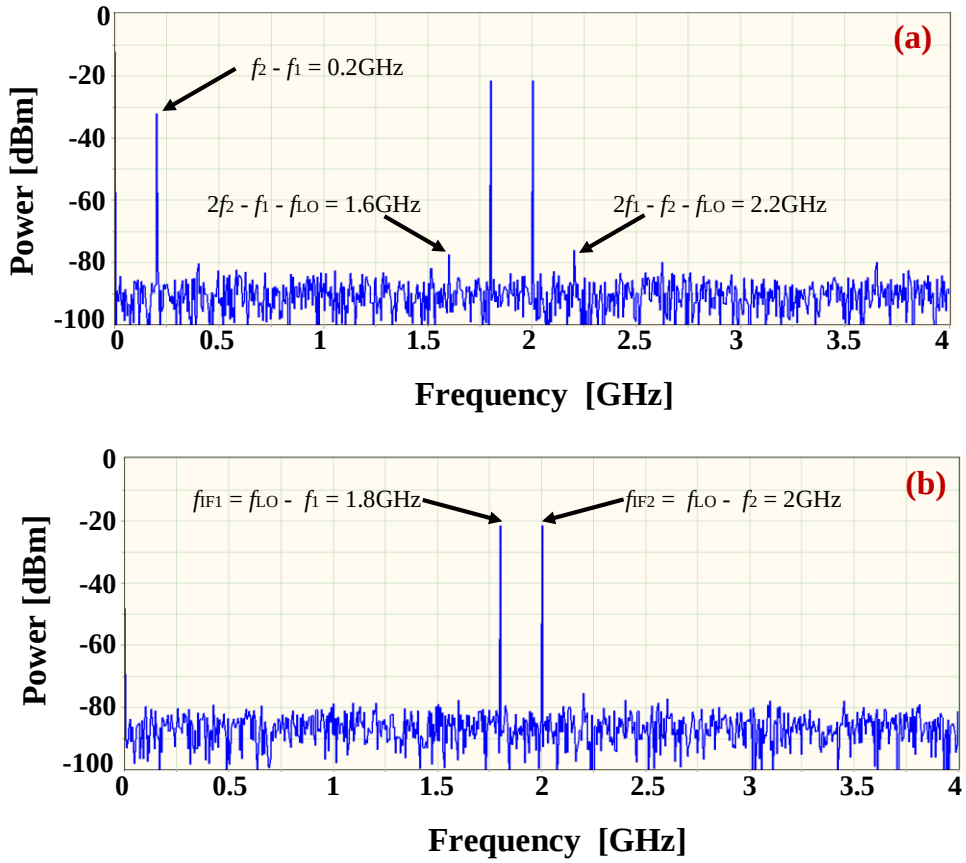

Figure 5.2: Output Electrical Spectrum; (a) Mixer without Linearisation; (b) Mixer with Linearisation technique

Figure 5.2 presents an electrical spectrum of the proposed photonic mixer and a comparison with a conventional photonic mixer based on a Dual-Parallel Mach Zehnder modulator (DPMZM) structure. The input RF signals 9GHz and 9.2GHz are down-converted to 1.8GHz and 2GHz, respectively. However, these input tones produce high-order intermodulation distortion, such as, 0.2GHz (200MHz) and 18.2GHz, which are referred to as Two-Tone IMD2. Furthermore, third-order

intermodulation distortion IMD3 ($2f_2$-f_1, $2f_1$-f_2) also interfere with the LO signal (f_{LO}), and consequently, further IMD3-IF ($2f_2$-f_1-f_{LO}, $2f_1$-f_2-f_{LO}) are produced. The IMD3-IF are significantly suppressed, but the model does not eliminate them. The results from the conventional photonic mixer are shown in Figure 5.2 (a). In Figure 5.2 (b), the result is achieved from the proposed method, which illustrates the elimination of 0.2GHz (Two-Tone IMD2).

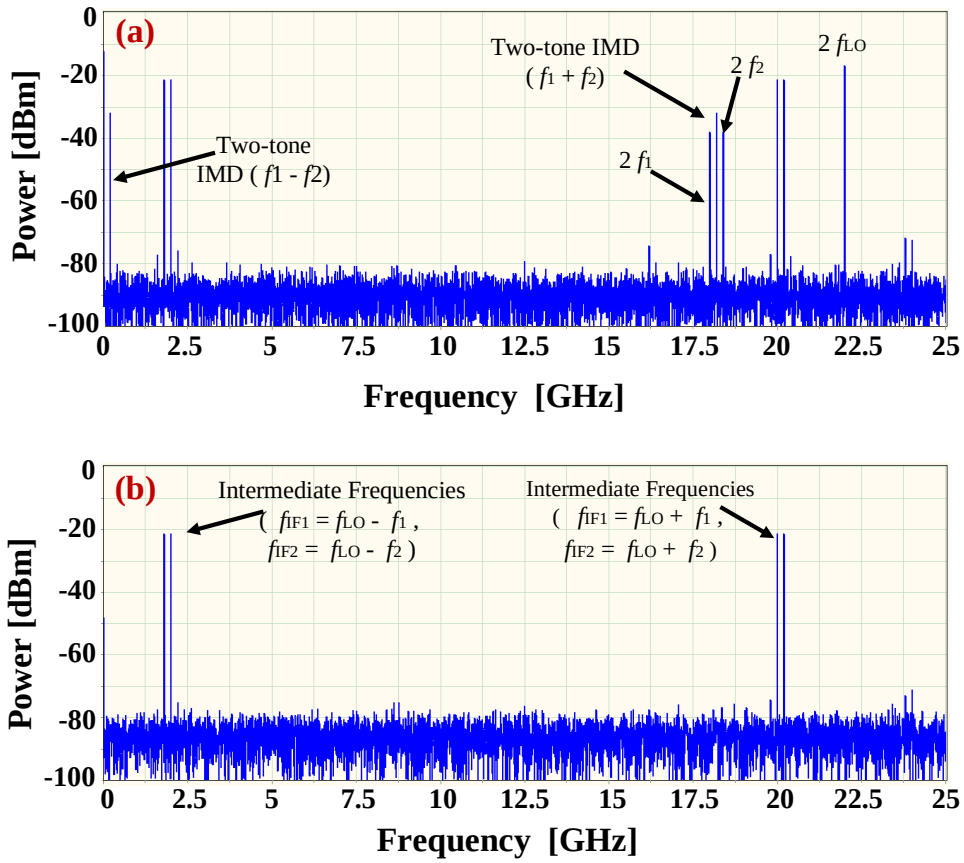

Figure 5.3: Full RF spectrum at the output; (a) without Linearisation technique; (b) with Linearisation technique

As it is well known that a photonic mixer usually produces down-converted IF (f_{LO}-f_1, f_{LO}-f_2) and upconverted IF (f_{LO}+f_1, f_{LO}+f_2) simultaneously. Up-converted IF appears at the higher frequency range, and it is generally surrounded by high-order distortion products as it can be seen from Figure 5.3 (a). In contrast to Figure 5.2, an expanded spectrum is shown in Figure 5.3 to illustrate the upper side of the frequency

band. SHD of Two-Tone signals (18GHz, 18.4GHz) along with the Two-Tone IMD2 (200MHz, 18GHz) are eliminated in Figure 5.3 (b). Additionally, SHD of the LO signal (22GHz) has also been eliminated with the proposed method of a linearised photonic mixer.

5.3.2 Adjustment of Optical Intensity

The above results have been further explored to present the limitation of the model. The model is comprised of three optical paths (Path 1, Path 2, Path 3). Since the model involves the splitting and combining of the optical beams at various points. Therefore, it can imply a mismatch in the intensity of optical signals, and consequently, the perfect elimination of the desired distortion products would not be possible. To overcome this issue, optical attenuators have been placed in the Optical Path 1 and Optical Path 3. The changes in attenuation $\Delta\alpha$ in each path is applied to observe the cancellation of Two-Tone IMD2 and 2LO, as shown in Figure 5.4. It should be noted that $\Delta\alpha$ in Path 3 has an impact on the suppression of 2LO because it adjusts the optical intensity of the sidebands in the Path 3 and potentially matches it with the intensity of 2LO in Path 2. In the simulation model, it was recorded that $\Delta\alpha$ in Path 3 needs to be ~0.67dB for the cancellation of 2LO harmonic. Similarly, $\Delta\alpha$ in Path 1 is optimised to alter the intensity of the sidebands of Two-Tone signals (f_1, f_2). In order to achieve the cancellation of beat frequencies of the Two-Tone signals (f_1, f_2), the intensity of sidebands should match with sidebands falling in Path 2. It was observed that $\Delta\alpha$ in Path 1 needs to be ~6.33dB to suppress the Two-Tone IMDs as shown in Figure 5.4.

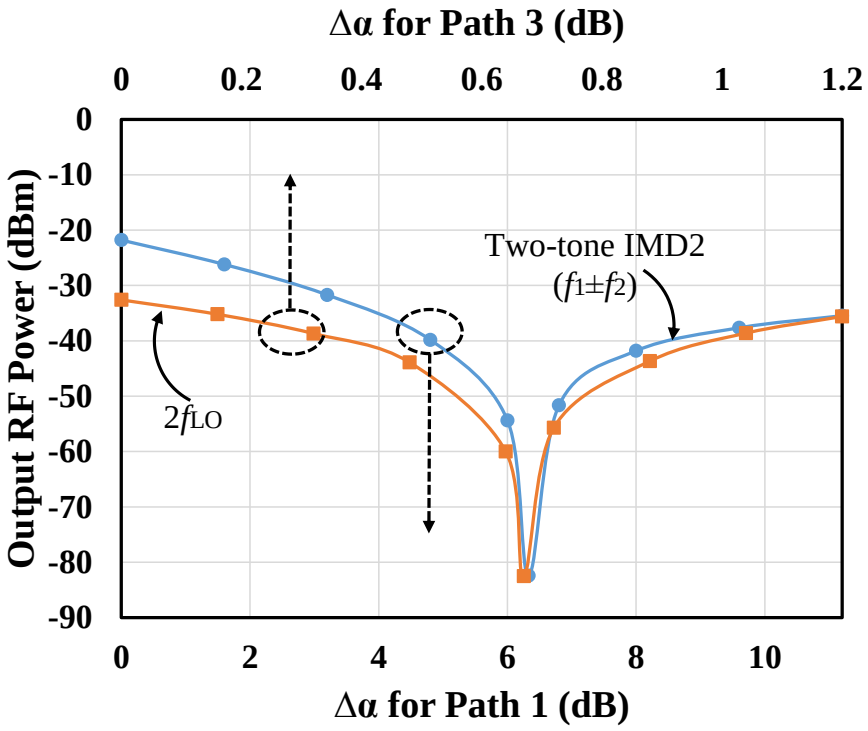

Figure 5.4: Optical Path adjustment

5.3.3 Spurious-free Dynamic Range Analysis

The Spurious-free Dynamic Range (SFDR) performance of the proposed system has been presented. It demonstrates a linearisation of the system, and it presents the dynamic range of Two-Tone IMD2 and IMD3-IF with respect to the noise floor of -170dBm/Hz. In the proposed link, the noise power is mainly limited by shot noise, and the other noise like RIN and ASE (caused by high optical power) are suppressed due to the BPD. In order to maintain the signal to noise ratio, the shot noise must be greater than the RIN and Intensity noise. Due to these reasons, the Noise floor is kept at -170dBm/Hz for the SFDR measurements. SFDR is measured by varying the input power of Two-Tone signals, and the power of the LO signal is kept constant for all measurements. Consequently, the power of the output signals is changed; the change in IF signal was by a factor of 1, whereas, the change in Two-Tone IMD2 and IMD3-IF is by a factor of 2 and 3, respectively. The SFDR of Two-Tone IMD2 is recorded at 106dB.Hz$^{1/2}$ and that of IMD3-IF is 119.5dB.Hz$^{2/3}$, as shown in Figure 5.5.

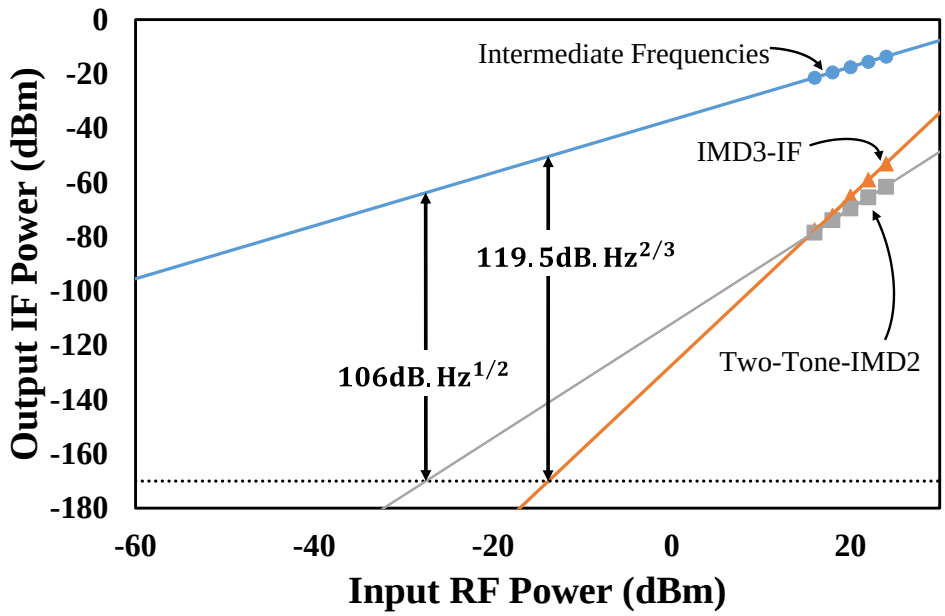

Figure 5.5: SFDR Performance of a linearized Two-Tone Photonic Mixer

5.4 Summary

In this chapter, a further investigation of a method presented in Chapter 4 has been carried out. Previously, the nonlinear distortion in a Two-Tone photonic mixer were eliminated, but the SHD of LO signal was not suppressed. Therefore, the proposed method in this chapter focused on eliminating SHD of the LO signal at the same time as the elimination of Two-Tone-IMD2. Initially, a mathematically model was presented, and then a simulation model was designed. The results achieved from the simulation were suitably analysed and discussed. Additional components used in the proposed model compared to the method in Chapter 4 were an extra laser source of wavelength 1540nm, MUX and De-MUX, and a photodetector PD3. These components were integrated into the proposed Two-Tone Photonic Mixer to specifically eliminate the SHD of LO signal along with Two-Tone IMD2. This integration created an extra optical path (Path 3), which led to a single photodetector PD3. The intensity in Path 3 and Path 1 was adjusted to achieve an optimal

cancellation of nonlinear distortions. Moreover, a slight disturbance in the optical intensity of each path was tested, and it was noted that $\Delta\alpha$ required in Path 1 and Path 3 must be ~6.3dB and ~0.66dB, respectively. Finally, SFDR performance for the nonlinear intermodulation distortions such as Two-Tone IMD2 and IMD3-IF of 106dB.$Hz^{1/2}$ and 119.5dB.$Hz^{2/3}$ were achieved, respectively. The work presented in this chapter has been filed for Patent rights by Leonardo UK Ltd, under an IP agreement, with a patent application number of GB1900552.9.

Chapter 6

6. Conclusion and Future Work

6.1 Conclusion

In order to fulfil the growing demand of transmitting high speed data, the conventional electrical links need to be replaced by radio over fibre RoF systems. RoF systems provides a unique way of transmitting signals, it uses a light source as a carrier to transmit electrical signals from one end to another. Conventionally, coaxial cables have been used between central unit and base stations, but these links incur huge losses and it is impossible for a signal to transmit over a long distance. In contrast, RoF possess a large number of benefits due to its natural properties like large bandwidth of light (in terahertz), low losses, and immunity to an interference from the electromagnetic waves. Due to these benefits, RoF systems are desirable for digital transmission as well as analogue transmission. However, the focus of this research is mainly on analogue transmission links, as it has a great importance in the radar systems, aircraft or debris detection systems, satellite communication links, and many other defence and aerospace applications.

In this thesis, the problems in the Analogue Photonic Link have been identified, and new improved configurations have been proposed to tackle such issues. At first, an in-depth study was undertaken to understand the system weaknesses. It was noticed that RoF system faces an inevitable dispersion from an optical fibre, which can only be compensated by including different dispersion compensation techniques. These fibre dispersion techniques have been reviewed and discussed in Chapter 2. Another important component of the APL is an electro-optic (EO) modulator, and it was understood that EO modulators incur a nonlinear transfer function. Due to this nonlinear behaviour, the modulated signal generates harmonics and high-order

intermodulation distortions, which reduces the dynamic range and limit the bandwidth of the link.

Based on the previously reported techniques an improved configuration of APL was proposed in Chapter 3. The model was initially developed in a VPI simulation software and then it was validated by implementing a mathematical and experimental model. The configuration involves two DPMZMs and a balanced photodetector. The principle used for the linearisation of APL was to suppress the optical carrier at the modulator and transmit the low biased modulated signal through an optical fibre toward the receiver. Both DPMZMs were set to operate at a minimum operating point so that an optical carrier can be eliminated. Another optical link was used to transmit the optical carrier signal directly from the laser source to the receiver. Consequently, IMD3 was suppressed and S/I ratio was increased. Additionally, the even-order distortion products (SHD, IMD2) were eliminated by using a BPD at the receiver. Hence, a multi-octave APL system was achieved. A single RF channel demonstrate a significant increase of Second-order Spurious-free Dynamic Range (SFDR2) and Third-order Spurious-free Dynamic Range (SFDR3) at 115dB.$Hz^{1/2}$ and 127dB.$Hz^{2/3}$, respectively. Same configuration was optimised for dual RF channels, and a mathematical model and experimental model was presented in Chapter 3. Therefore, the SFDR2 and SFDR3 for dual RF channel was measured at 108.5dB.$Hz^{1/2}$ and 110dB.$Hz^{2/3}$, respectively.

Microwave photonic mixers were investigated, and it was noticed that existing MPMs are vulnerable to the distortion products generated by multiple input RF signals. Conversion of multiple microwave signals simultaneously has serious consequences on the performance of a mixer, which is limited by not only IMDs but also the cross-modulation distortions. The self-beating between the input RF signals were successfully eliminated by a proposed novel technique presented in Chapter 4. This model was implemented in a VPI simulation software and the results were

analysed. Later, a mathematical model was created to realise the cancellation of distortion products. This technique involves two single MZM, where one was used to modulate input multiple RF signals and the other MZM was used for modulating the LO signal. The output of first MZM was split into two optical paths; one gets detected by a first photodiode of BPD, and second path combined with the output of second MZM to form a mixed signal. The combined signals were detected by the second photodiode. Hence the common distortion products were eliminated. As a result, the electrical spectrum was linearised, and the bandwidth of ADC was improved. Nevertheless, the proposed configuration could not eliminate the distortions related to the LO signal and the SFDR2 and SFDR3 of 89dB.$Hz^{1/2}$ and 114.5dB.$Hz^{2/3}$ was achieved, respectively.

To overcome the reported issue in a technique proposed in Chapter 4, a further investigation was undertaken to eliminate the distortion products related to the LO signal. A similar configuration was implemented in VPI simulation software, but an additional optical channel was created to modulate the LO signal at a second wavelength (1540nm). Due to an additional channel wavelength, an additional photodetector was used to detect the same distortion as they existed in previously mentioned configuration (Chapter 4). On combining the two electrical outcomes from both optical channels, the self-beating between input multiple signals and harmonics of the LO signals were eliminated. The mathematical model has been shown in the Chapter 5. The results achieved from the simulation model were analysed and the SFDR2 and SFDR3 of 106dB.$Hz^{1/2}$ and 119.5dB.$Hz^{2/3}$ was reported, respectively.

The outcome from the Chapter 3 has been sent for publication in two different journals and currently awaiting a decision. The proposed structures reported in the Chapter 4 and Chapter 5 have been submitted for patent grant, which is in a process of being published.

6.2 Future Work

The undertaken research has a great potential for further investigation in order to improve the performance and optimise the system for different applications. The prime focus of the proposed research in this thesis was to eliminate the distortion products in an Analogue Photonic Link (APL). However, the implementation of this system can be achieved by applying digital signals such as Quadrature Amplitude Modulation (QAM).

A linearisation model proposed in the Chapter 3 uses a short haul fibre, which needs to be tested for long haul transmission. Ideally, the APL was configured to make it viable for the applications that does not require long fibre links such as APL links deployed in an aircraft or a space station, and the short (few 100 metres apart) links between antennas and base stations. The practicality of this model will need to be tested for long haul applications like links between the central stations and base stations. The model will also need to be optimised for the digital signal transmission. Besides, the dual parallel modulation links will also need to be optimised in order to achieve a perfect balance in its optical arms. A further investigation may be required to match the extinction ratio of each arm or sub MZM.

A novel design was implemented for the linearisation of a multi-tone Microwave Photonic Mixer (MPM), which will need an experimental validation. The implication of optical intensity mismatch in the optical paths would be addressed. It was discovered that adjusting the optical attenuation in optical paths requires an automated system. This brings about another opportunity to design and develop an automated/adaptive attenuator, which will adjust the attenuation desirable for the IMD cancellation. Two independent MZMs used in the proposed configuration would be further investigated for the integration of both chips onto a single chip. The fabrication process of an MZM will be explored, which will potentially include two optical outputs; one output from an integrated optical splitter at first MZM output,

and second output from an integrated optical combiner at the output of second MZM and first MZM. At the receiver end, an in-depth study will need to be carried out. Currently, only balanced photodetector based on two photodiodes are available, however, further research would be done to investigate the integration of three photodiodes in a singular circuitry. Additionally, in a down-conversion or up-conversion process, an image frequency of Intermediate Frequency appears at the output, which is usually filtered out by bandpass filters. It would be appropriate to eliminate the image frequency by innovating the design of the MPM.

Publications

Published papers:

- Fadil Paloi, Taimur Mirza, Shyqyri Haxha, Optimisation of dispersion compensating in a long-haul fibre for RF transmission of up to 100 Gbit/s by using RZ and NRZ formats, in Optik - International Journal for Light and Electron Optics, Volume 131, February 2017, Pages 640-654.

- Fadil Paloi, Shyqyri Haxha, Taimur N Mirza, Mohammad Alom, "Microwave Photonic Downconversion With Improved Conversion Efficiency and SFDR," in IEEE Access, vol. 6, pp. 8089-8097, 2018.

- Shemsi Shaqiri, Shyqyri Haxha, and Taimur Mirza, "Elimination of Odd and Even Intermodulation Distortions of Analogue Microwave Photonics Link based on GaAs MZMs," in Optics Express, vol. 28, pp. 17521-17531, 2020.

Papers under review:

- Taimur Mirza, and Shyqyri Haxha, "A Linearized Analogue Microwave Photonic link with an Eliminated Even-order Distortions," in IEEE Systems Journal.

- Taimur Mirza, Shyqyri Haxha, and Amar Aggoun, "A Multi-Octave Dual-Channel Analogue Photonic Link over a Single Optical Wavelength with High Efficiency," in IEEE Systems Journal.

Patent Applications:

- Taimur Mirza, Shyqyri Haxha, and Ian Flint, "A Mixer", Patent application number GB1900552.9, 15th January 2019.

- Ian Flint, Taimur Mirza, and Shyqyri Haxha, An electro-optic modulator", Patent application number GB1821175.5, 24th December 2018.

References

[1] W. M. Steuart, T. C. Martin, A. V. Abbott, W. Mayer (Jr.), “Telephones and Telegraphs: 1902,” By United States. Bureau of the Census.

[2] J. P. Dakin, R. G. W. Brown, “Optical Transmission,” in Handbook of Optoelectronics, New York: Taylor & Francis, 2006.

[3] G. P. Agrawal, “Fibre-optic Communication systems”, 4th Edition, New York, Wiley, 2012.

[4] S. V. Kartalopoulos, "DWDM Networks, Devices and Technology", Wiley-Interscience, Piscataway, New Jersey, pp. 270-290, 2003.

[5] A.J. Cooper, "Fibre/radio' for the provision of cordless/mobile telephony services in the access network," in Electronics Letters, vol.26, no.24, pp.2054-2056, 22 Nov 1990

[6] A. J. Seeds, K. J. Williams, "Microwave Photonics," in Journal of Lightwave Technology, vol. 24, no. 12, pp. 4628-4641, Dec. 2006.

[7] H. B. Kim, "Radio over fibre architecture," Electronic and Information Technology, University of Berlin, Berlin, M.Sc. thesis, Chapter 3, 2005.

[8] X.N. Fernando, “Radio over fibre for wireless communications,” New York, Wiley-IEEE press, 2014

[9] S. Karabetos, S. Mikroulis, E. Pikasis, A. Nassiopoulos, “Radio-Over-Fibre Technology: a brief overview and the work at RDTL,” in International Conference on Telecommunications and Multimedia (TEMU), July 2008

[10] Epl/103. (2017). Transmitting equipment for radiocommunication. Radio-over-fibre technologies and their performance standard. System applications of radio over fibre technology. (Accessed on 31st January 2020)

[11] T. S. Rappaport, "Wireless communication principles and practice", Prentice Hall, Upper Saddle River, New Jersey, pp. 14-17, 1996.

[12] D. Wake, D. Johansson and D. G. Moodie, "The passive picocell - a new concept in wireless network infrasructiure", electron. Lett., vol. 33, pp. 404-406, 1997.

[13] International Civil Aviation Organization, International Standards and Recommended Practices, Annex 10 Aeronautical Telecommunications, Vol. IV, “Surveillance and Collision Avoidance Systems”, July 2014.

[14] C. H. Cox, “Analogue Optical Links: Theory and Practice,” Cambridge University press, 2004.

[15] C. Rumelhard, C. Algani, A. Billabert, “Microwave Photonic Links: Components and Circuit,” John Wiley and Sons, 2011.

[16] T. E. Darcie, and G. E. Bodeep, “Lightwave subcarrier CATV transmission system,” in IEEE Trans. Microwave Theory Tech. MIT-38, 524-533, 1990

[17] R. Olshansky, V. A. Lanzisera, S. Su, R. Gross, A. M. Forcucci and A. H. Oakes, "Subcarrier multiplexed broad-band service network: a flexible

platform for broad-band subscriber services," in Journal of Lightwave Technology, vol. 11, no. 1, pp. 60-69, January 1993.

[18] A. J. Seeds, "Microwave photonics," in IEEE Transactions on Microwave Theory and Techniques, vol. 50, no. 3, pp. 877-887, March 2002.

[19] J. Yao, "Microwave Photonics," in Journal of Lightwave Technology, vol. 27, no. 3, pp. 314-335, Feb.1, 2009.

[20] R. W. Ridgway, C. L. Dohrman and J. A. Conway, "Microwave Photonics Programs at DARPA," in Journal of Lightwave Technology, vol. 32, no. 20, pp. 3428-3439, Oct.15, 2014.

[21] J. Capmany and D. Novak, “Microwave photonics combines two worlds,” Nat. Photonics, vol. 1, no. 6, pp. 319-330, June 2007.

[22] F. Bredel, “Millimeter-Wave Radio-over-Fibre Links based on Mode-Locked Laser Diodes,” Kit Scientific Publications, 2013.

[23] Pooja, Saroj, Manisha, “Advantages and limitation of Radio over fibre system,” in IJCSMC, vol. 4, no. 5, pp. 506-511, May 2015.

[24] https://www.vpiphotonics.com/index.php, January 2020.

[25] I. Djordjevic, W. Ryan, B. Vasic, “Fundamentals of Optical Communication,” In Coding for Optical Channels, Springer US, pp. 25-73, 2010.

[26] S. P. Singh, N. Singh, "Nonlinear effects in optical fibres: origin, management and applications," in Progress in Electromagnetics Research, Vol. 73, 249-275, 2007.

[27] N. Massa, “Fibre optic Telecommunication,” in Fundamentals of Photonics, SPIE , Bellingham, Ch. 1.8, pp. 298-299,2008.

[28] C. Yao, “Optical Fibre Dispersion,” Fibre Optics for Sale, California, Sep 2010.

[29] I. Hong, “Dispersion compensation in fibre optic communication systems,” Master’s Thesis, San Jose State University, Paper 2319, 2002.

[30] G. P. Agrawal, “Dispersion-Compensating fibres,” in Fibre-Optic communication systems, John Wiley & Sons, pp 345-394, Oct 2010.

[31] M. A. Saifi, S. J. Jang, “Triangular-profile single-mode fibre,” in Optics Letters, Vol. 7, pp.43-45, Jan. 1982.

[32] S. J. Mihailov, "Fibre Bragg Grating Sensors for Harsh Environments," in Sensors, 12, no. 2, pp. 1898-1918, 2012.

[33] T. Pu, T. Fang, J. Zheng and L. Huang, "Dispersion compansation methods for radio over fibre system," Optical Communications and Networks (ICOCN), 2015 14th International Conference on, Nanjing, 2015, pp. 1-5.

[34] R. S. Kaler, A. K. Sharma, TS. Kamal, "Comparison of pre-, post and symmetric dispersion schemes for 10 GB/s NRZ links using standard and dispersion compensated fibres", in optics Communication, pp.107-123, 2002.

[35] R. Rajani, P. Pal, V. Sharma, “Comparison of Pre-, Post- and Symmetrical-dispersion Compensation Schemes for 10/15 GBPS using Different Modulation Formats at Various Optical Power Levels using Standard and Dispersion Compensated Fibres,” in International Journal of Computer Applications, vol. 50, no. 21, pp.6-13, July 2012.

[36] M. I. Hayee, A. E. Willner, “Pre- and post-compensation of dispersion and nonlinearities in 10-Gb/s WDM systems”, in IEEE Photon. Tech. Lett. 9, pp. 1271, 1997.

[37] O. Arora, A. K. Garg, S. Punia, “Symmetrical dispersion compensation for high speed optical links,” in International Journal of Computer Science Issues, vol 8(6), No.1, 371–376, 2011.

[38] C. Peucheret, “Direct and External Modulation of Light,” Experimental Course in Optical Communication, Department of Photonics Engineering, Technical University of Denmark, November 2009.

[39] “Tutorial Note 5 – Modulation Schemes”, by SHF communication Technologies AG, Berlin Germany, Available at: https://www.shf.de/wp-content/uploads/appnotes/shf_tutorial_note_modulation_schemes.pdf (Accessed on 1st December 2019)

[40] S. S. A. Obayya, S. Haxha, B. M. A. Rahman, C. Themistos and K. T. V. Grattan, "Optimisation of the optical properties of a deeply etched semiconductor electrooptic modulator," in Journal of Lightwave Technology, vol. 21, no. 8, pp. 1813-1819, Aug. 2003.

[41] Ebrahim Mortazy, Ke Wu, Microwave and millimeter-wave losses in conventional optoelectronic devices, Optics & Laser Technology, Volume 43, Issue 4, June 2011, Pages 852-857.

[42] “Introduction to iXBlue Mach Zehnder Modulators Bias Controllers”, iXblue S.A.S Photonic Solutions, France.

[43] N. A. Al-Shareefi et al., "A study in OCS millimeter-wave generation using two parallel DD-MZMs," 2013 IEEE 11th Malaysia International Conference on Communications (MICC), Kuala Lumpur, 2013, pp. 418-421.

[44] S. A. Tretter, “Double Sideband Suppressed Carrier Amplitude Modulation and Coherent Detection,” in Communication System design using DSP algorithms, Springer, 2008.

[45] E. Cura, “Experiment 3: Double Sideband Modulation,” in The university of Texas at Dellas, 2012, Accessed online at: http://www.utdallas.edu/~mtacca/courses/EE3150/Spring-2012/Exp3.pdf

[46] S. A. Tretter, “Single-sideband Modulation and Frequency Translation,” in Communication System design using DSP algorithms, Springer, 2008.

[47] B. Kolner and D. Dolfi, “Intermodulation Distortion and Compression in an Integrated Electrooptic Modulator,” Appl. Optics, vol. 26, no. 17, pp. 3676–3680, Sep 1987.

[48] M. S. Islam, T. B. Chau, and M. C. Wu, “Distributed balanced photodetectors for high-performance RF photonic links," in IEEE Photonics Technology Letters, vol. 11, no. 4, pp. 457-459, April 1999.

[49] Di Peng, Zhiyao Zhang, Yangxue Ma, Yali Zhang, Shangjian Zhang, and Yong Liu, "Broadband linearization in photonic time-stretch analogue-to-digital converters employing an asymmetrical dual-parallel Mach-Zehnder modulator and a balanced detector," in Optics Express, vol. 24, pp. 11546-11557, 2016.

[50] M. Saiful h, T. Chau, S. Mathai, T. Itoh, M. Wu, D. Sivco, and A. Cho, “Distributed balanced photodetectors for broad-band noise suppression,” IEEE Trans.Microw. Theory Tech., vol. 47, no. 7, pp. 1282–1288, Jul 1999.

[51] X Xie, Y. Dai, Y. Ji, K. Xu, Y.Li, J. Wu and J. Lin, "Broadband Photonic Radio-Frequency Channelization Based on a 39-GHz Optical Frequency Comb," in IEEE Photonics Technology Letters, 24 (8), 661-663 (2012).

[52] S. Shaqiri, and S. Haxha, ”Linearisation and Down-Conversion of Microwave Photonics Signal based on Dual-drive Dual-parallel Mach-Zehnder Modulator with Eliminated 3rd Intermodulation and 2nd Distortions,” in Optik, 164103, (2019).

[53] D. A. Hall, “Understanding Intermodulation distortion Measurements,” in Engineering Essentials-Electronics design, October 2013.

[54] X. Meng, “Designing high dynamic range microwave photonic links for radio applications,” in Fibre and Integrated Optics, vol.23, pp1–56, 2004.

[55] C. Henn, “Intermodulation Distortion (IMD),” in Application Bulletin, Burr-Brown, USA, April 1994.

[56] G. Gonzalez, “Microwave Transistor Amplifier: Analysis and Design,” 2nd edition, City: Prentice Hall, 1997.

[57] J. Garcia, S. G. LaJeunesse, D. Bartow, “Measuring Spurious free dynamic range in a D/A converter,” Technical Brief, Intersil, January 1995.

[58] T. Pu, T. Fang, J. Zheng and L. Huang, "Dispersion compensation methods for radio over fibre system," Optical Communications and Networks (ICOCN), 2015 14th International Conference on, Nanjing, 2015, pp. 1-5.

[59] R. S. Kaler, A. K. Sharma, TS. Kamal, "Comparison of pre-, post and symmetric dispersion schemes for 10 GB/s NRZ links using standard and dispersion compensated fibres", in optics Communication, pp.107-123, 2002.

[60] A. Yariv and P. Yeh, Photonics: Optical Electronics in Modern Communications, 6th ed. New York: Oxford University Press, 2007.

[61] W. van Etten, Introduction to Random Signals and Noise. Chisester, West Sussex: JohnWiley & Sons, 2005.

[62] Naval Air warfare Centre, “Receiver Sensitivity/Noise,” in Electronic Warfare and Radar Systems Engineering Handbook, NAWCWD Technical Publication 8347, Fourth Edition, October 2013.

[63] Application note, “Optical Signal-to-Noise Ratio and the Q-Factor in Fibre-Optic Communication Systems,” in Maxim Integrated, 2008.

[64] Z-h. Zhu, S-h. Zhao, Y-j. Li, X-c. Chu, H. Zhang, X. Wang, and G-h. Zhao, “Optimization of optically pre-amplified inter-satellite microwave photonics links,” in Journal of Optoelectronics Laser vol. 24, no. 3, pp. 500-507, 2013. (in Chinese)

[65] W. Zhou, X-h. Zou, W. Pan, L-s. Yan, B. Luo, and B. Lu, “Photonic generation of microwave signals with a 24 multiplied frequency using cascaded Mach-Zehnder modulators and four-wave mixing”, in Journal of Optoelectronics Laser vol. 24, no. 132332 (2013). (in Chinese)

[66] Z. Wang, J-x. Ma, R-j. Zhang, Y-j. Li, Q-q. Zhang, Q. Zhang, R-h. Liu, and J-g. Yu,” Study on direct detection optical OFDM-RoF system based on single-sideband modulation,” in Journal of Optoelectronics Laser, vol. 25, no. 9, pp. 1709-1714, 2014. (in Chinese)

[67] Z. Zhu, S. Zhao, Q. Tan, W. Jiang, Y. Li, X. Li, "A Linearized Optical Single-Sideband Modulation Analogue Microwave Photonic Link Using Dual Parallel Interferometers," in IEEE Photonics Journal, vol. 5, no. 5, pp. 5501712-5501712, Oct 2013.

[68] G. H. Smith, D. Novak, and Z. Ahmed, “Technique for optical SSB generation to overcome dispersion penalties in fibre radio systems”, in Electronic Letter, vol. 33, no. 1, pp. 74–75, Jan. 1997.

[69] Xuan Li, Zihang Zhu, Shanghong Zhao, Yongjun Li, Lei Han and Jing Zhao, “An intensity modulation and coherent balanced detection intersatellite microwave photonic link using polarisation direction control,” in Optics & Laser Technology, vol. 56, pp. 362-366, March 2014.

[70] X. Li, S. Zhao, Z. Zhu, Y. Li, J. Zhao, and Y. Liu, “Dynamic range improvement of broadband microwave photonic links using a linearized single-sideband modulator,” in optics communications, vol. 350, pp. 170-177, April 2015

[71] S.Y. LI, X.P. Zheng, and B.K. Zhou, “Simultaneous multi-wavelength optical SSB generation for WDM radio-over-fibre systems using a DGD element and a polarizer,” in proc. SPIE, vol. 6353 Optical Transmission, Switching, and Subsystems IV, 63532P (19 October 2006).

[72] Z. Zhu, S. Zhao, X. Li, K. Qu, and T. Lin, “A linearized analogue photonic link based on a single z-cut LiNbO3 dual-output Mach Zehnder modulator,” in IEEE Photonics Journal, vol. 9, no.3, pp. 1-10, June 2017.

[73] G. Q. Zhang, X. P. Zheng, S. Y. Li, H. Y. Zhang, B. K. Zhou, “Postcompensation for nonlinearity of Mach–Zehnder modulator in radio-over-fibre system based on second-order optical sideband processing” in Optics Letter, vol. 37, no.5, pp.806–808, 2012.

[74] G. Zhang, S. Li, X. Zheng, H. Zhang, B. Zhou, and P. Xiang, “Dynamic range improvement strategy for Mach-Zehnder modulators in microwave/millimeter-wave ROF links,” Opt. Express 20(15), 17214–17219 (2012).

[75] Y. Cui, Y. Dai, F. Yin, J. Dai, K. Xu, J. Li, and J. Lin, “Intermodulation distortion suppression for intensity-modulated analogue fibre-optic link incorporating optical carrier band processing,” Opt. Express, 21 (20), 23433-23440 (2013).

[76] J. L. Brooks, G. S. Maurer, and R. A. Becker, “Implementation and evaluation of a Dual parallel linearisation system for AM-SCM video transmission,” in Journal of Lightwave Technology, vol. 11, no. 1, pp. 34-41, January 1993.

[77] J. Li, Y. Zhang, S. Yu, T. Jiang, Q. Xie, and W. Gu, "Third-order intermodulation distortion elimination of microwave photonics link based on integrated dual-drive dual-parallel Mach–Zehnder modulator," Opt. Lett., 38 (21), 4285-4287 (2013).

[78] W. Jiang, Q. Tan, W. Qin, D. Liang, X. Li, H. Ma, and Z. Zhu, "A Linearisation Analogue Photonic Link With High Third-Order Intermodulation Distortion Suppression Based on Dual-Parallel Mach–Zehnder Modulator," in IEEE Photonics Journal, 7 (3), 1-8 (2015).

[79] G. Zhu, W. Liu and H. R. Fetterman, "A Broadband Linearized Coherent Analogue Fibre-Optic Link Employing Dual Parallel Mach–Zehnder Modulators," in IEEE Photonics Technology Letters, vol. 21, no. 21, pp. 1627-1629, Nov.1, 2009.

[80] S. Kim, W. Liu, Q. Pei, L. R. Dalton, and H. R. Fetterman, "Nonlinear intermodulation distortion suppression in coherent analogue fibre optic link using electro-optic polymeric dual parallel Mach-Zehnder modulator," in Optics Express, vol. 19, pp.7865-7871, 2011.

[81] S. Li, X. Zheng, H. Zhang and B. Zhou, "Highly Linear Radio-Over-Fibre System Incorporating a Single-Drive Dual-Parallel Mach–Zehnder Modulator," in IEEE Photonics Technology Letters, vol. 22, no. 24, pp. 1775-1777, Dec.15, 2010.

[82] D. Zhu, J. Chen, and S. Pan, "Multi-octave linearized analogue photonic link based on a polarisation-multiplexing dual-parallel Mach-Zehnder modulator," Opt. Express, 24 (10), 11009-11016 (2016).

[83] Y. Wang, H. Zhang, D. Wang, T. Zhou, F. Yang, D. Yang, and X. Zhong, "Microwave Photonic Link With Flexible Even-Order and Third-Order Distortion Suppression," in IEEE Journal of Quantum Electronics, vol. 55, no. 3, pp. 1-9, June 2019.

[84] Q. Tan, Y. Gao, Y. Fan, and Y. He, “Multi-octave analogue photonic link with improved second- and thid-order SFDRs,” in optics communications, vol. 410, no. 1, pp. 685-689, March 2018.

[85] C. K. Sun, R. J. Orazi and S. A. Pappert, "Efficient microwave frequency conversion using photonic link signal mixing," in IEEE Photonics Technology Letters, vol. 8, no. 1, pp. 154-156, Jan 1996.

[86] T. R. Clark and M. L. Dennis, "Photonic downconversion and linearisation of an X-band fibre optic link using optical I/Q demodulation," in Conference on Lasers and Electro-Optics/Quantum Electronics and Laser Science

Conference and Photonic Applications Systems Technologies, OSA Technical Digest Series (CD) (Optical Society of America, 2007), paper CTuAA2.

[87] T. R. Clark and M. L. Dennis, "Experimental Demonstration of Coherent Optical I/Q Demodulation of Analogue RF Signals," in Optical Amplifiers and Their Applications/Coherent Optical Technologies and Applications, Technical Digest (CD) (Optical Society of America, 2006), paper CFA5.

[88] K. E. Alameh, “Frequency downconverter for high-capacity fibre grating based beamformers for phased arrays,” in Electron. Lett., vol. 35, no. 1, pp. 66–67, Jan 1999.

[89] A. Agarwal, T. Banwell, and T. K. Woodward, “Optically filtered microwave photonic links for RF signal processing applications,” in J. Lightw. Technol., vol. 29, no. 16, pp. 2394–2401, Aug 2011.

[90] C.-S. Brès, S. Zlatanovic, A. O. J. Wiberg, and S. Radic, “Reconfigurable parametric channelized receiver for instantaneous spectral analysis,” in Optics Express, vol. 19, no. 4, pp. 3531–3541, Feb 2011.

[91] B. Glance and T. E. Darcie, "An Optical Heterodyne Image-Rejection Mixer," in Conference on Lasers and Electro-Optics, G. Bjorklund, E. Hinkley, P. Moulton, and D. Pinnow, eds., OSA Technical Digest (Optical Society of America, 1986), paper ThU7.

[92] G. K. Gopalakrishnan, R. P. Moeller, M. M. Howerton, W. K. Burns, K. J. Williams, and R. D. Esman, “A low-loss down-converting analogue fibre-optic link,” in IEEE Trans. MTT, vol. 43, pp. 2318–2323, 1995.

[93] G. K. Gopalakrishnan, W. K. Burns and C. H. Bulmer, "A LiNbO3 microwave-optoelectronic mixer with linear performance," 1993 IEEE MTT-S International Microwave Symposium Digest, Atlanta, GA, USA, vol.2, pp. 1055-1058, 1993.

[94] S. J. Strutz and K. J. Williams, "An 8-18-GHz all-optical microwave downconverter with channelization," in IEEE Transactions on Microwave Theory and Techniques, vol. 49, no. 10, pp. 1992-1995, Oct. 2001.

[95] G. Gopalakrishnan, R. Moeller, M. Howerton, W. Burns, K. Williams, and R. Esman, “A low-loss downconverting analogue fibre-optic link,” in IEEE Trans. Microwave Theory Tech., vol. 43, no. 9, pp. 2318–2323, 1995.

[96] C. K. Sun, R. J. Orazi, S. A. Pappert and W. K. Burns, "A photonic-link millimeter-wave mixer using cascaded optical modulators and harmonic carrier generation," in IEEE Photonics Technology Letters, vol. 8, no. 9, pp. 1166-1168, Sept. 1996.

[97] K. P. Ho, S. K. Liaw, and C. Lin, “Frequency doubling photonic mixer with low conversion loss,” in Proc. OFC’97, pp. 356–357, 1997.

[98] M. M. Howerton, R. P. Moeller, G. K. Gopalakrishnan, and W. K. Burns, “Low-biased fibre-optic link for microwave downconversion,” IEEE Photon. Technol. Lett., vol. 8, no. 12, pp. 1692–1694, 1996.

[99] J. T. Gallo, K. D. Breuer, and J. B. Wood, “Millimeter wave frequency converting fibre optic link modelling and results,” in SPIE, vol. 3160, pp. 106–113, 1997.

[100] E.H.W. Chan, K.E. Alameh, and R.A. Minasian, “A photonics-based wideband linearised mixer,” in Microwave Optical Technology Letter, vol. 39, pp. 500-502, 2003.

[101] E. H. W. Chan and R. A. Minasian, "Microwave Photonic Downconverter With High Conversion Efficiency," in Journal of Lightwave Technology, vol. 30, no. 23, pp. 3580-3585, Dec 2012.

[102] Z. Tang, F. Zhang, S. Pan, "Photonic microwave downconverter based on an optoelectronic oscillator using a single dual-drive Mach–Zehnder modulator", in Optics Express, vol. 22, no. 1, pp. 305-310, Jan 2014.

[103] T. Jiang, S. Yu, R. Wu, D. Wang, W. Gu, "Photonic downconversion with tunable wideband phase shift", in Optics Letter, vol. 41, no. 11, pp. 2640-2643, Jun 2016.

[104] B. M. Haas, J. D. McKinney, "Multi-band RF downconversion over fibre with a single modulator", IEEE Photon. Technol. Lett., vol. 30, no. 18, pp. 1633-1636, Sep 2018.

[105] X. Liang, Y. Dai, F. Yin, X. Liang, J. Li, K. Xu, "Digital suppression of both cross and inter-modulation distortion in multi-carrier RF photonic link with down-conversion", in Optics Express, vol. 22, no. 23, pp. 28247-28255, Nov. 2014.

[106] X. Xie et al., “Digital nonlinearities compensation based on forward distortion information acquisition in channelized RF photonic links,” in Proc. Int. Topical Meet. Microw. Photon, pp. 88–91, 2012.

[107] Y. Cui, Y. Dai, F. Yin, Q. Lv, J. Li, K. Xu, and J. Lin, "Enhanced Spurious-Free Dynamic Range in Intensity-Modulated Analogue Photonic Link Using Digital Postprocessing," in IEEE Photonics Journal, vol. 6, no. 2, pp. 1-8, April 2014.

[108] A. Agarwal, T. Banwell, P. Toliver, and T. K. Woodward, “Predistortion compensation of nonlinearities in channelized RF photonic links using a dual-port optical modulator,” in IEEE Photon. Technol. Lett., vol. 23, no. 1, pp. 24–26, 2011.

[109] H. Yu, P. Li, M. Chen, R. Shi, H. Chen, S. Yang, and S. Xie, Photonic downconversion and linearisation of microwave signals from the X- to K-Band,” in IEEE Photonics Technology Letters, vol. 27, no. 19, pp. 2015-2018, 1 Oct.1, 2015.

[110] G. Li, T. Shang, Y. Zhang, and D. Chen, “SFDR and gain enhancement in photonic downconversion link by linearisation and full spectrum utilization,” in applied Optics, vol. 58, no. 3, pp. 579-587, January 2019.

[111] V. J. Urick, "Long-haul analogue links tutorial," Optical Fibre Communication, collocated National Fibre Optic Engineers Conference, San Diego, CA, pp. 1-39, 2010.

[112] D. Inoue, T. Hiratani, K. Fukuda, T. Tomiyasu, T. Amemiya, N. Nishiyama, and S. Arai, "Low-bias current 10 Gbit/s direct modulation of GaInAsP/InP membrane DFB laser on silicon," in Optical Express, vol. 24, no. 16, pp. 18571-18579, 2016.

[113] F. Paloi, S. Haxha, T. N. Mirza, and M. S. Alom, "Microwave Photonic Downconversion with Improved Conversion Efficiency and SFDR," in IEEE Access, vol. 6, pp. 8089-8097, 2018.

[114] W. L. Stewart II, and J. G. Blaylock, "RF Photonics for aerospace applications," in Journal of Aerospace, vol. 113, no. 1, pp. 1629-1640, 2004

[115] R. G. Walker, N. Cameron, Y. Zhou, and S. Clements, "Electro-Optic modulators for space using Gallium Arsenide," Proc. SPIE 10562, International Conference on Space Optics-ICSO 2016, 105621A, September 2017.

[116] R. G. Walker, I. Bennion, and A. C. Carter; "Low voltage, 50Ω GaAs/AlGaAs travelling-wave electro-optic modulator with bandwidth exceeding 25GHz", Electron. Lett., 25(23), pp. 1549–1550, 1989

[117] X. J. Meng and A. Karim, "Microwave photonic link with carrier suppression for increased dynamic range," Fibre Integr. Opt., vol. 25, no. 3, pp. 161–174, 2006.

[118] W. Qin and W. Jiang, "The performance analysis of microwave photonic frequency conversion using double-sideband suppressed-carrier and balance detection," in IEEE International Conference on Communication Problem-Solving (ICCP), pp. 582-585, Guilin, 2015.

[119] C. Middleton and R. DeSalvo, "High performance microwave photonic links using double sideband suppressed carrier modulation and balanced coherent heterodyne detection," MILCOM 2009 - 2009 IEEE Military Communications Conference, Boston, MA, , pp. 1-6, 2009.

[120] J. Kim, W. B. Johnson, S. Kanakaraju, W. N. Herman, C. H. Lee, "Demonstration of balanced coherent detection using polymer optical waveguide integrated distributed traveling-wave photodetectors", Opt. Express, vol. 17, no. 22, pp. 20242-20248, 2009

[121] D. Marpaung, C. Roeloffzen, A. Leinse, and M. Hoekman, "A photonic chip based frequency discriminator for a high performance microwave photonic link," Opt. Express, vol. 18, pp. 27359-27370, 2010.

[122] F. V. C. Mendis, M. K. Haldar, and J. Wang, "Cross-modulation distortion in subcarrier multiplexed optical systems," in Proceedings of 1994 Nonlinear Optics: Materials, Fundamentals and Applications, Waikoloa, HI, USA, pp. 338-340, 1994.

[123] W. L. Stewart II and J.G. Blaylock, "The challenge of transmitting super-high-frequency radio signals over short fibre-optic networks on aerospace platforms," 21st IEEE Digital Avionics Systems Conference, Track 4, 4D3, 2002.